Technical Report Documentation Page

1. Report No.	2. Government Accession No.	3. Recipient's Catalog No.
FHWA/TX-02/0-4372-1		

4. Title and Subtitle	5. Report Date
Improved Design Economy for Drilled Shafts in Rock - Introduction, Literature Review, Selection of Field Test Sites for Further Testing, and Hardware	15 November 2002
	6. Performing Organization Code

7. Author(s)	8. Performing Organization Report No.
Nam, M. S., Liang, R., Cavusoglu, E., O'Neill, M. W., Liu, R., and Vipulanandan, C.	0-4372-1

9. Performing Organization Name and Address	10. Work Unit No. (TRAIS)
University of Houston Department of Civil and Environmental Engineering N107 Engineering Building 1 Houston, Texas 77204-4003	11. Contract or Grant No. 0-4372

12. Sponsoring Agency Name and Address	13. Type of Report and Period Covered
Texas Department of Transportation Research and Technology Implementation Office P. O. Box 5080 Austin, Texas 78763-5080	Technical Report / 1 Sep 01 - 31 Aug 02
	14. Sponsoring Agency Code

15. Supplementary Notes
Research performed in cooperation with U. S. Dept. of Transportation, Federal Highway Administration
Research Project Title: Improved Design Economy for Drilled Shafts in Rock

16. Abstract

Published studies relating to the design of drilled shafts for axial loading in soft rock are reviewed, including previous load tests performed by TxDOT. A process whereby this information can be incorporated into improved design rules for drilled shafts in soft rock is described. This process involves the use of computer models that will be calibrated by existing load test and rock data as well new data to be acquired later in the project, which will focus especially on borehole roughness as produced by augers and core barrels. A new series of load tests that will be conducted on drilled shafts in the Dallas, Texas, area is proposed, and candidate test sites in both clay-shale and limestone are identified. Initial rock strength and Texas DOT penetrometer data from from five sites in the Dallas area are summarized, and the design of test shafts at three of these sites is shown. The Osterberg Cell method of loading will be used at those sites. The shafts will be tested in clay-shale, clay-shale and soil overburden, and limestone. Data from the two Dallas area test sites not selected for new load tests will also be used later in the project. Documentation is provided for a laser profiling device that will be used to quantify borehole roughness at the test sites and for a simple penetrometer device that is proposed for the routine delineation of clay-shale from overlying soil.

17. Key Words	18. Distribution Statement
Drilled shafts, design, axial capacity, load testing, soft rock, roughness, TxDOT penetrometer	No restrictions. This document is available to the public through NTIS: National Technical Information Service 5285 Port Royal Road Springfield, Virginia 22161

19. Security Classif.(of this report)	20. Security Classif.(of this page)	21. No. of Pages	22. Price
Unclassified	Unclassified	146	

Form DOT F 1700.7 (8-72) **Reproduction of completed page authorized**

Contents

List of Figures

List of Tables

Chapter 1: Introduction

General

Drilled shafts are used heavily for foundations for bridges and other transportation structures in geographical areas in Texas where rock lies near the ground surface, principally because they are cost-effective relative to driven piles and spread footings. They are constructed by excavating into the rock, forming a cylindrical socket, and the sockets are concreted, usually with steel reinforcing. The "rock socket" resists loads through a combination of skin friction (Q_s) and point bearing (Q_b) in the rock and in the "overburden" (soil). A schematic of a typical rock-socketed drilled shaft is shown in Figure 1. The arrows along the side of the shaft in the overburden indicate that in addition to shear capacity in the rock socket, some shear capacity may also be provided in the softer overburden that can be added to the capacity developed in the rock socket.

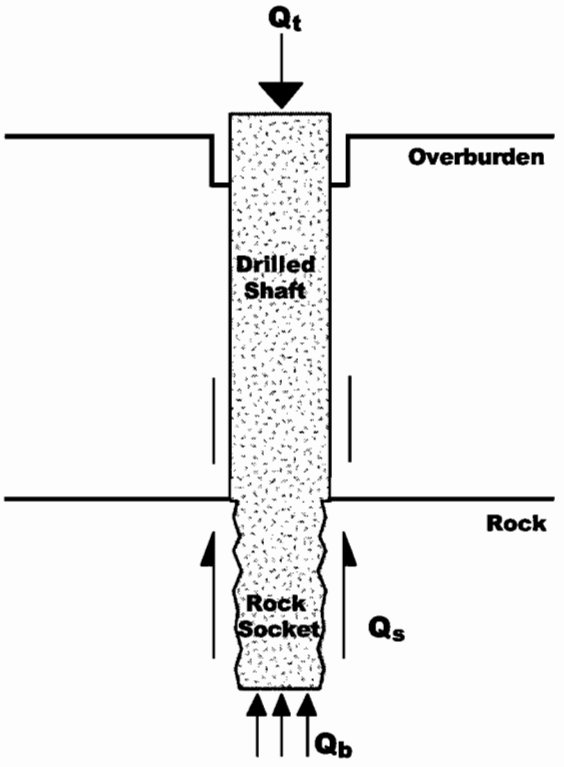

Figure 1.1. A Schematic of a Typical Rock-Socketed Drilled Shaft

Even though rock sockets are sometimes difficult to excavate, they usually provide excellent resistance to load. Rock sockets can be cut into the rock for a very short distance, in which case most of the working load is resisted in point bearing, or they can penetrate further into the rock, in which case most of the working load will be resisted in skin fiction.

Definition of Rock and Intermediate Geomaterial

Generally, to the geologist the term "rock" applies to all constituents of the earth's crust. To the civil engineer, especially the geotechnical engineer, the term "rock" is understood to apply to the hard and solid (cemented) formations of the earth's crust. From a genetic point of view, rocks are usually divided into the three groups:

- Igneous rocks (e. g., granite, diorite, basalt)
- Sedimentary rocks (e. g., shale, siltstone, sandstone, conglomerate, limestone, lignite, chert, and gypsum)
- Metamorphic rocks (e. g., gneiss, schist, slate, marble)

Igneous rocks form when hot molten silicate material from within the earth's crust solidifies. Sedimentary rocks form from deposition and accumulation of sediments of other rocks, plant remains, and animal remains by wind, or water at the earth's surface, followed by their later solidification into rock. Metamorphic rocks form when existing rocks undergo changes by recrystallization in the solid state at high pressure, temperature, and/or by chemical action at some time in their geological history.

The rock formations of greatest interest to the Texas DOT (i. e., those in which the greatest amount of highway construction occurs) are sedimentary rocks belonging to formations from the upper Cretaceous to lower Eocene periods (Del Rio Clay / Georgetown Limestone, Eagle Ford Shale / Buda Limestone, Navarro Group / Marlbrook Marl / Pecan Gap Chalk / Ozan Formation, Midway Group, and Wilcox Group, progressing from oldest to youngest, and from west to east according to the positions of their outcrops). These rocks, which are found along the "I-35 corridor" along and west of I-35 between a point north of Dallas to a point south and west of San Antonio, can almost always be classified as shales, limestones or marls (shales with carbonate cementation, or "limey shales"). Some units in the shale and marl formations exhibit

characteristics of very heavily overconsolidated clays (slake and swell easily) rather than those of true rock. The general location of these formations is shown in Figure 1.2.

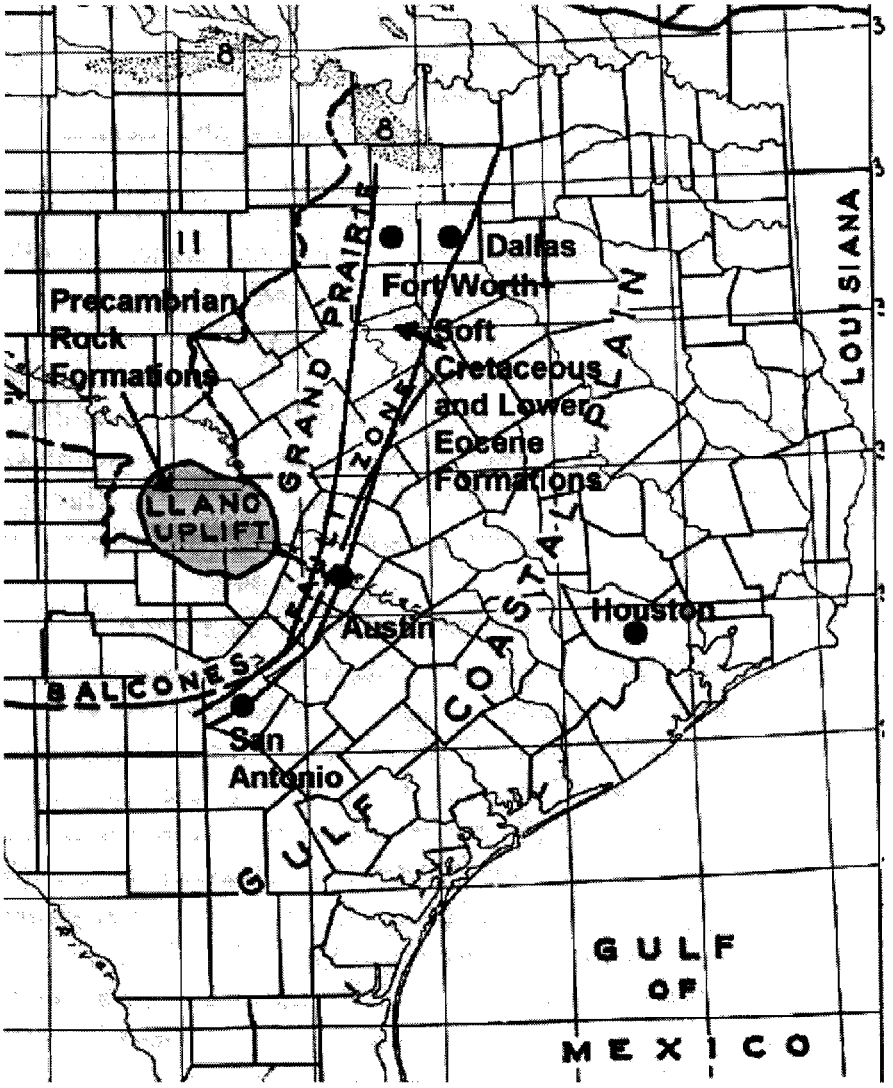

Figure 1.2. Map of East and Central Texas Showing Locations of Soft Upper Cretaceous to Lower Eocene Formations along the I-35 Corridor and Precambrian Rock Formations of the Llano Uplift (after Sellards et al., 1932)

From an engineering perspective, Deere and Miller (1966) provide a description of intact rock in terms of its uniaxial compressive strength and its stiffness relative to strength, as seen in Table 1.1.

Table 1.1. Engineering Classification of Intact Rock on the Basis of Strength and Modulus (after Deere and Miller, 1966)

On the basis of strength

Class	Description	Uniaxial Compressive Strength, q_u (MPa)	Rock Material
A	Very high strength	~ 220	Quartzite, diabase, dense basalts
B	High strength	~ 110 to ~ 220	Majority of igneous rocks, strong metamorphic rocks, weakly cemented sandstones, hard shales, majority of limestones, dolomites
C	Medium strength	~ 55 to ~ 110	Many shales, porous sandstones and limestone, schistose varieties of metamorphic rocks
D	Low strength	~ 28 to ~ 55	Porous low-density rocks, friable sandstone, tuff, clay shales, weathered and chemically altered rocks of any lithology
E	Very low strength	< 28	

On the basis of modulus ratio

Class	Description	Modulus Ratio (E_{t50} / q_u)
H	High	> 500
M	Average (medium)	200 ~ 500
L	Low	< 200

For purposes of this research two different terms for very soft rock will be used. These are the terms given by O'Neill and Reese (1999): (1) "intermediate geomaterial" for geomaterials having 73 psi (0.5 MPa) < q_u < 725 psi (5.0 MPa), and (2) "rock" for any cohesive geomaterial having a $q_u \geq$ 725 pounds per square inch (5.0 MPa). Most, but not all, of the near-surface rock formations along the I-35 corridor tend to fall into Category E in Table 1.1.

Some harder igneous rock formations outcrop at scattered locations along the I-35 corridor but are found more frequently in the Pre-Cambrian Llano Uplift region of west-central Texas

(Figure 1.2), where metamorphic and sedimentary rock formations are also found. These rocks are often in Categories B and C in Table 1.1. Pre-Cambrian formations, mostly hard and very complex geologically, are also found in the Trans-Pecos Region in the vicinity of Van Horn.

This research will focus on the softer shale and limestone formations along the I-35 corridor. In addition to being soft, these rock formations often contain frequent joints and solution cavities that are either closed, open or open and filled with debris. From an engineering perspective one way to describe the degree and effect of jointing is to assign two indexes. The first is the percent recovery from core samples. The percent recovery is defined as follows:

$$\text{Percent Recovery} = \frac{\text{sum of lengths of all segments recovered in a core barrel}}{\text{total length cored}} \times 100(\%) .$$

The second is the rock quality designation (or "RQD"), which is defined as follows:

$$\text{RQD} = \frac{\text{sum of lengths of rock core segments, the length of which are 100 mm (4 in.) and longer}}{\text{total length cored}} \times 100(\%).$$

It is generally accepted that rocks and intermediate geomaterials with lower RQD's and percent recoveries will produce rock sockets with lower capacities and greater settlements than those with higher RQD's and percent recoveries.

A third index, which is used by TxDOT to design rock sockets, is the cone penetration resistance (PR). The PR is obtained by driving a 76-mm (3-inch) diameter, 60-degree solid steel cone into rock at the bottom of a standard borehole. The cone, termed the TxDOT cone, is affixed to the bottom of a string of N-rod and driven by a 170-lb (0.76 kN) hammer dropped 24 inches (610 mm) onto a flat steel plate at the head of the string of N rod successively for 100 blows. The penetration resistance is the distance that the tip of the cone advances in 100 blows. If that value is 12 inches (305 mm) or less, the geomaterial is classified as a rock for design purposes. RQD and percent recovery are not used explicitly in design because it is assumed that the PR value will reflect seams, joints and cavities within the rock. It is the desire of TxDOT that any design parameters that arise from the current research be correlated to the PR.

Current TxDOT Design Method (2000)

The current TxDOT design method for rock sockets is described in the TxDOT Geotechnical Manual (TxDOT, 2000). Figure 1.3 was taken from that manual. The designer simply uses this graph to convert the number of millimeters (or inches) of penetration of the TxDOT cone per 100 blows of the hammer into allowable values of unit skin friction and point bearing. These are then multiplied by the nominal perimeter and cross-sectional areas of the socket, respectively, and the results are summed to obtain the allowable capacity of the socket. The unit values obtained from these figures contain inherent factors of safety of 3.0 for skin friction and 2.0 for point bearing. Figure 1.3 was redrawn as Fig. 1.4 without the indicated factors of safety in Fig. 1.3. That is, Fig. 1.4 relates PR in mm / 100 blows to ultimate unit resistance. The highest ultimate unit point bearing values that are permitted are for CPR values of 2 inches (50 mm) of penetration per 100 blows [900 psi or 6200 kN/m^2]. Correspondingly, the highest permissible unit skin friction values (for the same 50 mm per 100 blow penetration) is 141 psi (975 kN/m^2). The origins of Fig. 1.3 are not clear. TxDOT geotechnical engineers indicate that it appeared in a 1951 publication with no reference to how the values were obtained.

The TxDOT Geotechnical Manual indicates that if the shaft is socketed into or tipped on hard geomaterial [3 in. (75 mm)/100blows] skin friction in all softer overlying soil (overburden) is usually neglected because the movements necessary to mobilize point bearing resistance in the rock are too small to allow for the development of substantial skin friction in the overlying soft soil. Otherwise, presumably, skin friction from the overlying soil is added to the capacity of the rock socket to yield the overall capacity of the drilled shaft. Procedures for estimating skin friction in softer geomaterials (overburden) are given in the TxDOT Geotechnical Manual (2000) and will not be repeated here.

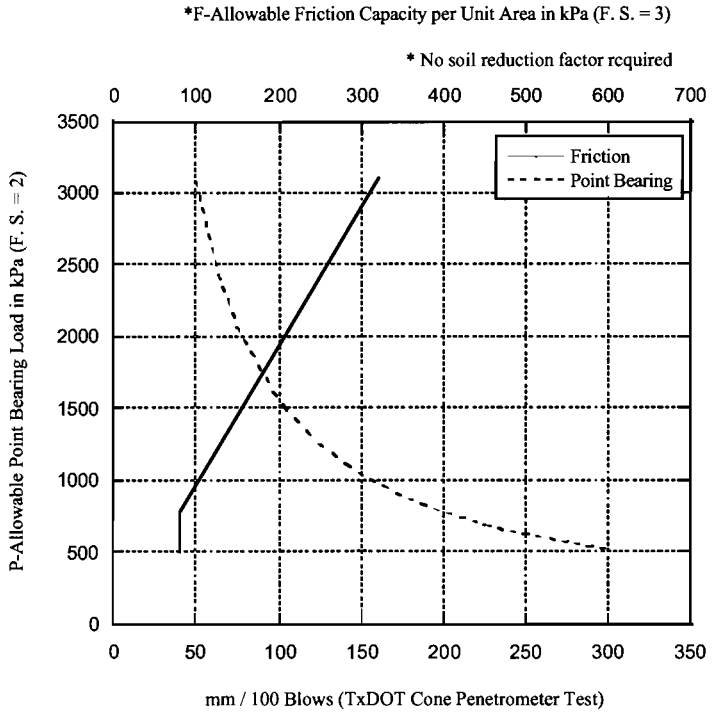

Figure 1.3. Allowable Point Bearing and Skin Friction Values for PR > 100 Blows/300 mm (foot) (TxDOT Geotechnical Manual, 2000)

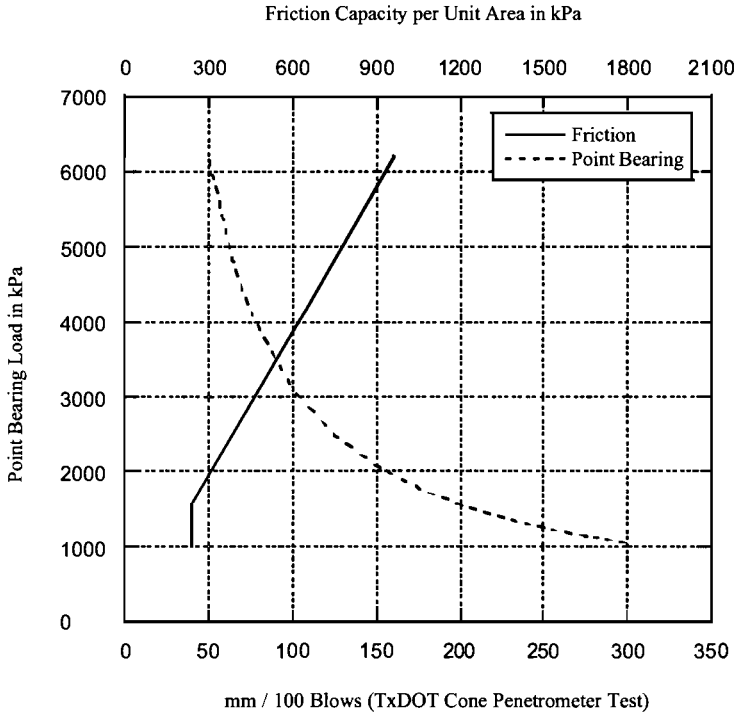

Figure 1.4. Ultimate Point Bearing and Skin Friction Values for PR > 100 Blows/300 mm (foot) (Modified after TxDOT Geotechnical Manual, 2000)

TxDOT has identified several concerns relating to the current design method for rock sockets, including:

1. The accuracy and appropriateness of the current design chart (Fig. 1.3) over its entire range of PR values.
2. The appropriateness of current upper limits to both unit skin friction and point resistance values permitted in TxDOT's current design method.
3. The appropriateness of adding load transfer in the overburden soil to the resistance in the socket for design purposes.
4. The need for assessing the elevation of the top of rock in clay-shale formations, in which rock is difficult to identify on the basis of cuttings brought to the surface on drilling tools.

Issues 1 and 2 are influenced by the effect of discontinuities and soft soil seams within the rock on load transfer from the socket to the rock; the roughness and cleanliness of the sides and base of the rock socket; the strength and stiffness of the intact rock; and perhaps other factors, including the length of time that the borehole for the socket remains open and allowing for the occurrence of the negative results of stress relief.

The current design chart (Fig. 1.3) was apparently developed though correlations with relatively few drilled shaft load tests, although details are not available. It is the general suspicion of TxDOT design personnel that the values of unit skin friction and point bearing in Figs. 1.3 and 1.4 may be too conservative.

Objectives and Limitations

The objectives of this project are as follows:

1. Develop updated design charts for skin friction and point bearing resistance in rock sockets, focusing on the very soft rocks and intermediate geomaterials along the I-35 corridor in Texas and focusing on the TxDOT cone test as the principal geomaterial characterization tool.

2. Assess whether skin friction in overburden soils can be added to rock socket capacities to give total drilled shaft capacities when the rock sockets are in the soft rocks found along the I-35 corridor.
3. Assess methods to determine the location of the top of rock during the construction of rock sockets.

The methodology for addressing these objectives will be covered in detail in Chapter 3 and beyond. In general, the research will proceed through the following steps:

- Identify analysis tools and design models for rock sockets that have been developed by others (Chapter 2).
- Acquire rock socket test data from selected soft rock sites, most likely from outside the state of Texas, at which as a minimum q_u and RQD have been obtained.
- Develop a convenient device for obtaining borehole roughness profiles.
- Locate three sites along the I-35 corridor at which field studies can be performed. These sites should be in soft limestone and clay-shale and should be sites at which the borehole can be drilled dry with or without the use of surface casing (to accommodate the laser profiler).
- Take rock core samples at these test sites and conduct TxDOT CPR tests in nearby boreholes in parallel with rock coring.
- Perform compression tests with stiffness measurements on the cores and assign percent recovery and RQD values for all cores taken.
- Perform alternate lab tests as surrogates for compression tests (splitting tension, point load) so that correlations can be developed to estimate compressive strength in very low RQD rock without standard 100-mm-long cores.
- Install full-sized boreholes at the three test sites (multiple holes at each site), measuring side roughness profiles with the laser profiler developed above.

- Develop, from the above data, correlations between rock type, drilling tool characteristics, and some measure of borehole roughness (e. g., mean asperity height).
- Install one test socket at each of the three test sites, with in-place Osterberg load cells. At one site carry the socket through the overburden to ascertain whether the skin friction in the overburden can be added to the socket resistance.
- Load-test the three test sockets to determine the maximum skin friction and a lower bound to maximum point bearing resistance and the degree to which overburden skin friction can be added to socket resistance.
- In parallel, use the data from the test-site cores (compression strength, modulus, etc.), the joint patterns (RQD and percent recovery) and the roughness measurements in one to three design models to predict socket capacity (skin friction and point bearing resistance) for all three test sockets.
- Compare the results from the design and/or models with measurements at the three test sites, and modify the design models if necessary to obtain agreement between predictions and measurements. In order to expand the base of correlations for test results and design/analysis models, these models will also be adjusted to give high-level correlations at other selected sites, outside the state of Texas, from which data can be obtained.
- Develop design curves similar to the current TxDOT design curves, but based upon q_u and rock type (and possibly the type of drilling tool), in which it would be expected that the rock type and drilling tool would be an indicator of roughness.
- Develop relations between TxDOT cone penetration resistance and compressive strength of the cores at various sites, using surrogate tests for the cores (point load, splitting tension) where necessary. Data will be collected from TxDOT from other subsurface exploration sites as such data become available.
- Using the cone correlations above convert the design charts that are related to q_u to design charts that are related to TxDOT cone penetration resistance,

which will give design charts that have the appearance of the current design charts, but which may be specific to a certain type of rock (clay-shale, or limestone).

The limitations of the study are:

1. There will be no attempt to re-evaluate factors of safety, as too few data will be available to permit evaluation of the statistical parameters necessary to relate factor of safety to level of reliability.
2. The design relations involving TxDOT cone penetration resistance will not be explicitly calibrated for hard rock (e. g., granitic rock from the Llano Uplift region).

During the field phase of the work a techniques will be assessed to determine when the borehole has reached the surface of rock.

This page is intentionally blank.

Chapter 2: Literature Review

Rock Socket Behavior

Various methods of design and analysis of rock sockets will be reviewed in this chapter. However, it is first useful to review the principles on which many of these methods are based.

Principles

Skin friction in rock sockets can develop in one of three ways: (1) through shearing of the bond between the concrete and the rock that develops when cement paste penetrates into the pores of the rock (bond); (2) sliding friction between the concrete shaft and the rock when the cement paste does not penetrate into the pores of the rock and when the socket is smooth (friction); and (3) dilation of an unbonded rock-concrete interface, with increases in effective stresses in the rock asperities around the interface until those asperities shear off, one by one (dilation). Dilational behavior is also accompanied by frictional behavior. Dilation at the rock-concrete interface produces increases in rock strength at the interface since any pore water pressures that develop during shear in the rock near the interface dissipate very rapidly because of the proximity of gaps at the interface and the high stiffness of the rock framework. These phenomena are illustrated schematically in Figure 2.1, below.

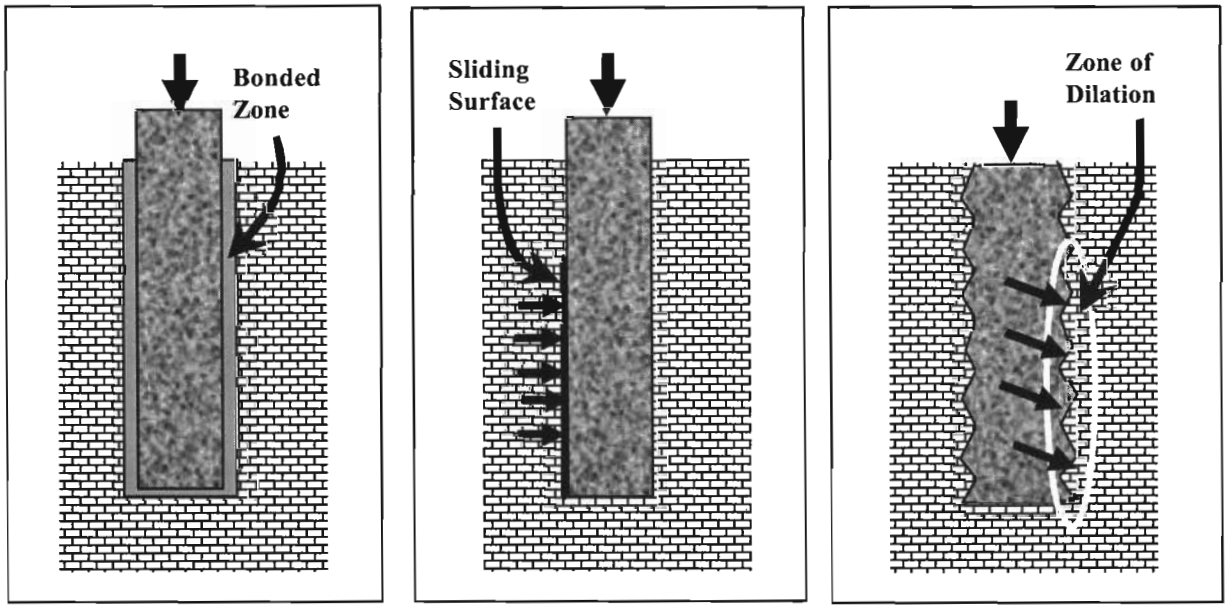

(a) Bond condition (b) Friction condition (c) Dilation condition

Figure 2.1. Schematic Representation of Interface Conditions in Rock Sockets.

It is not likely that only one of these phenomena is present in a given rock socket. Rather, all three occur simultaneously, with one being dominant. Rock that does not have large pores or in which the action of the drilling tool forces fine cuttings into the pores (or in which drilling mud plugs the pores), thus limiting filtration of the cement paste into the formation, will not exhibit the bond condition. Instead, rock-concrete interfaces will exhibit either the friction condition or the dilation condition. This behavior may be more characteristic of argillaceous rocks such as clay-shales than of carbonaceous or arenaceous rocks, such as limestones or sandstones.

Skin Friction

Interface Roughness and Smear. While friction may be important in rock sockets that drill smoothly and that have low permeability, any degree of surface roughness on the interior face of the borehole can produce significant capacity through dilation. In a purely frictional (smooth) socket O'Neill and Reese (1999) suggest estimating unit skin friction as the product of the fluid concrete pressure at the time of construction and the tangent of the angle of rock-soil friction, typically about 30° in Texas clay shales (Hassan, 1994). If the socket is rough, and dilation occurs, the process of modeling skin friction becomes complicated. Many of the methods described in this chapter assume some degree of interface roughness. The effect of this roughness is handled through (1) empirical correlations, (2) finite element simulation of the kinematics associated with shear movement at a regular (e. g., sinusoidal) interface (e. g., Hassan, 1994), or (3) limit equilibrium amongst rock asperities in a statistically defined interface (e. g., Baycan, 1996).

The stress conditions computed using a finite element model around rock or IGM asperities at the socket-rock interface are shown for a sinusoidal interface pattern in Figure 2.2. Shearing failure occurs by "gouging" the asperity out of its parent rock, or development of lateral bearing capacity failure of the concrete on the rock asperities. Very crudely, the shear strength of the rock asperity is proportional to the radial effective stress produced by the concrete pushing the rock outward as it slides past the rock asperity. The normal radial strain in the rock is proportional to the asperity height divided by the shaft radius if the rock behaves elastically. This suggests that if the roughness pattern does not change with the radius of the socket borehole and the rock is radially elastic up to the point of shear failure, the shearing resistance at the rock-concrete interface will decrease linearly as the diameter or radius of the socket increases. O'Neill et al. (1996) found that the ratio of skin friction in rock sockets in soft rock varied by an

average factor of 2.7 from a socket diameter of 152 mm (6 inches) to one of 914 mm (36 inches). However, Baycan (1996) found this phenomenon to be true only for small socket diameters [less than 0.61 m (24 inches)] in Melbourne mudstone. In sockets with diameters larger than about 0.61 m (24 inches), the effect of interface dilation was found not to vary significantly with socket diameter. This may be a result of the effect of stress relief on the rock asperities and underlying rock due to drilling the socket, which weakens large-diameter sockets (which take longer to excavate) more than small-diameter sockets. Kalinski et al. (2001) found that in stiff clays stress relief due to excavating a borehole resulted in reduced stiffness in the geomaterial to within about one borehole radius of the side of the borehole for a borehole with a diameter of 1.07 m. It is speculated that the width of the zone of influence for stress relief (resulting in reduced rock moduli) may be smaller relative to the borehole radius as the radius increases, thus accounting for the phenomenon observed by Baycan. Based on Baycan's observations it is concluded that test sockets for the current project should be at least 0.61 m (24 inches) in diameter and that the results of the research will in all likelihood not be applicable to sockets of smaller diameter.

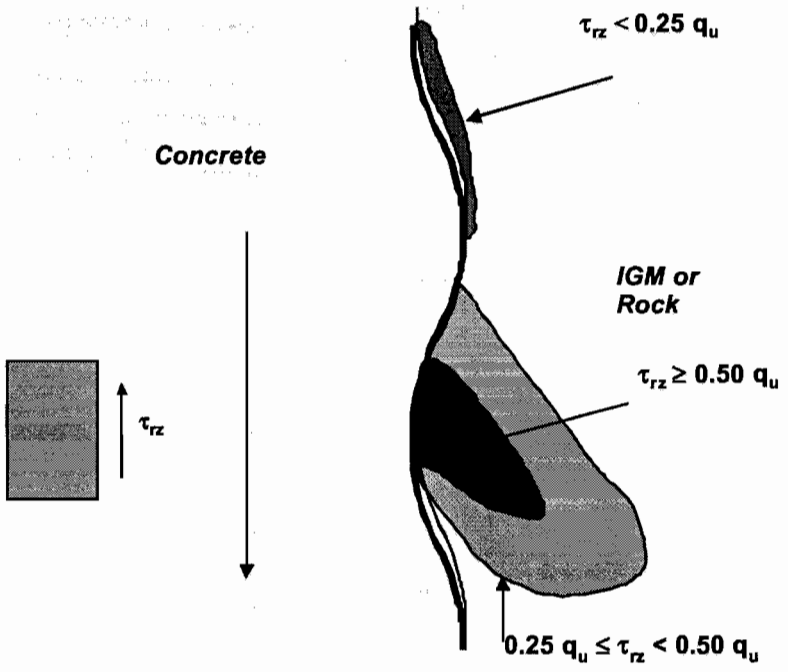

Figure 2.2. Stress Condition Around Rock or IGM Asperity at Incipient Shear Failure Via Finite Element Analysis (after Hassan, 1994)

Rock powder that is produced by the drilling process can mix with free water in the borehole and produce a paste-like covering, or "smear," on the surface of the borehole. A similar phenomenon can sometimes be produced by the accumulation of mud cake from mineral drilling slurry. Smear is more common in argillaceous rock than in other kinds of rock; however, it is possible in any rock type. Figure 2.3, from the slides for the NHI short course on drilled shafts, illustrates smeared geomaterial on the surface of a rock socket as well as a lower zone in which smear has been removed.

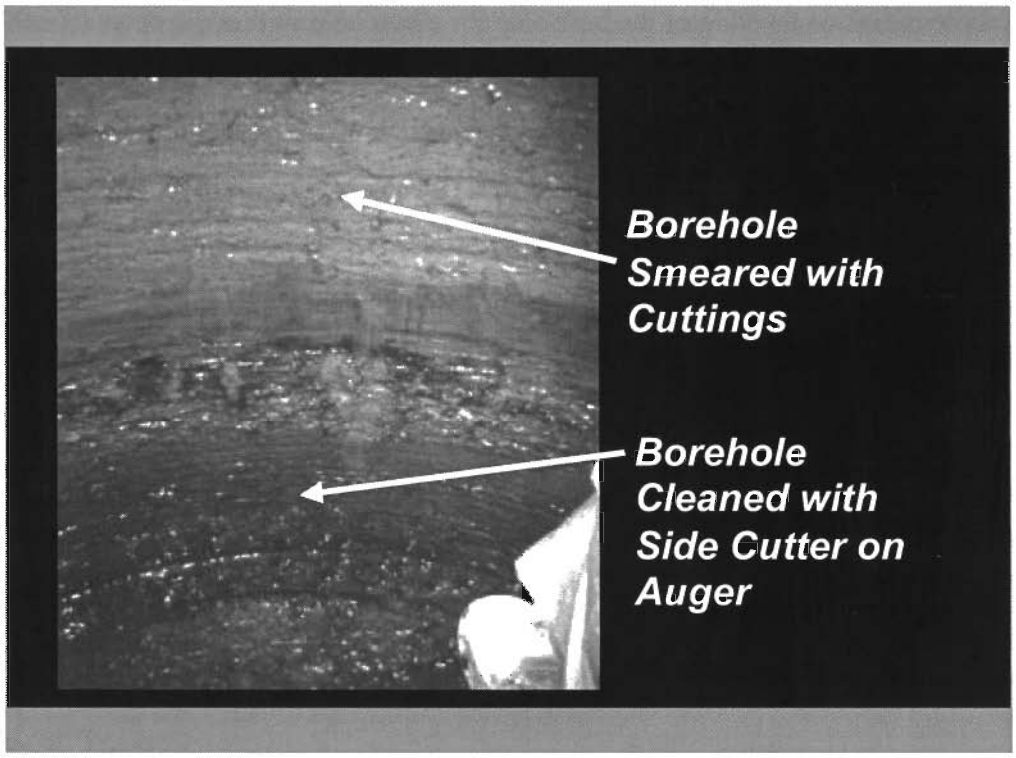

Figure 2.3. Photo of Borehole with Smeared Geomaterial Cuttings (Above) and Borehole Cleaned of Smear (Below)

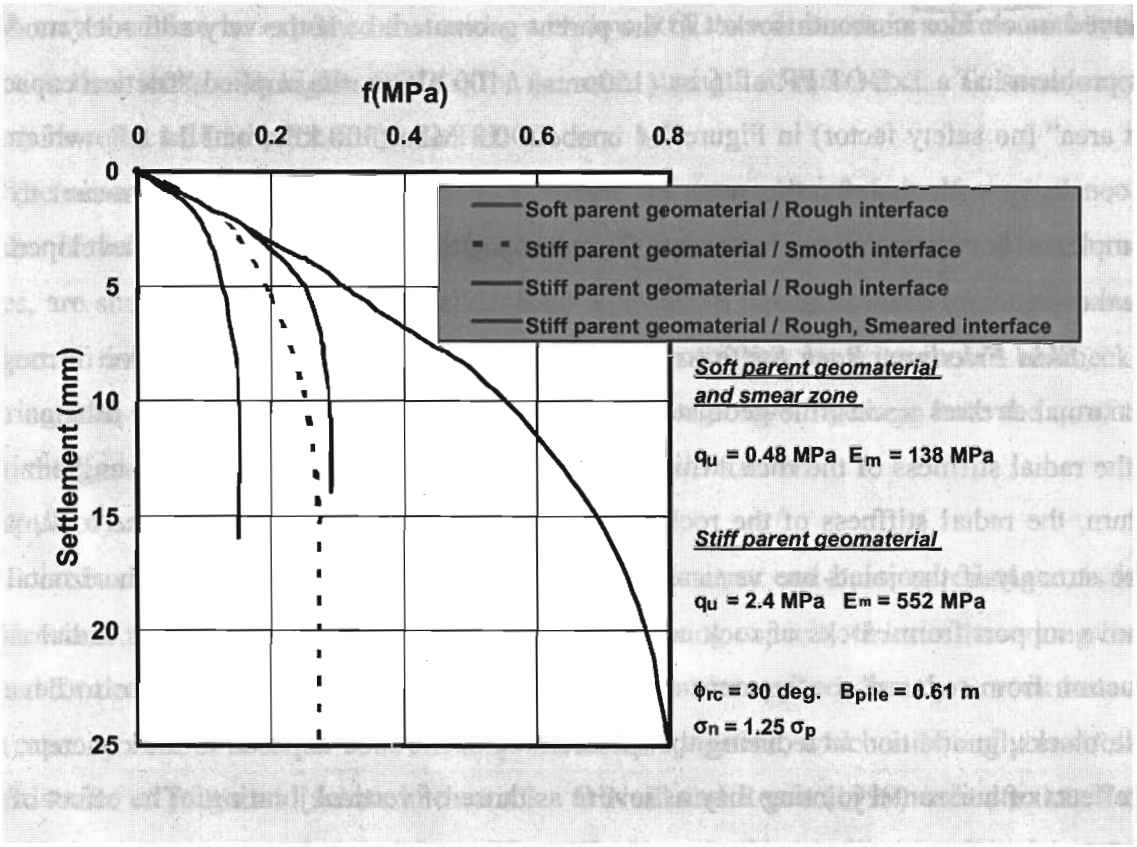

Figure 2.4. Effect of Smear on a Rock Socket in Very Soft Clay-Shale (Hassan and O'Neill, 1997).

Figure 2.4 shows graphs of developed unit skin friction (f) vs. settlement as computed from finite element analyses of rough and smooth sockets, clean and smeared. The rough interface pattern was a sinusoidal pattern with an asperity amplitude of 25.4 mm (1 in.) and a wave length of 1 m (39 in.). The smeared geomaterial was located at the interface, was 12.7 mm thick and had a compressive strength of 20 per cent of that of the stiff parent geomaterial. σ_n/σ_p is the normal concrete pressure on the sides of the borehole prior to loading, in atmospheres. The curve on the right considers a rough socket with no smear, which develops a maximum unit skin friction of 0.80 MPa (8.35 tsf). The curve to the left of that curve shows a rough socket with smear, as defined above, in which f_{max} = 0.28 MPa (2.92 tsf). The dashed curve, by comparison, considers a smooth socket in the same parent geomaterial but with no smear. The maximum unit skin friction value f_{max} is also 0.28 MPa (2.92 tsf). That is, the presence of smear to half of the asperity height essentially completely destroyed the salient effect of roughness, and the socket

behaved much like a smooth socket in the parent geomaterial. If the very soft rock modeled in this problem has a TxDOT PR of 6 in. (150 mm) / 100 blows, the implied "friction capacity per unit area" (no safety factor) in Figure 1.4 is about 0.3 MPa (300 kPa, or 3.14 tsf), which would be consistent with that for the smeared interface. (This observation is only meant to be an example of how correlations between PR and capacity might ultimately be developed. The actual correlation. between q_u and PR is yet to be established.)

Skin Friction: Rock Stiffness and Jointing. In a socket with any degree of roughness, the normal stresses against the geomaterial at the interface that are generated by dilation depend on the radial stiffness of the rock, which can crudely be characterized by its Young's modulus. In turn, the radial stiffness of the rock depends on the degree of jointing in the rock, perhaps more strongly if the joints are vertical than if they are horizontal. However, horizontal joints remove support from blocks of rock adjacent to the interface and allow both for radial stiffness reduction from reduced confinement of the rock and premature shearing failure to develop in those blocks, in addition to reducing the surface area of the rock exposed to the concrete, so that the effects of horizontal jointing may as severe as those of vertical jointing. The effect of lateral geomaterial stiffness is illustrated schematically in Figure 2.5.

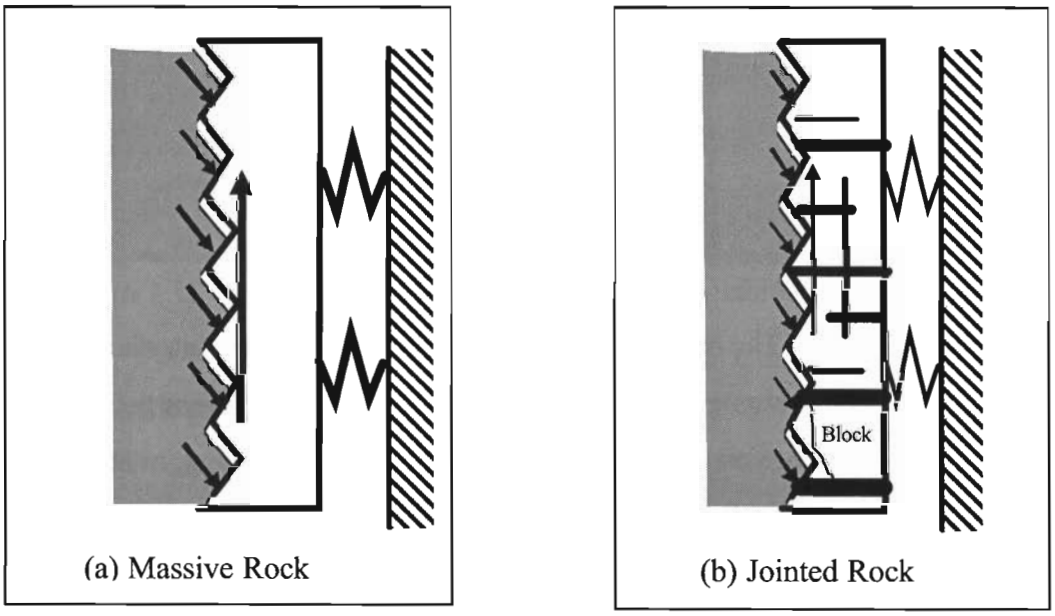

Figure 2.5. Schematic of the Effect of Rock Jointing on Dilative Skin Friction

It may therefore be expected that rocks with low RQD's will result in sockets with lower skin friction than rocks with higher RQD's, for the same strength of intact rock. To some extent, RQD may be reflected in the PR from the TxDOT cone test.

The observation is made that side shear failure does not always occur through the rock asperities. If the rock is stronger than the concrete, the concrete asperities, rather than the rock asperities, are sheared off. This effect is not likely to occur in the soft rock formations that are the subject of this study; however, in harder rock, the skin friction capacity should be checked considering both possibilities. This is often done at the design level by using both the q_u of the rock and the f'_c of the concrete in the design formulae for skin friction.

Point Bearing

Point bearing, also called base resistance, toe resistance or end-bearing resistance, is less well understood for rock sockets than is skin friction. Bearing capacity theories have long been developed for deep foundations in soil; however they cannot be applied directly to rock because bearing capacity in rock is often controlled by fracture propagation, which is strongly controlled by the existence of joints and seams in the rock. O'Neill and Reese (1999) indicate that if the rock is massive (no joints) and if the base of the socket is embedded in sound rock (assumed by the authors to be 1.5 socket diameters below the top of discernable rock), the ultimate point bearing capacity will be 2.5 times the median q_u of the rock to 2 socket diameters below the base of the socket. Experience within TxDOT suggests that in Texas rock formations an embedment of 1.0 socket diameters is sufficient to use the point bearing values in Figure 1.3.

Where the rock is jointed below the base of the socket, the point bearing capacity is reduced severely because the joints accelerate the development of fractures in the rock on which the socket is bearing. Some simple bearing capacity models have been developed using limit equilibrium principles for prescribed jointing patterns, and some have been developed using finite element analyses for prescribed jointing patterns and varying properties of gouge (debris within the joints). The most common design models, however, are those that were derived semi-empirically by correlating load test results with jointing patterns in the subsurface rock below the base of the socket. These models normally prescribe net, rather than gross, bearing capacities, so that the weight of the drilled shaft need not be considered as a load.

An important issue in the determination of point resistance is the value of settlement at which the maximum unit bearing capacity (q_{max}) occurs. If this value is much greater than the

value in which f_{max} occurs, and if the sides of the socket are brittle in shear, the maximum side shearing resistance should not be added to the maximum point resistance to determine the ultimate capacity of the shaft. A similar statement can be made about allowable capacity. If the settlement needed to develop q_{max} in the socket is smaller than that needed to develop the full skin friction in the overburden, it may not be prudent to use the full skin friction in the overburden when computing the capacity of the entire drilled shaft (socket plus overburden). TxDOT's current practice is to ignore skin friction in the overburden, which is conservative. There are no documented cases in load tests on sockets in soft rock in which settlement needed to develop q_{max} has been less than the settlement need to develop f_{max} in the socket, so this possibility will not be considered here.

Design Methods

Numerous design methods for rock sockets, other than the TxDOT design method, have been developed throughout the world. Most of these methods use q_u as a measure of rock capacity. A few use standard penetration test (SPT) resistance values (in granular intermediate geomaterials). Only a very few consider socket roughness and jointing along the sides of the socket in any explicit manner. Some of these methods provide a means for estimating socket settlement, but most address only socket capacity, carrying the tacit assumption that settlement is not an important design issue for sockets in rock (other than as indicated in the preceding section). A number of design methods were identified in this study that will be summarized below. Ordinarily, ultimate side resistance and base resistance are computed, reduced by factors of safety and added together to give the allowable capacity of the drilled shaft in compression.

AASHTO Design Method

The AASHTO method (*AASHTO*, 1996) prescribes that the ultimate side resistance, or skin friction capacity (Q_{SR}), for shafts socketed into rock be determined using the following:

$$Q_{SR} = \pi B_r D_r (0.144\, q_{SR}) \quad , \tag{2.1}$$

where B_r = Diameter of rock socket (ft),

D_r = Length of rock socket (ft), and

q_{SR}= Ultimate unit shear resistance along shaft/rock interface (psi), referred to elsewhere herein as f_{max}.

Fig. 2.6 gives values of q_{SR} as a function of q_u for massive rock. For uplift loading Q_{SR} of a rock socket is limited to $0.7Q_{SR}$ (for compression).

The design of rock sockets is based on the unconfined compressive strength of the rock *mass* (q_m) or concrete (σ_c) , whichever is weaker. q_m may be estimated using the following relationship:

$$q_m = \alpha_E q_u \quad , \tag{2.2}$$

where α_E = 0.0231(RQD%) – 1.32 ≥ 0.15 [Reduction factor based on RQD to estimate rock mass modulus and uniaxial compression strength for the rock mass (considering joints) from the modulus and uniaxial strength from the intact rock (dimensionless), given in AASHTO (1996)], and

q_u = uniaxial compressive strength of intact rock (units of pressure).

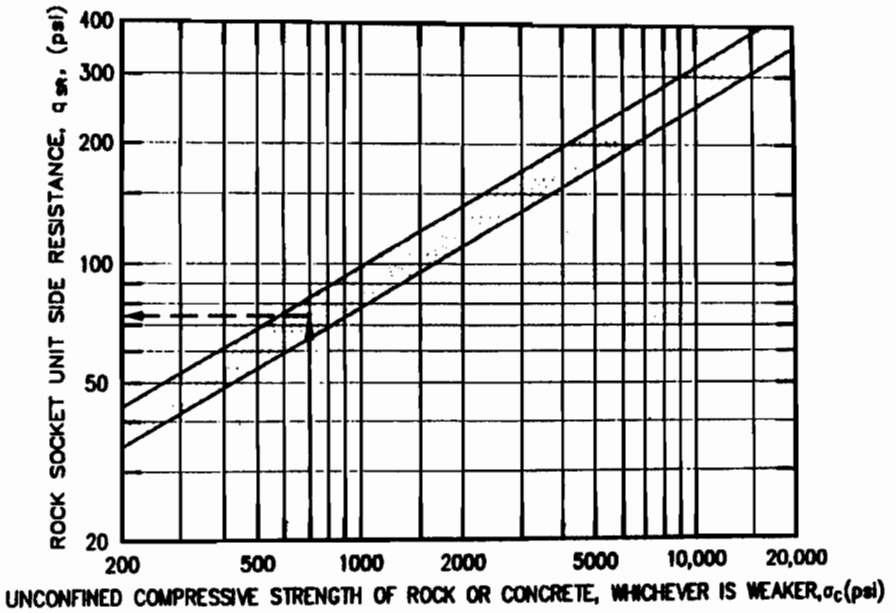

Figure 2.6. Procedure for Estimating Average Unit Side Shear for Smooth-Wall, Rock-Socketed Shafts (adapted from Horvath, et al., 1983)

Evaluation of ultimate point resistance (Q_{TR}) for rock-socketed drilled shafts considers the influence of rock discontinuities. Q_{TR} for rock-socketed drilled shafts is determined from:

$$Q_{TR} = N_{ms}\, q_u\, A_t \quad , \tag{2.3}$$

where N_{ms} = coefficient factor to estimate q_{ult} for rock (dimensionless), and

A_t = Area of shaft tip (base or point) (m^2 or ft^2, per units of q_u)

Table 2.1 Values of Coefficient N_{ms} for Estimation of the Ultimate Capacity of Footings on Broken or Jointed Rock (Modified after Hoek, 1983)

Rock Mass Quality	General Description	RMR[1] Rating	NGI[2] Rating	RQD[3] (%)	N_{ms}[4] A	B	C	D	E
Excellent	Intact rock with joints spaced > 10 feet apart	100	500	95-100	3.8	4.3	5.0	5.2	6.1
Very good	Tightly interlocking, undisturbed rock with rough unweathered joints spaced 3 to 10 feet apart	85	100	90-95	1.4	1.6	1.9	2.0	2.3
Good	Fresh to slightly weathered rock, slightly disturbed with joints spaced 3 to 10 feet apart	65	10	75-90	0.28	0.32	0.38	0.40	0.46
Fair	Rock with several sets of moderately weathered joints spaced 1 to 3 feet apart	44	1	50-75	0.049	0.056	0.066	0.069	0.081
Poor	Rock with numerous weathered joints spaced 1 to 20 inches apart with some gouge	23	0.1	25-50	0.015	0.016	0.019	0.020	0.024
Very poor	Rock with numerous highly weathered joints spaced < 2 inches apart	3	0.01	<25	Use q_{ult} for an equivalent soil mass				

[1]Geomechanics Rock Mass Rating (RMQ) System—Bieniawski, 1988.
[2]Norwegian Geotechnical Institute (NGI) Rock Mass Classification System, Barton, et al., 1974.
[3]Range of RQD values provided for general guidance only; actual determination of rock mass quality should be based on RMR or NGI rating systems.
[4]Value of N_{ms} as a function of rock type; refer to Table 4.4.8.1.2B for typical range of values of C_o for different rock type in each category.

Preferably, values of q_u should be determined from the results of laboratory testing of rock cores obtained within 2 socket diameters of the base of the socket. Where rock strata within this interval are variable in strength, the rock with the lowest capacity (q_u) should be used to determine Q_{TR}. For rocks defined by very poor quality, the value of Q_{TR} cannot be less than the value of Q_T for an equivalent soil mass. The AASHTO method makes no specific allowance for the use of dynamic penetrometers, such as the TxDOT penetrometer, for use as a surrogate for q_u.

Formation-Specific Design Method of O'Neill and Hassan

O'Neill and Hassan (1993) describe a method for estimating the skin friction capacity of drilled shafts in the Eagle Ford Formation in Dallas, Texas. The Eagle Ford Formation is an upper Cretaceous clay-shale (soft rock) containing several lithological units whose compression strengths vary widely. This method is empirical and is based on analysis of the results of six full-scale compression load tests at four sites in the Eagle Ford Formation in the Dallas area. O'Neill and Hassan proposed a design formula for unit skin friction in that specific geologic formation that considers the strength of the clay-shale, as measured in unconfined compression tests, variability of the strength of the rock within the socket (joints and discontinuities) and construction factors (roughness and smear):

$$\frac{f_{\max}}{q_u} = \alpha\beta\varepsilon\sigma \quad , \tag{2.4}$$

where f_{max} = the maximum, nominal unit skin friction (i. e., unfactored),

q_u = unconfined compression strength of the rock (not including inclusions of stiff clay, which occur within the Eagle Ford Formation),

α = a rock strength reduction factor to account for the effects of drilling disturbance and stress relief on the rock surrounding the socket,

β = a factor to account for the presence of discontinuities within the rock,

ε = a borehole surface roughness or texture factor (function of drilling details), and

σ = a "smear" factor that accounts for the remolding effects produced by drilling in the presence of water without subsequent cleaning.

Based on the paper, the authors proposed that α be taken as 0.36 for 200 kN/m^2 $\leq q_u \leq$ 5000 kN/m^2. β was recommended to be equal to 1, since the discontinuities in the Eagle Ford clay-shale at the sites where the load tests were carried out are horizontal laminations that are typically closed. The value of ε was suggested to be 0.69 for ordinary auger drilling and 1.0 for any case in which the borehole was artificially roughened. Finally, it was suggested that σ be taken as a function of average rock strength, q_u, as follows:

$$\sigma = 1.1 - 0.48 \log_{10}\left[\frac{q_u\left(MN/m^2\right)}{0.19\left(MN/m^2\right)}\right] \quad . \tag{2.5}$$

As stated, the factor, the factor σ takes into account the presence of smear at the concrete-rock interface.

O'Neill and Hassan displayed the gross results of their analysis as shown in Figure 2.7 and suggested a simpler, but less accurate, design equation, Eq. (2.6). This equation is a simple analytical representation of the solid line in Figure 2.7, which is a fit to the field data.

$$\alpha_q = \frac{f_{\max}(avg)}{q_u(avg)} = 0.275 - 0.125 \log_{10} \frac{q_u(MPa)}{0.19MPa} \quad , \qquad q_u \le 5MPa \tag{2.6}$$

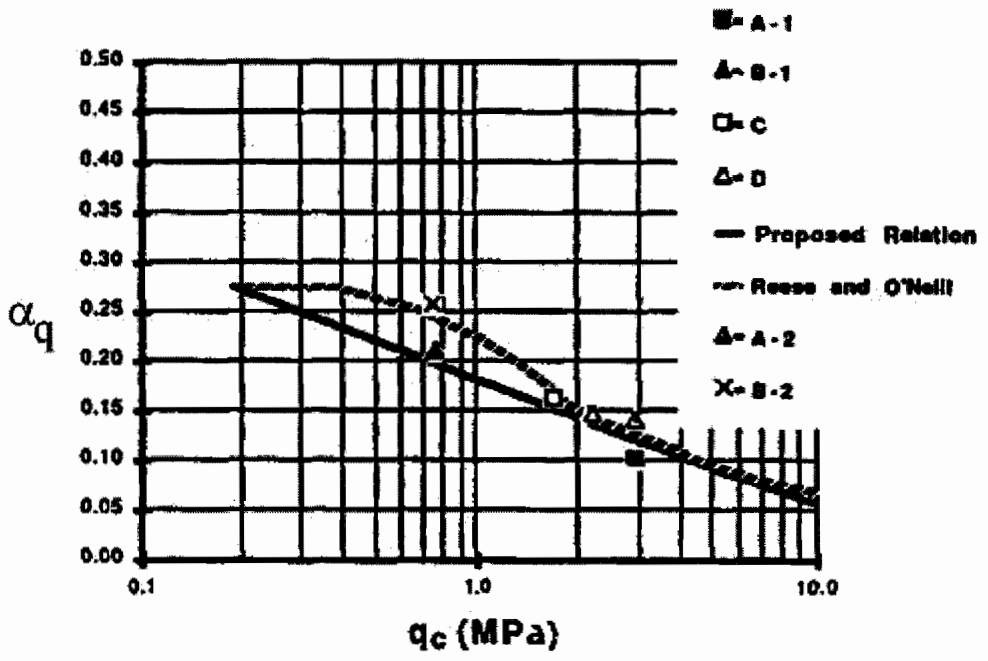

Figure 2.7. α_q vs. q_u for Loading Tests in the Eagle Ford Formation
(O'Neill and Hassan, 1993)

While no borehole roughness, TxDOT cone or RQD data were available for these tests, the clay-shale at the test sites was always observed to be finely laminated and to have undrained compressive strengths that generally fell in the "intermediate geomaterial" range. Figure 2.7 displays the results of the skin friction measurements made in the load tests, which were

performed on instrumented drilled shafts loaded to compressive displacements of at least 5 per cent of the diameter of the test shaft. α_q is the ratio of average maximum unit side shearing resistance (f_{max}) to average q_u (from core tests) along the socket. These tests are important to the objectives of this study because the Eagle Ford formation is economically very important to the Texas Department of Transportation, since many structural foundations are socketed into it.

General Design Method of O'Neill and et al.

O'Neill et al. (1996) focused on predicting the resistance-settlement behavior of individual axially loaded drilled shafts in intermediate geomaterials (IGM's). Three categories of IGM's were established for design purposes:

- Category 1: Argillaceous IGM's, or IGM's derived predominantly from clay minerals and that are prone to smearing according to the definition for water sensitivity.
- Category 2: Carbonaceous IGM's, or IGM's derived predominantly from calcite and dolomite (limestones), and soft sandstones with calcareous cementation, or argillaceous IGM's that are not prone to smearing.
- Category 3: Granular IGM's, such as residual, completely decomposed rock and glacial till.

The design model included the variables described earlier and has a sound analytical basis. Its appropriate use, however, requires high-quality, state-of-the-practice sampling and testing and attention to construction details. The method is based on the finite element model of Hassan (1994) for skin friction and models developed by others for point resistance, which were verified at several test sites (in Texas, Florida, Massachusetts, and Hawaii) by conducting full-scale load tests.

Point Bearing. Point bearing (q_{max}) calculations require knowledge of the thickness and spacing of discontinuities in the IGM within about 2 socket diameters beneath the base. If such discontinuities exist, and they are primarily horizontal, q_{max} is computed according to the Canadian Foundation Manual (1985) method as follows,

$$q_{\max} = 3K_{sp}\Theta q_u \quad , \tag{2.7}$$

where, K_{sp} = a dimensionless bearing capacity factor based on geomaterial jointing characteristics, given by

$$K_{sp} = \frac{3 + \frac{s_v}{B}}{10\sqrt{1 + 300\frac{t_d}{s_v}}} \quad , \tag{2.8}$$

where, s_v = average vertical spacing between joints in the rock on which the base bears,

t_d = average thickness or "aperture" of those joints (open or filled with debris), and

Θ = dimensionless factor related to the ratio of the depth of penetration of the socket into the rock layer (D_s) (not the depth below the ground surface) to the socket diameter (B), given by

$$\Theta = 1 + 0.4(D_s / B) \leq 3.4 \quad . \tag{2.9}$$

If the rock discontinuities are primarily vertical, q_{max} is estimated as follows [using methods developed by Carter and Kulhawy (1988)].

- Vertical joints are open and spaced horizontally at a distance less than socket diameter, B.

$$q_{max} = q_u \text{ (of the rock mass, per AASHTO)} \quad . \tag{2.10}$$

- Vertical joints are closed and spaced horizontally at a distance less than the shaft diameter, B.

$$q_{max} \text{ (gross)} = (1 + N_q/N_c)\, c\, N_c + 0.3\, B\gamma N_\gamma + (1 + \tan\phi)\, \gamma L\, N_q \tag{2.11}$$

where, N_c, N_γ, N_q = Bell's bearing capacity factors,

c = cohesion of the rock mass,

ϕ = angle of internal friction of the rock mass,

L = total depth of the socket below the ground surface, and

γ= unit weight of the rock mass (buoyant if the rock is beneath the phreatic surface).

- Vertical joints are open or closed and spaced horizontally at a distance greater than the socket diameter, B. In this case, vertical splitting of the rock beneath the base of the shaft will occur, and failure will be governed by that condition. The appropriate equation is:

$$q_{max} = J\, c\, N_{cr} \quad , \tag{2.12}$$

where, N_{cr} = bearing capacity factor that is based on the horizontal spacing of the rock joints S relative to the base diameter B and the angle of internal friction of the rock mass,

J = correction factor for spacing of horizontal joints, if they exist, with a vertical spacing of H, and

c = cohesion of the rock mass.

Graphs for Bell's bearing capacity factors and for N_{cr} and J are given by O'Neill et al. (1996) and are reproduced later in connection with the method of Carter and Kulhawy. The above equations only cover the case of "blocky" rock. If the rock beneath to socket is preferentially sloping, methods given by Carter and Kulhawy can be used. Otherwise, if discontinuities are minimal or nonexistent (for example, core recovery of 100 percent and RQD = 100 percent), q_{max} is computed as follows,

$$q_{max} = 2.5\, q_u \quad , \tag{2.13}$$

where q_u is the median (rather than average) compression strength of cores within 2 B of the base of the socket.

Skin Friction. The first method proposed assumed a bonded interface. First, f_a, the apparent maximum average unit side shear at infinite displacement for *Category 1 or 2 IGM's, smooth or rough boreholes (with bonding)*, is estimated as follows:

$$f_a = c_r + \sigma_n \tan\phi_r \quad , \tag{2.14}$$

where c_r = drained cohesion of the soft rock or IGM

σ_n = normal (horizontal) stress at the borehole wall before loading the shaft, and

ϕ_r = drained angle of internal friction for the soft rock or IGM.

σ_n is estimated as the concrete pressure after placement of concrete in the borehole at the middle of the socket. The authors give a simple method for estimating σ_n in the referenced report. If the interface shear strength parameters are not known, use the following approximation:

$$f_a = \frac{q_u}{2} \quad . \tag{2.15}$$

Second, if the borehole-concrete wall is assumed to be non-bonded, estimate f_a, the apparent maximum average unit side shearing resistance at infinite displacement for *Categoiy 1 or 2 IGM's, smooth boreholes*, as follows:

$$f_a = \alpha_q \, q_u$$

where, α_q = constant of proportionality that is determined from Figure 2.8.

The factor σ_p in Figure 2.8 is the value of atmospheric pressure in the units employed by the designer. Figure 2.8 is based on the use of ϕ_{rc} (angle of rock-concrete sliding friction) = 30 degrees, which is a value that was measured at a test site in the Eagle Ford clay-shale that is believed to be typical of clay-shales and mudstones in the United States. If evidence indicates that ϕ_{rc} is not equal to 30 degrees, then α_q should be adjusted to:

$$\alpha_q = \alpha_{q\,Figure\,2.8} \frac{\tan\phi_{rc}}{\tan 30^\circ} \quad . \tag{2.16}$$

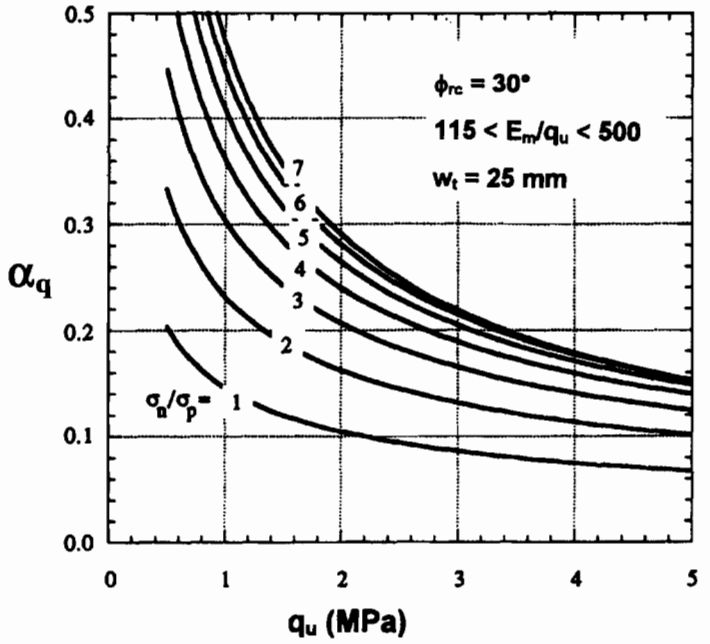

Figure 2.8. Factor α_q for Smooth Category 1 or 2 IGM's (From O'Neill et al., 1996)

O'Neill et al. (1996) recommend that the socket be considered *smooth* and non-bonded for design purposes unless wall bonding can be demonstrated through load testing or the socket walls are artificially roughened and the effect of the roughening can be verified during construction. A drilling tool fixture that will produce grooves nominally 50 mm deep or deeper into the socket wall is recommended when roughening is to be carried out. The reason for this conservative recommendation is that bonding and roughness measurements had not been made in sufficient detail at the time of the study (1996) to evaluate how roughly various drilling tools drilled the socket walls in various types of rock and whether bonding could be demonstrated under certain circumstances.

Once f_a has been evaluated, it is modified downward if the RQD of the rock is less than 100% to account for the presence of soft seams that reduce the elastic stiffness of the rock. O'Neill et al. recommend using a series of tables from Carter and Kulhawy (1988). However, those tables can be subsumed under one table, Table 2.2, which gives adjusted apparent values of f_{max} (f_{aa}).

Table 2.2. Adjustment of f_a for Presence of Soft Seams (From O'Neill et al., 1996).

RQD (%)	f_{aa}/f_a	
	Closed joints	Open Joints
100	1	0.84
70	0.88	0.55
50	0.59	0.55
20	0.45	0.45
< 20	unclear	unclear

Note is made that f_{aa} may be achieved only at very large displacements in some rocks, so it is recommended by the authors that the load-settlement behavior of the socket be computed and that the ultimate resistance be taken as the load on the socket that produces a settlement of 1 inch (25 mm). A procedure based on parametric finite element studies, which is suitable for spreadsheet analysis, is given by the authors.

Some soft rocks such as clay-shales and mudstones exhibit considerable creep settlement. A method proposed by Horvath and Chae (1989) is suggested to estimate the additional settlement produced by long-term creep. First, a normalized settlement, S_N is defined:

$$S_N = \frac{E_m B}{2Q_{socket}} w_{socket} \quad , \tag{2.17}$$

where, E_m is the secant mass modulus at one-half of the compressive strength of the soft rock,

Q_{socket} refers to the load (Q) applied to the socket, and

w_{socket} is the deflection (w) at the top of a rock socket with diameter B.

If creep settlement is defined as the settlement occurring in the period after 1 day of sustained load, ΔS_N, the normalized creep settlement, can be expressed as:

$$\Delta S_N = c_{nrp} \log_{10} [t_p\ (days)] + c_{nrs} \log_{10} [t\ (days) - t_p\ (days)] \quad , \tag{2.18}$$

where, c_{nrp} is a normalized primary creep coefficient in mm/log cycle of time in days,

c_{nrs} is a secondary creep coefficient in the same units,

t_P is the time required to achieve primary creep (approximately 100 days for the tests reported by Horvath and Chae in shales of southern Ontario), and

t is the time after application of the sustained load for which ΔS_N desired.

Test results indicated that both creep coefficients are dependent on the roughness of the borehole wall. For smooth interfaces, c_{nrp} is approximately 0. 1, and c_{nrs} is approximately 0.03. For rough interfaces, c_{nrp} is approximately 0.06, and c_{nrs} is approximately 0.01, which indicates that rough interfaces are less prone to creep.

Design Method of Rowe and Armitage

Rowe and Armitage (1987a) provided theoretical solutions from which a comprehensive design method was developed to estimate rock socket settlement and to assure safety against bearing failure. Neither the exact nature of concrete-rock interaction (bonding, friction, dilatancy) nor the side shear or point capacities are considered explicitly, but the analytical solutions that are referenced suggest frictional-dilational behavior was indirectly assumed at the interface. These solutions relate a displacement influence factor (I) at the top of the socket to the fraction of total load transferred to the base of the socket (P_b / P_T), and the length-to-diameter ratio (L_P /D_P) of the socket, under elastic or "slip" (side shear failure) conditions.

Rowe and Armitage (1987b) outline a specific design method for soft rock, based on the LRFD concept, using the solutions from Rowe and Armitage (1987a). The design process begins by defining an acceptable settlement w_p under the factored axial load P_T for the head of the rock socket. Ordinarily, P_T can be assumed to be the load at the head of the drilled shaft if the overburden is relatively shallow. Then, a value of socket diameter, D_p, is selected. Based on laboratory unconfined compression tests of the rock, representative values of q_u and E_p (modulus of the socket material) are selected. (A representative value of q_u might be the median value from a statistically significant number of core samples.) The, design values for unit skin friction and mass modulus of the rock are estimated from Eqs. (2.19) and (2.20):

$$f_{\max}(MPa) = 0.7\alpha\,[q_u(MPa)]^{0.5} \quad , \tag{2.19}$$

where, $\alpha = 0.45\ [q_u(\text{MPa})]^{0.5}$ for clean sockets, with roughness Rl, R2 or R3, as defined in Table 2.3, according to Pells et al. (1980), and

$\alpha = 0.60\ [q_u(\text{MPa})]^{0.5}$ for clean sockets with roughness R4.

Table 2.3 Roughness Classification for Sockets in Rock (after Pells et al., 1980)

Roughness Class	Description
R1	Straight, smooth sided socket, grooves or indentations less than 1.0 mm deep
R2	Grooves of depth 1 to 4 mm, width greater than 2 mm, at a spacing of 50 to 200 mm
R3	Grooves of depth 4 to 10 mm, width greater than 5 mm, at a spacing of 50 to 200 mm
R4	Grooves or undulations of depth greater than 10 mm, width greater than 10 mm, at a spacing of 50 mm to 200 mm

The factor 0.7 can be viewed as a resistance factor that takes account of the error involved in evaluating q_u. If the socket cannot be presumed to be clean, f_{max} should be taken to be zero.

$$E_r\,(MPa) = 0.7\,\{215\,[q_u\,(MPa)]^{0.5}\}\quad , \tag{2.20}$$

Again, the factor 0.7 can be viewed as a factor of uncertainty in evaluating E_r. Eqs. (2.19) and (2.20) apply to massive rock (no joints or seams). If the rock modulus below the base of the socket appears to be different form that above the base (along the sides), the same expression can be used to compute the rock modulus at the base, E_b.

If the rock contains seams of softer material, both the values of f_{max} and E_b must be reduced. To do this a parameter termed S is introduced:

$$S = \frac{\sum(seam\ thicknesses)}{Length\ \ cored}\quad . \tag{2.21}$$

[For practical purposes, S can be assumed conservatively to be (1 – recovery ratio), where the recovery ratio is the percent recovery in a core barrel expressed as a ratio. Obviously,

engineering judgement is necessary in the selection of a value for this parameter.] If it is assumed that the shear strength of the seam material is negligible compared to the shear strength of the rock, then the values of f_{max}, E_r and E_b that should be used for design, according to Rowe and Armitage, f_{max}*, E_r*, and E^*_b are given by:

$$f_{max}^{*} = (1-S) f_{max} \quad , \tag{2.22}$$

$$E_r^* = (1-S) E_r \quad , \tag{2.23}$$

$$E_b^* = (1-S) E_b \tag{2.24}$$

Ratios E_p/E^*_r and E^*_b/E^*_r are next estimated, where E_p is the composite Young's modulus of the structural material in the socket. Then a displacement influence factor (I_d) is computed. I_d is defined as follows:

$$I_d = \frac{w_p D_p E_r^*}{P_T} \quad . \tag{2.25}$$

Next, the ratio of socket length (L_p) to socket diameter (D_p) corresponding to the development of the full average value of design skin friction and zero tip resistance is computed. This value is termed $(L/D)_{d\,max}$:

$$\left(\frac{L}{D}\right)_{d\,max} = \frac{P_T}{\pi D_p^2 f_{max}^*} \quad . \tag{2.26}$$

Then, a design chart is used to estimate the ratio of base or tip resistance to the factored applied load P_T. A family of design charts to be used for this purpose for different values of E_b/E_r and E_p/E_r, developed from the analytical solutions (Rowe and Armitage, 1987a) are given by Rowe and Armitage (1987b). One such chart is shown in Figure 2.9. It is used as indicated to compute P_b, the load transferred to the base or point, corresponding to the selected value of settlement. In

practice, unless the rock is completely without joints or seams, as indicated by 100 per cent core recovery, E_r and E_b are, respectively, taken as E^*_r and E^*_b.

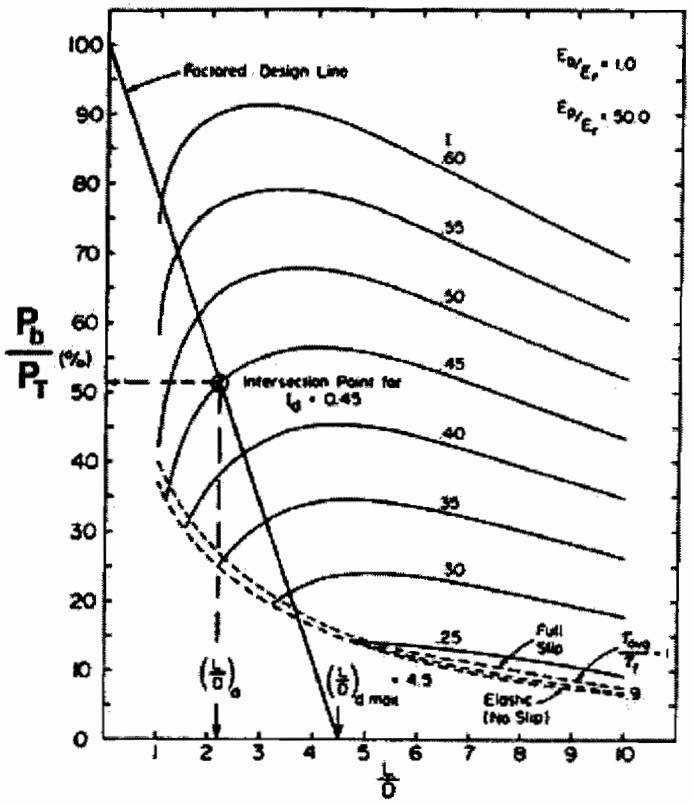

Figure 2.9. Typical Design Chart for a Complete Socket, E_b / E_r = 1.0, and E_P / E_r = 50 (from Rowe and Armitage, 1987b)

In Figure 2.9, a line is drawn from the horizontal axis at (L/D) = (L_p/D_p) = $(L/D)_{d\ max}$ [Eq. (2.26)] to the vertical axis at P_b/P_T = 100%. The point at which this line crosses the contour line for the estimated value of I_d [Eq. (2.25)] defines both the needed value of L_p/D_p for the socket and the ratio of base or point resistance (P_b) to applied load (P_T) for that value of L_p/D_p. The maximum stress in the socket, $\sigma_c = P_T/(\pi D_p^2/4)$, should be less than the factored resistance value permitted by structural codes. The maximum point resistance, $q_b = P_b/(\pi D_p^2/4)$, should be $\leq q_u$ (median) for one base diameter beneath the base, provided there are no rock joints or the rock

joints are tightly closed (no gouge or compressible material in the joints) and provided q_u (median) ≤ 30 MPa (4350 psi). [Note that, although not stated by Rowe and Armitage, when gouge-filled or open joints are present within this bearing zone, the maximum net point bearing pressure should be ≤ 0.4 q_{max} given by Eq. (2.9) or other appropriate method that considers the effects of joints in the bearing zone.]

One more criterion that is suggested is that

$$q_{max} \geq \frac{P_T}{\pi D_p^2 / 4} - 4 f^*_{max} \frac{L_p}{D_p} \quad . \tag{2.27}$$

If the expression on the right-hand side of the inequality is negative, $q_{max} = 0$. This criterion is given to assure a measure of safety against ultimate bearing failure of the socket.

There is a possibility that an intersection will not be found in Figure 2.9. Rowe and Armitage (1987b) discuss procedures to follow in that case.

Design Method of Kulhawy and Phoon

Kulhawy and Phoon (1993) developed expressions for the unit skin friction (shaft resistance) for drilled shafts in soil and for rock sockets from the analysis of 127 load tests in soil and 114 load tests in rock. No procedure for estimating q_{max} is provided. Since their data were acquired from both soil and rock, they elected to define their adhesion factor, α, in relation to undrained shear strength, c_u, rather than unconfined compressive strength, q_u. The adhesion factor, α_c, is as follows:

$$\alpha_c = f_{max} / c_u = 2\alpha_q \quad . \tag{2.28}$$

Their results are plotted as adhesion factor, α_c, versus normalized shear strength, defined as either c_u / p_a or $q_u / 2P_a$, where, p_a is atmospheric pressure, as shown in Figure 2.10.

On the basis of the load test data, Kulhawy and Phoon also suggest that peak unit skin friction, f_{max}, be computed in general for rock sockets from Eq (2.29):

$$\frac{f_{max}}{p_a} = \psi\left(\frac{q_u}{2p_a}\right)^{0.5} \quad , \tag{2.29}$$

where, p_a = atmospheric pressure in the units selected for q_u and f_{max},

ψ = quantitative roughness factor for design,

= 3 when the borehole is very rough (e.g., roughened artificially),

= 2 for normal drilling conditions, and

= 1 for conditions that produce "gun-barrel-smooth" sockets.

Eq. (2.29) is purportedly applicable over a range of q_u from 4 to 500 atmospheres.

Note that with this method rough boreholes produce about three times the skin friction produced in smooth boreholes, which is consistent with Figure 2.4, developed by mathematical modeling by Hassan and O'Neill.

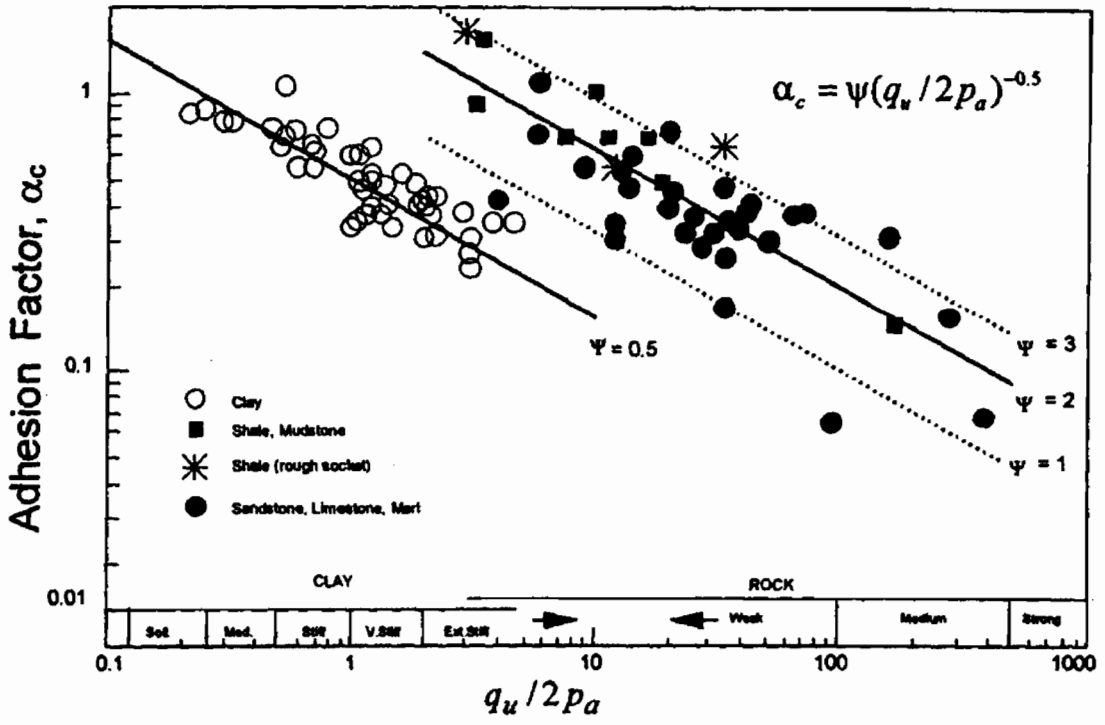

Figure 2.10. Adhesion Factor versus Normalized Shear Strength (From Kulhawy and Phoon, 1993)

Design Method of Carter and Kulhawy

Carter and Kulhawy (1988) provide comprehensive solutions for drilled shafts socketed into rock with joints. Separate solutions are given for response in the elastic range and in the range beyond the elastic range.

If the rock has relatively uniform mass strength below the base, three point (base) failure conditions are envisioned, as governed by the jointing pattern in the rock:

- Vertical joints are open and spaced horizontally at a distance less than shaft diameter, D. Here:

$$q_{max} = q_u \text{ (rock mass)} \tag{2.30}$$

- Vertical joints are closed and spaced horizontally at a distance less than the shaft diameter, D. Here, Bell's bearing capacity theory for shear wedge failure is used, which assumes that no friction is developed along the joints. For practical approximations, the gross bearing capacity of a socket with diameter D can be computed as:

$$q_{max} \text{ (gross)} = (1 + N_q/N_c)\, c\, N_c + 0.3\, D\gamma N_\gamma + (1 + \tan\phi)\, \gamma L\, N_q \quad , \tag{2.31}$$

where N_c, N_γ, N_q = Bell's bearing capacity factors, given in Figure 2.11,

c = cohesion of the rock mass,

ϕ = angle of internal friction of the rock mass, and

γ = unit weight of the rock mass (buoyant if the rock is beneath the phreatic surface).

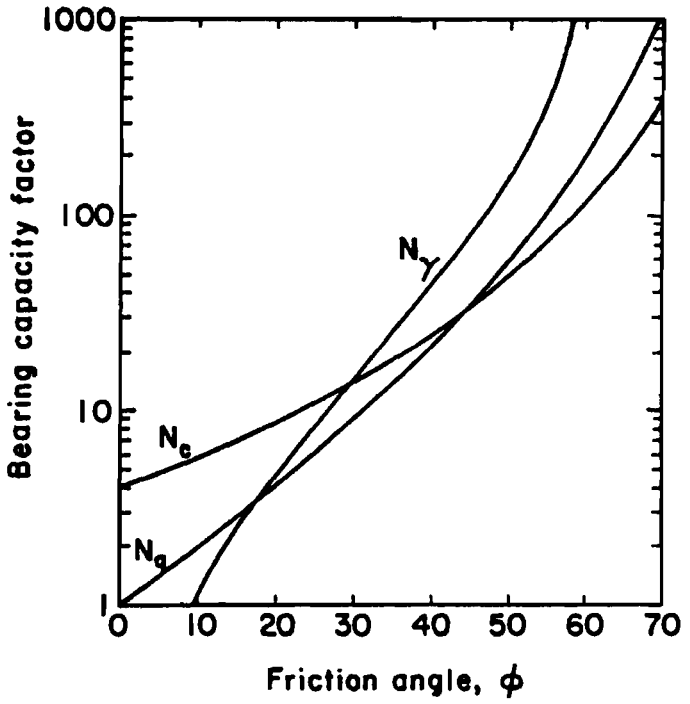

Figure 2.11. Bearing Capacity Factors for Bell's Theory (©1988. Reproduced by O'Neill et al. (1996) with permission of Electric Power Research Institute [EPRI], Palo Alto, CA)

- Vertical joints are open or closed and spaced horizontally at a distance greater than the shaft diameter, D. In this case, vertical splitting of the rock beneath the base of the shaft will occur, and failure will be governed by that condition. The appropriate equation is:

$$q_{max} = J\,c\,N_c \quad , \tag{2.32}$$

where, N_c = a bearing capacity factor that is based on the horizontal spacing of the rock joints S relative to the base diameter of the socket D and the angle of internal friction of the rock mass, given in Figure 2.12,

J = correction factor for spacing of horizontal joints, if they exist, with a vertical spacing of H, given in Figure 2.13, and

c = cohesion of the rock mass.

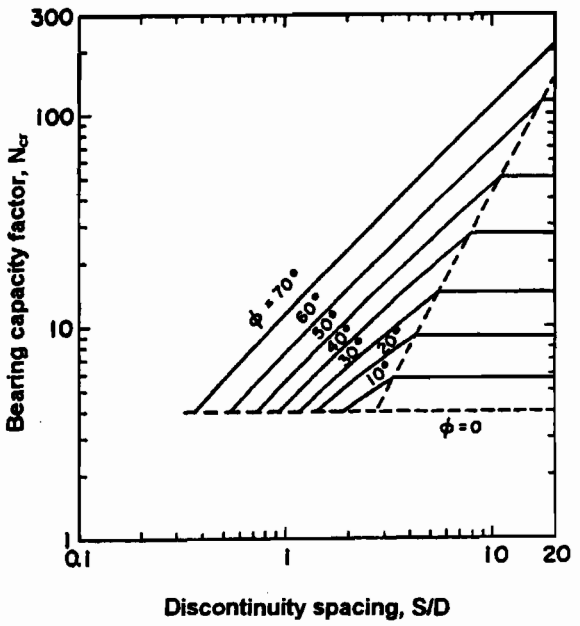

Figure 2.12. N_{cr} versus S/D (©1988. Reproduced by O'Neill et al. (1996) with permission of Electric Power Research Institute [EPRI], Palo Alto, CA)

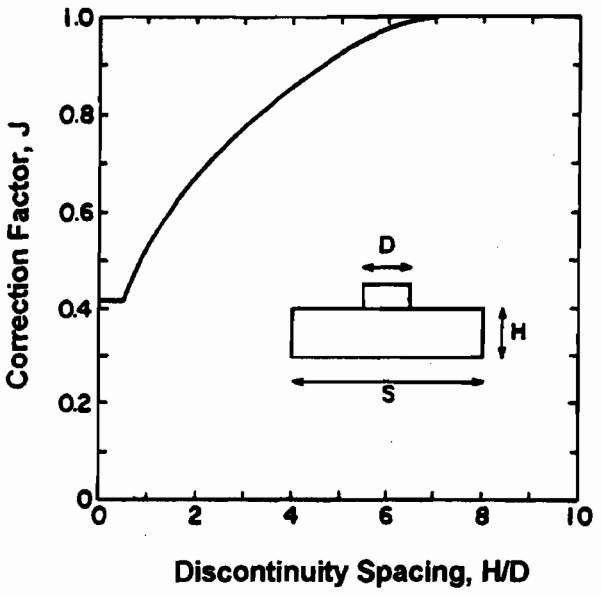

Figure 2.13. J versus Rock Discontinuity Spacing (©1988. Reproduced by O'Neill et al. (1996) with permission of Electric Power Research Institute [EPRI], Palo Alto, CA)

Note is made that q_{max} as used here is a gross bearing capacity for which the weight of the shaft must be considered part of the load. In all of the equations in this method, c and ϕ are rock mass properties, not properties measured from tests on rock cores (intact rock). Carter and Kulhawy suggest that the value of ϕ for the rock mass be taken to be about one-half of the value measured from the intact rock, if ϕ for the intact rock is measured through direct shear or triaxial shear testing on rock cores in the laboratory. Conservatively, ϕ for the rock mass can be taken as zero in the calculation of base resistance.

In order to compute q_u (rock mass), for example, for use in Eq. (2.30), the following equation is recommended to estimate the equivalent q_u of the rock mass.

$$q_u \text{ (mass)} = \alpha_E \, q_u \text{(intact)} \quad . \tag{2.33}$$

Factor α_E can be obtained accurately if the RQD, percent core loss, Young's modulus of the intact rock, and normal stiffness of the material in the joints are known. Appropriate graphs are given by Carter and Kulhawy to evaluate α_E for the case when such detailed information is available for the rock. However, a simple approximation for most rock is to take $\alpha_E = 0.1$ for RQD equal to or less than 70 percent, $\alpha_E = 0.6$ for RQD = 100 percent, and to assume a linear variation of α_E between RQD of 70 and 100 percent. Note that this is a more severe reduction for joints and seams than is suggested by Rowe and Armitage based on percent recovery.

Once ϕ (mass) and q_u (mass) have been evaluated, c (mass) can then be computed from:

$$c(mass) = \frac{q_u(mass)}{2\tan\left[45^\circ + \frac{\phi(mass)}{2}\right]} \quad . \tag{2.34}$$

Carter and Kulhawy also give closed-form solutions for load-movement relationships for five cases of rock-socketed drilled shafts:

- Complete socket (combined base and side resistance) loaded in compression.
- Socket with side resistance only (implying a void beneath the base) loaded in compression.
- Socket with side resistance only loaded in uplift at the head of the socket.

- Socket with side resistance only loaded in uplift at the base of the socket.
- Socket with side resistance only loaded in uplift at the base of the socket by jacking upward on the base with a compression reaction against the rock at the bottom of the void (e. g., loading in a test through a flat-jack-type load cell.)

The load-settlement curve at the head of the socket is presumed to have the shape shown in Figure 2.14. In the initial part of the curve, both side (interface) and base response are completely elastic, and there has been no debonding of the concrete in the shaft from the rock walls. At point A, slip begins to occur between the concrete and the rock at the sides of the socket at some point along the shaft, and slip then progresses along the shaft until point B is reached due to debonding of the shaft concrete from the rock. Beyond point B, base response remains elastic, while side shear response is fictional-dilative, rather than cohesive, as is the case for the elastic region of loading.

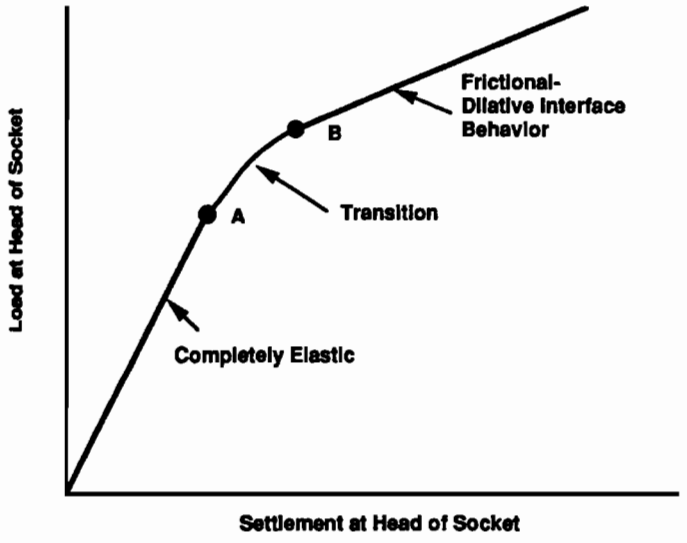

Figure 2.14. Conceptual Load-Settlement Curve for Rock Socket.

Within the elastic range, the settlement at the top of the socket w_t can be related to the load at the top of the socket Q_t by Eq. (2.35), adapted from Randolph and Wroth (1978), which is

shown here for the case where the elastic stiffness of the rock mass below the base is equal to the elastic stiffness along the sides of the shaft.

$$w_t = \left[\frac{2Q_t}{DG_m}\right]\frac{1+\left(\frac{4}{1-\nu}\right)\left(\frac{1}{\pi\lambda}\right)\left(\frac{2L}{D}\right)\left[\frac{\tanh(\mu L)}{\mu L}\right]}{\left(\frac{4}{1-\nu}\right)+\left(\frac{2\pi}{\zeta}\right)\left(\frac{2L}{D}\right)\left[\frac{\tanh(\mu L)}{\mu L}\right]} \quad . \tag{2.35}$$

The value of the load carried by the base under elastic conditions is:

$$Q_b = \frac{Q_t\left(\frac{4}{1-\nu}\right)\left[\frac{1}{\cosh(\mu L)}\right]}{\left(\frac{4}{1-\nu}\right)+\left(\frac{2\pi}{\zeta}\right)\left(\frac{2L}{D}\right)\left[\frac{\tanh(\pi L)}{\pi L}\right]} \quad , \tag{2.36}$$

where G_m = shear modulus of the rock mass $= \frac{E_m}{2(1+\nu)}$,

ν = Poisson's ratio of the rock mass,

$\lambda = E_c / G_m$, where E_c is the composite Young's modulus of the shaft concrete/steel,

$\mu = \frac{2}{D}\sqrt{\frac{2}{\lambda\zeta}}$, and

$\zeta = \ln\left[5(1-\nu)\frac{L}{D}\right]$

The settlement of the base w_b can then be computed approximately from:

$$w_b = \frac{Q_b}{A_b}\frac{\pi}{2}\left(\frac{1-\nu^2}{E_m}\right)\frac{D}{2} \quad , \tag{2.37}$$

where, A_b = bearing area of the base,

$\nu = 0.25 \sim 0.30$ (for soft rock), and

$E_m = \alpha_E E_{rock}$ (intact) .

Point B corresponds approximately to complete debonding of the concrete from the rock, which occurs at:

$$Q_s = Q_t - Q_b = c \text{ (interface) } \pi D L$$

Note that c(interface), the adhesive bond strength between the concrete and rock, can be as high as the value of c(mass) if the interface is free of any remolded rock or "smear." The value of c for the rock is usually less than q_u (mass) / 2.

In order to predict the load-settlement relationship beyond point B, an analytical solution that involves frictional resistance at the concrete-rock interface is employed. It is also assumed that both dilation and drainage occur at the interface at the side of the socket. The dilatancy phenomenon was illustrated conceptually in Figure 2.5, which shows the concrete and rock in the vicinity of the interface. Since the interface is frictional, the shearing resistance on the interface increases as w (socket displacement) increases, which partially explains the positive slope of the load-settlement curve beyond point B in Figure 2.14. As the slip mechanism develops, it is assumed that c (interface) drops to zero. The interface asperities in the rock and in the concrete are both assumed to be nondeformable. The behavior of the rock in the field outside the interface is entirely elastic.

Design Method of Horvath, et al.

Horvath et al. (1983) suggested a correlation between shaft resistance, f_{max}, and compressive strength of the weaker socket material (concrete or rock), q_u or f'_c, for large-diameter conventional sockets in soft rock. This correlation is shown in Figure 2.15. It represents curves of best fit for 202 data points for conventional socketed shafts. The suggested correlations in Figure 2.15 (denoted "Conventional Piers") can be approximated by:

$$q_s \ (= f_{max}) \ (MPa) = b\sqrt{q_u \ (MPa)} \quad , \tag{2.38}$$

where, b = 0.2 ~ 0.3 for large-diameter sockets, presumably with B > 410 mm.

In Figure 2.15, q_s is equivalent to f_{max}.

Furthermore,

$$q_s(MPa) \leq b\sqrt{f'_c\,(MPa)} \quad , \tag{2.39}$$

which can control if the rock has a higher compressive strength than the concrete. Therefore, the term σ_{cw} in Fig. 2.15 is the lesser of q_u (rock) and f'_c (concrete).

The authors also proposed a method for estimating the effects of socket wall roughness on the value of side resistance using a roughness factor, RF. The roughness factor, RF, is given by the expression

$$RF = \frac{\overline{\Delta r}}{r_s}\frac{L_t}{L_s} \quad , \tag{2.40}$$

where, $\overline{\Delta r}$ = the average height of the interface asperities,

r_s = nominal socket radius,

L_s = nominal socket length, and

L_t = total travel distance along the socket wall profile.

RF is easily estimated for sockets that have a designed grooving pattern.

They also suggested an empirical relationship between roughness factor, RF, and normalized shaft resistance, NSR, where,

$$NSR = \frac{f_{max}}{q_u} \quad , \quad (q_u < f'_c) \quad . \tag{2.41}$$

This relationship is shown in Figure 2.16, where q_s is equivalent to f_{max}, and σ_{cw} is the smaller of q_u and f'_c.

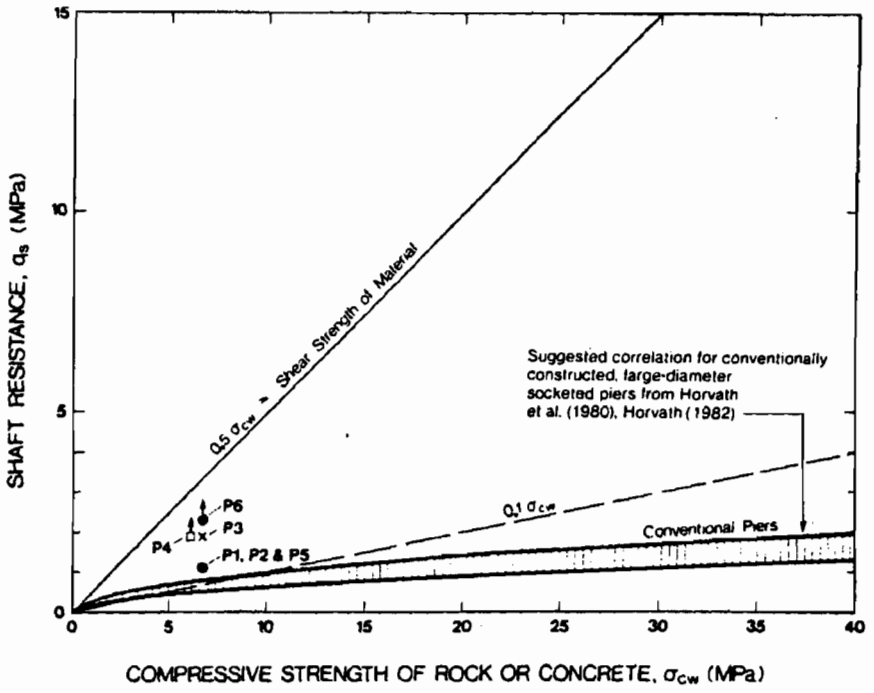

Figure 2.15. Empirical Correlation of Shaft Resistance with Material Strength for Large-Diameter Sockets (Horvath et al., 1983)

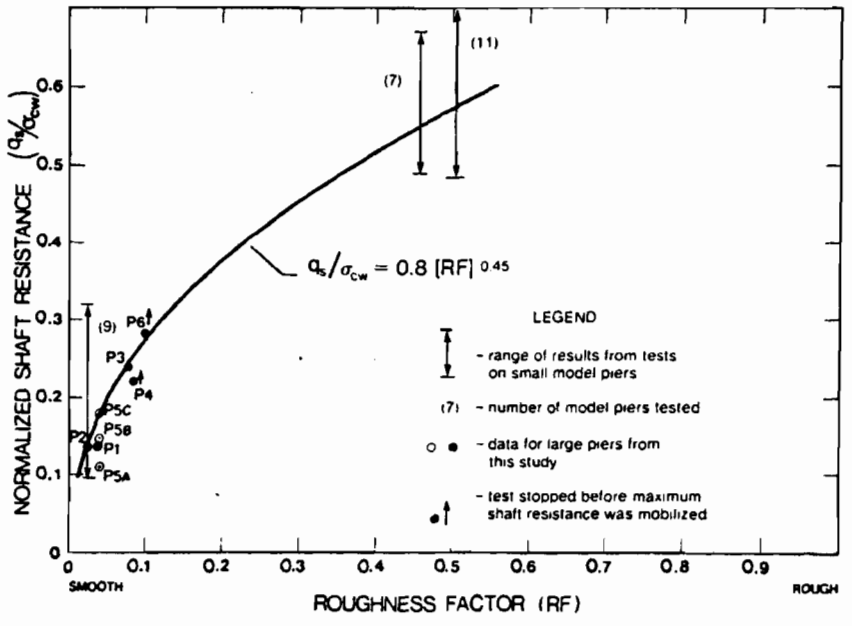

Figure 2.16. Normalized Shaft Resistance versus Roughness Factor (Horvath et al., 1983)

Design Method of Williams

Williams (1980) developed a design method based on observations of axial loading tests of drilled shafts and shaft segments in Melbourne mudstone in Victoria, Australia, and upon elastic pile-soil interaction analyses. The method is applied through the concept of normalized elastic and inelastic side shear and base resistances to predict the load-settlement response of soft rock sockets. The elastic (finite element) solution for an elastic pile in a semi-infinite halfspace was applied into predict the total load, Q_e, at a given target settlement, corresponding to elastic conditions for the socket.

$$Q_e = \frac{w_t E_m D}{I} \quad , \tag{2.42}$$

where w_t = target settlement at the socket head,

E_m = average mass modulus of elasticity of the soft rock along the socket,

D = socket diameter, and

I = an elastic influence factor, based on the geometry of the shaft, determined from analytical procedures for elastic behavior and shown in Figure 2.17.

In Figure 2.17, E_c is the composite Young's modulus of elasticity of the drilled shaft concrete and reinforcing steel. The percentage of Q_e that is transferred to the base, defined as Q_{be}, is then determined by reference to Figure 2.18, also based on analytical procedures for elastic behavior. Figure 2.18 serves a purpose similar to that of Figure 2.9 for Rowe and Armitage.

The portion of Q_e carried in side shear, Q_{se}, is then equal to $Q_e - Q_{be}$. The "elastic" unit side shear, f_e, and the "elastic" unit end bearing, q_e, are then determined as:

$$f_e = \frac{Q_{se}}{\pi L D} \quad , \qquad \text{and} \tag{2.43}$$

$$q_e = \frac{4 Q_{se}}{\pi D^2} \quad . \tag{2.44}$$

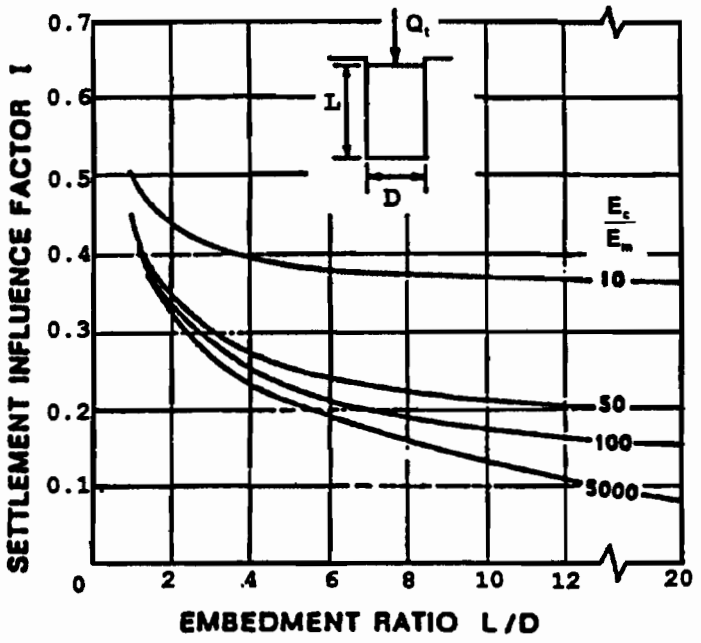

Figure 2.17. Influence Factor I (Reproduced by O'Neill et al. (1996) with permission of A. A. Balkema, Rotterdam, Netherlands)

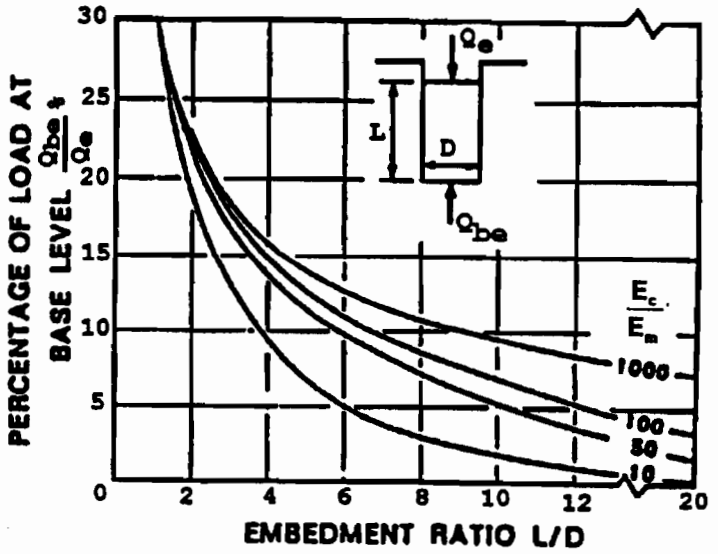

Figure 2.18. Q_{be} / Q_e (Reproduced by O'Neill et al. (1996) with permission of A. A. Balkema, Rotterdam, Netherlands)

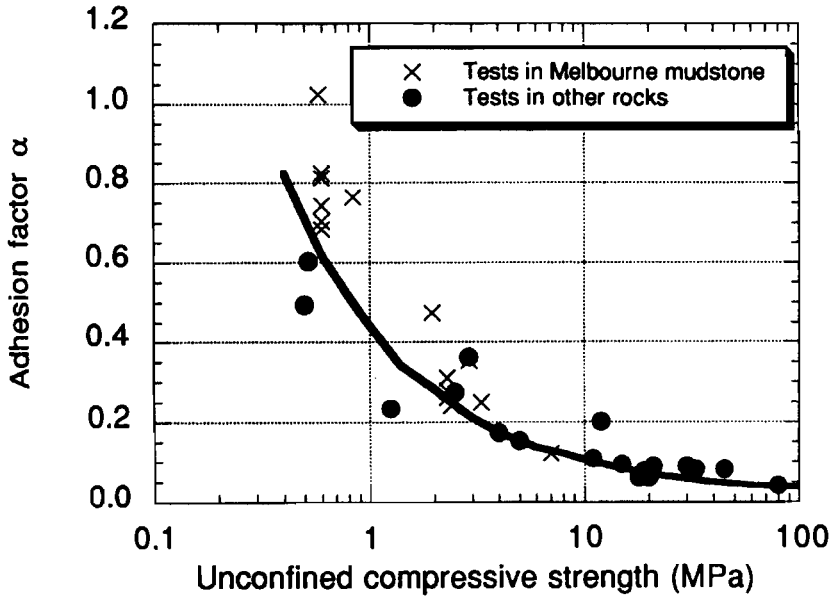

Figure 2.19. α / q_u (Reproduced by O'Neill et al. (1996) with permission of A. A. Balkema, Rotterdam, Netherlands)

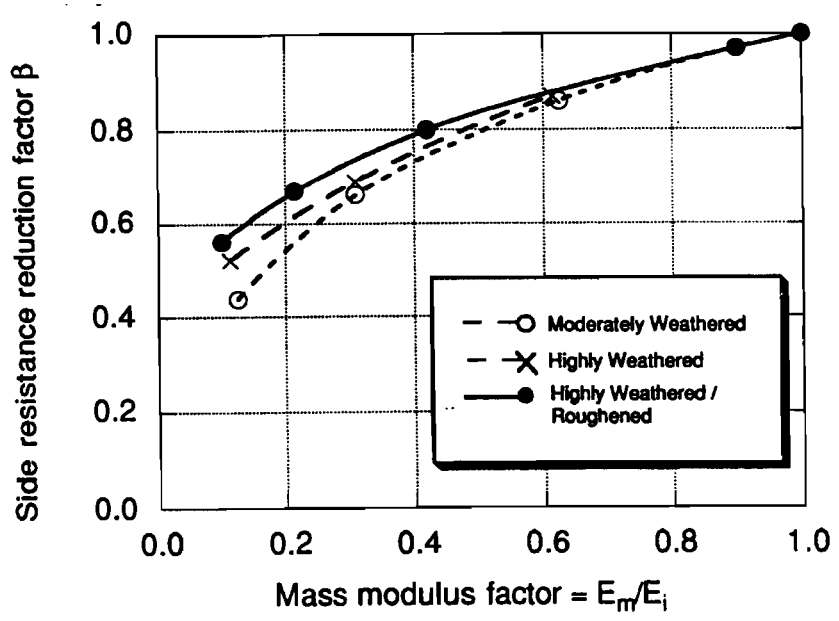

Figure 2.20. β versus Mass Factor (Reproduced by O'Neill et al. (1996) with permission of A. A. Balkema, Rotterdam, Netherlands)

The value of f_{max} is then determined from Figure 2.19 for soft rock without open discontinuities or borehole wall disturbance (smear), in which:

$$f_{max} = \alpha \, q_u \quad , \tag{2.45}$$

where q_u = (median) unconfined compression strength (q_u) of rock cores in the vicinity of the socket, excluding the effects of soft seams. If there are soft seams within the rock mass, f_{max} is determined from Figures 2.19 and 2.20 using

$$f_{max} = \alpha \, \beta \, q_u \quad . \tag{2.46}$$

In Figure 2.20, f_{max} is reduced according to the ratio of mass modulus of the rock to modulus of the rock cores, based on the concept that f_{max} accrues from normal interface stress due to dilation, and that dilation depends directly on the radial Young's modulus of the rock. Therefore, in Figure 2.20 E_m = Young's modulus of elasticity of the rock mass, including the effects of soft seams or joints, and E_i = Young's modulus of elasticity measured from the intact rock cores. [As a commentary, E_m/E_i is an elusive factor in practice. An alternate method for evaluating β might be to use $\beta = f_{aa}/f_a$ from Table 2.2, which is based partially on an analysis of Williams' data.]

Williams' method recognizes that actual load-settlement behavior will not be elastic. The deviation from elastic behavior is quantified by using the normalized graph shown in Figure 2.21, which was derived with empirical evidence from full-scale loading tests on rough-walled sockets in Melbourne mudstone. Factors (unit skin friction values) termed f_e and f_p are shown in that figure. Factor f_p relates to the loss of unit shaft resistance that occurs due to plastic yielding for the value of settlement, w_t. Therefore, the shaft resistance Q_s corresponding to the target settlement w_t is given by:

$$Q_S = (f_e - f_p) \, \pi \, L \, D \quad . \tag{2.47}$$

The ultimate (limit) unit base resistance, q_l, is defined as the net bearing stress corresponding to a settlement of 0.01 D, in which:

$$q_l = N_s q_u \quad . \tag{2.48}$$

where, N_s = function of L/D given in Figure 2.22.

Base resistance is also decreased through plastic losses, so q_t must be reduced by an amount q_p according to Figure 2.23. Finally, the base resistance for the selected value of w_t is

$$Q_b = (q_e - q_p)\frac{\pi D^2}{4} \quad . \tag{2.49}$$

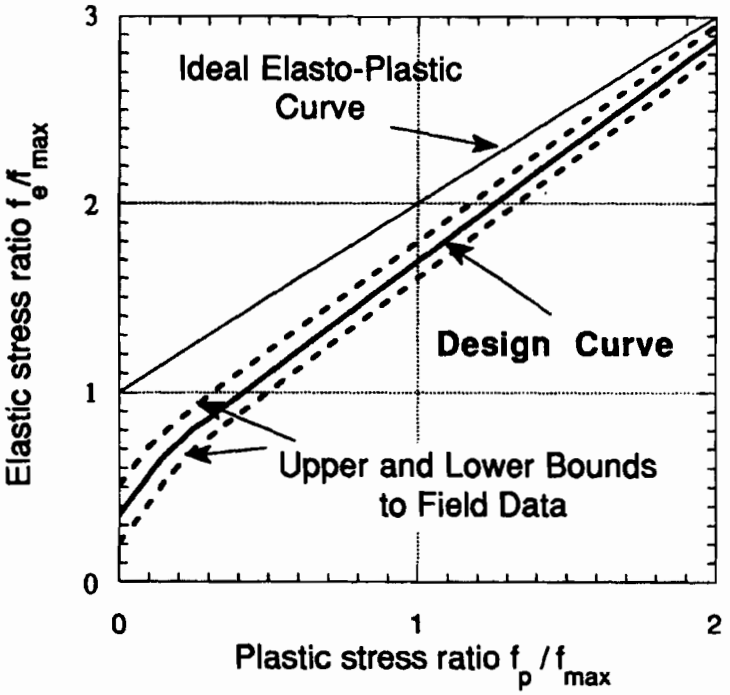

Figure 2.21. Design Curve for Side Resistance (Reproduced by O'Neill et al. (1996) with permission of A. A. Balkema, Rotterdam, Netherlands)

For a given load, if the socket behaves completely elastically, Q_{be} can be obtained from Figure 2.18, assuming that the load on the socket is Q_e. Q_{se}, the side resistance under purely elastic conditions, is then given by

$$Q_{se} = Q_e - Q_{be} \quad . \tag{2.50}$$

Therefore,

$$f_e = Q_{se} / \pi D L \quad . \tag{2.51}$$

Since f_{max} can be estimated from Eq. (2.46), f_e/f_{max} (elastic stress ratio) can be computed for use in Figure 2.21. Once this value is known, f_p/f_{max} can be determined form Figure 2.21 using the design curve (black line) as the pivot. This defines f_e and f_p for a given load, and Eq. (2.47) is then used to compute Q_s for the settlement, w_t, associated with the applied load Q_e, which is obtained from Figure 2.17. A similar process is followed to compute Q_b using Figure 2.23. That value of Q_b also corresponds to the same settlement, w_t.

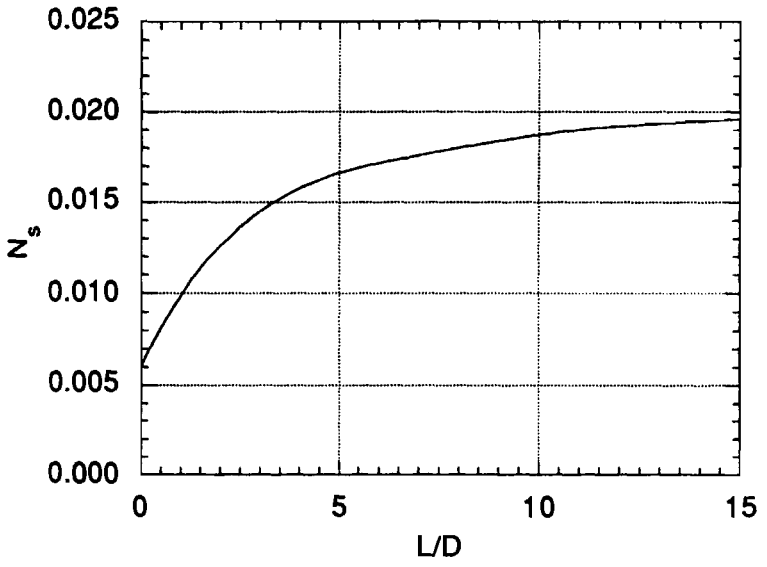

Figure 2.22. Base Bearing Capacity Factor N_s (Reproduced by O'Neill et al. (1996) with permission of A. A. Balkema, Rotterdam, Netherlands)

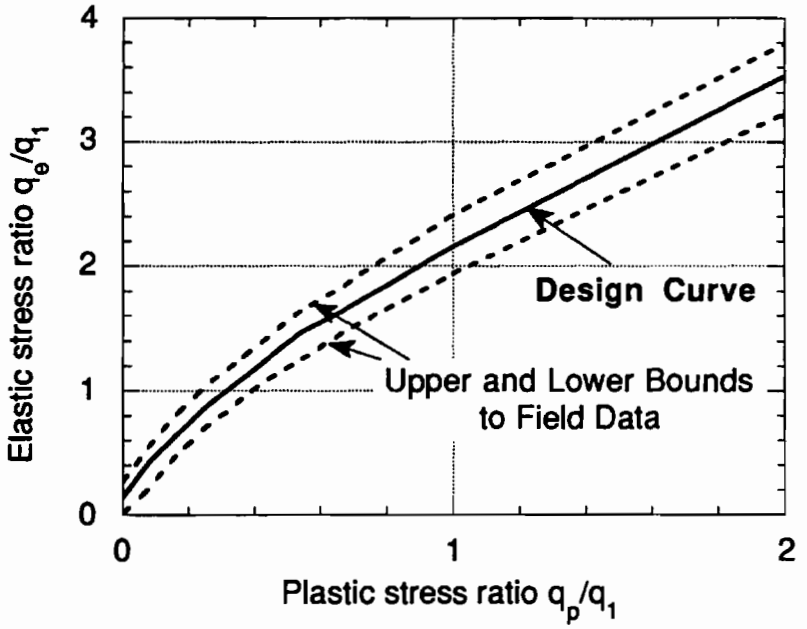

Figure 2.23. Design Curve for Base Resistance (Reproduced by O'Neill and et al. (1996) with permission of A. A. Balkema, Rotterdam, Netherlands).

Finally,

$$Q_t = Q_s + Q_b \quad , \tag{2.52}$$

Note that Q_t, which corresponds to settlement w_t, will be equal to or less than Q_e. In essence, Williams computes the settlement and distribution of transferred load to side and base resistance using elastic solutions and then relaxes the side and base resistances while keeping a constant socket settlement, w_t, to accommodate nonlinear behavior of the rock.

Williams et al. suggest that if the applied load Q_t is a factored load, partial factors of safety of about 1.4 and 2.0 are appropriate for side and base resistance when the geomaterial properties are well defined, unless the shaft supports only side resistance, in which case the partial factor of safety for side resistance should be at least 2.0.

Design Method of McVay et al.

McVay *et al.* (1992) proposed a design method for side-resistance-only drilled shaft sockets that applies to IGM's and harder rock, mainly limestone. This method addresses only side resistance, and it does not include an estimation of settlement or base resistance. The premise of this method is that the side resistance in limestone will be cohesive and not frictional. That is, cement paste from the socket concrete will penetrate the rock and form a true cohesive bond, leading to a value of f_{max} equal to the cohesion c of the limestone. Because of the cohesive nature of the bond, interface dilation will not develop. The method also presumes that base resistance will not be included in the design because of the possibility that cavities will exist below the base and that probing for such cavities and deepening shafts in the event that cavities are found is not a cost-effective construction process.

Since for design purposes f_{max} = c in this method, and since limestone is a c-ϕ material, owing to its propensity to drain, some simple method is needed to evaluate c in a c-ϕ material. The ultimate skin friction, f_{max} was derived from a consideration of the Mohr's circles at failure for unconfined compression and splitting tension tests in which

$$f_{max} = \frac{1}{2}\sqrt{q_u}\sqrt{q_t} \quad , \tag{2.53}$$

where q_t is the splitting tension strength of the geomaterial. The derivation of this expression presumes that the normal effective stress on the failure plane is zero, that is, that there is no frictional component to f_{max}. This is contrary to most of the other methods considered in this chapter, which generally considers the interface to be frictional-dilative with zero cohesion. That condition is conceivably more appropriate for clay-based rocks such as clay-shales.

Alternatively, if ϕ (rock) can be estimated, f_{max} can be determined only from q_u, as follows:

$$f_{max} = q_u \frac{1-\sin\phi}{2\cos\phi} \quad . \tag{2.54}$$

Simplified FHWA Design Method

O'Neill and Reese (1999) discuss simplified design methods for point bearing in rock, considering the pattern of discontinuities in the rock, principally by reference to other studies. If the rock is massive (RQD = 100 %) and the depth of the socket, D_s, in the rock ≥ 1.5 B, the point bearing capacity, q_{max}, at and below the base is

$$q_{max} = 2.5\, q_u \ . \tag{2.55}$$

If the rock has an RQD value between 70 and 100 %, all joints are closed, the closed joints are approximately horizontal, and $q_u > 0.5$ MPa, the recent method of Zhang and Einstein (1998) is used.

$$q_{max}(MPa) = 4.83\,[q_u\,(MPa)]^{0.51} \ . \tag{2.56}$$

If the rock is jointed, the joints have random orientation, and the condition of the joints can be evaluated from cuts in the geographical area or from test excavations, q_{max} can be evaluated by one of the methods summarized by Carter and Kulhawy (1988):

$$q_{max} = \left[S^{0.5} + \left(mS^{0.5} + S\right)^{0.5}\right] q_u \ , \tag{2.57}$$

where q_u is a (median) value measured on intact cores from within 2D below the base of drilled shaft socket, q_{max} has the units of q_u, and S and m are properties of the rock mass that can be estimated from Tables 2.4 and 2.5.

The side of the socket borehole in soft rock or cohesive IGM should be classified as *smooth* or *rough.* It is recommended that a *rough* condition be applied only where the borehole is specified to be artificially roughened by grooving. Otherwise, the socket should be considered *smooth.*

For a *smooth* rock socket, the ultimate skin friction, f_{max}, is taken as:

$$f_{max} = 0.65 p_a \left[\frac{q_u}{p_a}\right]^{0.5} \leq 0.65 p_a \left[\frac{f'_c}{p_a}\right]^{0.5}, \quad (2.58)$$

where f'_c = 28-day compressive cylinder strength of the concrete in the socket,

p_a = atmospheric pressure in the units used for q_u, and

q_u = median value for q_u along the socket.

For a *grooved* (mechanically roughened) rock socket, the ultimate skin friction, f_{max} (as recommended by Horvath et al., 1983) is

$$f_{max} = 0.8 \left[\frac{\Delta r}{r}\left(\frac{L'}{L}\right)\right]^{0.45} q_u, \quad (2.59)$$

where q_u should not exceed 0.75 f'_c. The remaining terms refer to the geometry of the socket and are defined in Figure 2.24.

Table 2. 4. Description of Rock Types.

Rock Type	Description
A	Carbonate rocks with well-developed crystal cleavage (e.g., dolostone, limestone, marble)
B	Lithified argillaceous rocks (mudstone, siltstone, shale, slate)
C	Arenaceous rocks (sandstone, quartzite)
D	Fine-grained igneous rocks (andesite, dolerite, diabase, rhyolite)
E	Coarse-grained igneous and metamorphic rocks (amphibole, gabbro, gneiss, granite, diorite, quartz-diorite)

Table 2. 5. Values of S and m (Dimensionless) Based on Classification in Table 2. 4.

Quality of Rock Mass	Joint Description and Spacing	S	Value of m as Function of Rock Type (A - E) from				
			A	B	C	D	E
Excellent	Intact (closed); spacing > 3 m	1	7	10	15	17	25
Very Good	Interlocking; Spacing of 1 to 3 m	0.1	3.5	5	7.5	8.5	12.5
Good	Slightly weathered; Spacing of 1 to 3 m	4×10^{-2}	0.7	1	1.5	1.7	2.5
Fair	Moderately weathered; Spacing of 0.3 to 1 m	10^{-4}	0.14	0.2	0.3	0.34	0.5
Poor	Weathered with Gouge (soft material); Spacing of 30 to 300 mm	10^{-5}	0.04	0.05	0.08	0.09	0.13
Very Poor	Heavily weathered; spacing of less than 50 mm	0	0.007	0.01	0.015	0.017	0.025

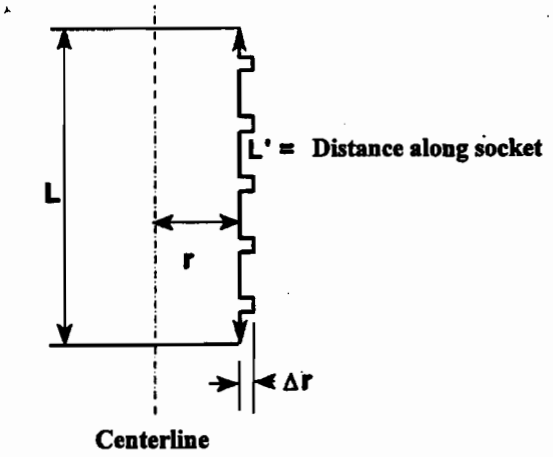

Figure. 2.24. Definition of Geometric Terms in Equation for a *Grooved* Rock Socket

ROCKET Model [Collingwood (2000) and Seidel and Collingwood (2001)]

Collingwood (2000) and Seidel and Collingwood (2001) describe a model for predicting the shearing resistance of the side of a rock socket using a simulation program, developed at Monash University, in Australia, called ROCKET (ROck soCKET). ROCKET models the interface between the concrete drilled shaft and the rock using a series of triangular asperities that may have variable sizes. They recommend the use of principles of fractal geometry to reproduce any general pattern of interface roughness that is expected to develop with a particular drilling method in a particular rock formation, from which the triangular asperity patterns can be selected. ROCKET is the outgrowth of a large fundamental research program on the behavior of rock-socketed piles that has been conducted over the past 15 years at Monash University. This research was based on extensive constant normal stiffness direct shear testing of interfaces between concrete and various types of weak rock. The experimental results have provided guidance in both the development and validation of ROCKET, which simulates the process.

The principles of ROCKET are described as follows. Figure 2.25 shows an idealized section of a rock socket. On application of an axial load to the shaft (concrete), the shaft and rock mass will displace together elastically until such time as the shear stress at the interface causes slip between the concrete and rock. Geometric constraints require this sliding displacement to generate dilation at the interface, and an increase, $\Delta D = 2\Delta r$, in the socket diameter. This dilation occurs against a surrounding rock mass that must deform to compensate for the enlargement of the socket diameter, and an increased normal stress at the pile/rock interface therefore results. (This is furthermore an increase in effective stress in the rock mass at the interface, since the Monash experiments show that most saturated soft rocks, unlike many soils, drain almost instantaneously when subjected to slowly applied normal or shear stresses.) The expansion of the rock socket can be approximated by the expansion of an infinite cylindrical cavity in an infinite elastic space. As long as the rock remains elastic, the increase in normal (effective) stress at the interface, $\Delta\sigma_n$, for a socket can be related to the interface dilation, Δr, as:

$$\Delta\sigma_n = \frac{E_m}{(1+\nu)}\frac{\Delta r}{r} \quad , \tag{2.60}$$

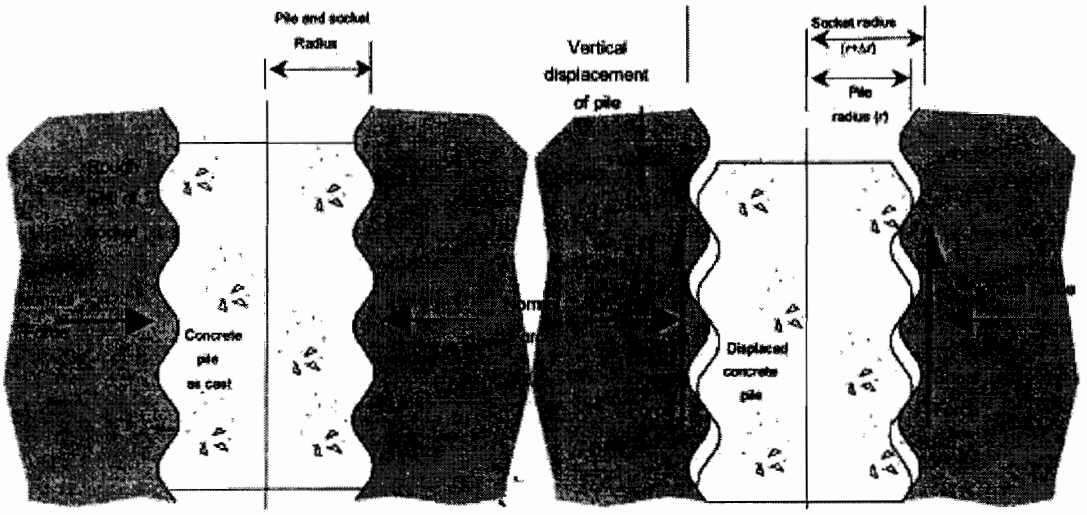

Figure. 2.25. An Idealized Section of a Rock Socket (Seidel and Collingwood, 2001)

where r is the original rock socket radius and E_m and ν are the rock mass modulus and Poisson's ratio of the rock, respectively. This expression can be rearranged to compute the stiffness normal to the borehole wall, K, as follows:

$$K = \frac{\Delta\sigma_n}{\Delta r} = \frac{E_m}{r(1+\nu_m)} . \tag{2.61}$$

Since the increase in socket radius, Δr, is much smaller than the initial radius, the normal stiffness, K, can effectively be assumed constant, which is a premise of the ROCKET model.

The behavior of pile sockets is therefore modeled as being governed by a constant normal stiffness (CNS) condition, as progressive slip displacements of the pile prior to peak resistance cause increasing normal effective stresses, and therefore increasing interface strength.

The interface asperities are modeled by a series of chords (straight lines) with length l_a and height Δr. These straight lines define triangular rock asperities in two dimensions. The shear stress, τ, at which slip is initiated on these triangular asperities is a function of the shear strength parameters at the planar concrete/rock interface (c_s, ϕ_s), the normal stress acting

upon the interface, σ_n, and the inclination of the interface to the socket axis, θ, as follows:

$$\tau = c_s + \sigma_n \tan(\phi_s + \theta) \quad . \tag{2.62}$$

For actual rock sockets, interface surfaces will consist of asperities over a range of inclinations rather than a constant value. Seidel (1993) showed that for a socket of total perimeter area, A, in an elastic medium consisting of a distribution of n asperities, with individual contact areas, a_i, with interface cohesion (c_s) equal to zero, and bcal normal stresses, $\sigma_{n,i}$, the shear stress at slip can be computed as follows:

$$\tau = \frac{1}{A}\sum_{i=1}^{i=1}\left[a_i \sigma_{n,i} \tan(\phi_s + \theta_i)\right] \quad . \tag{2.63}$$

After the initial interface slip occurs, the contact area between the concrete and the surrounding rock gradually reduces from the full contact area to smaller contact areas as shear displacement progresses. Figure 2.26 shows a simple two-dimensional model of the reduction of asperity contact area with progressive shear. Local normal stresses increase both as a consequence of the reduced contact area and the interface dilation in combination with the constant normal stiffness condition. A critical normal stress is reached at which the asperity can no longer sustain the loading, and individual asperity shear failure occurs.

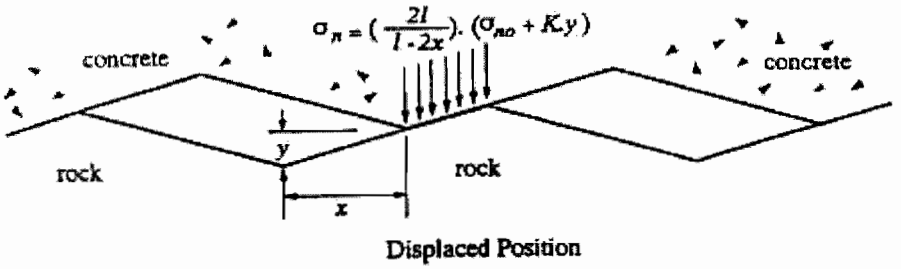

Figure 2.26. Reduction of Asperity Contact Area with Progressive Shear Displacement (Collingwood, 2000)

In Fig. 2.26, l is the length of a chord used to define the triangular asperity, K is the normal stiffness [Eq. (2.61)], and σ_{no} is the initial normal stress at the interface (before translating the concrete past the rock), which Seidel and Collingwood (2001) state has a minor effect. [The denominator of the term for σ_n in Fig. 2.26 should be 1 – x, rather than 1 – 2x..] The critical normal stress for an asperity is a function not only of the intact shear strength of the rock, but also of the geometry of the asperity. Observations of CNS direct shear tests on triangular asperities demonstrated what Seidel terms a 'door-stopper' effect, in which, after initial shear of the asperity, movement occurs both between the concrete and a wedge of failed rock and between the wedge of failed rock and the underlying intact rock.

Figure 2.27 is a schematic of post-peak shear displacement. The shearing resistance between the concrete and rock for the condition depicted in Figure 2.27 is governed by the internal shear strength parameters for the rock (c, ϕ) and is computed over a unit length of socket using principles of limit equilibrium (i. e., Hoek and Brown, 1980).

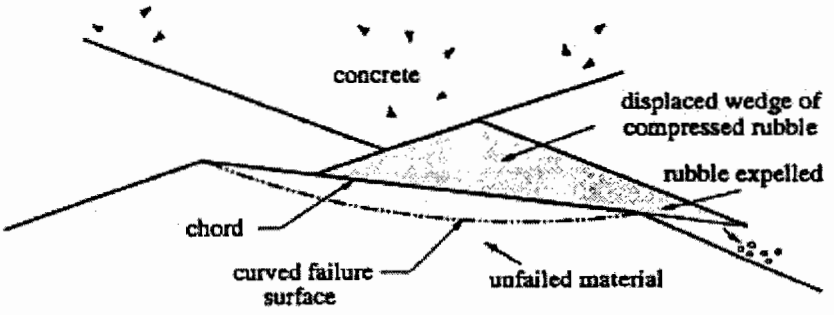

Figure 2.27. Schematic Representation of Post-Peak Shear Displacement (Collingwood, 2000)

ROCKET describes the geometry of the interface surface as follows, with reference to Figure 2.28.

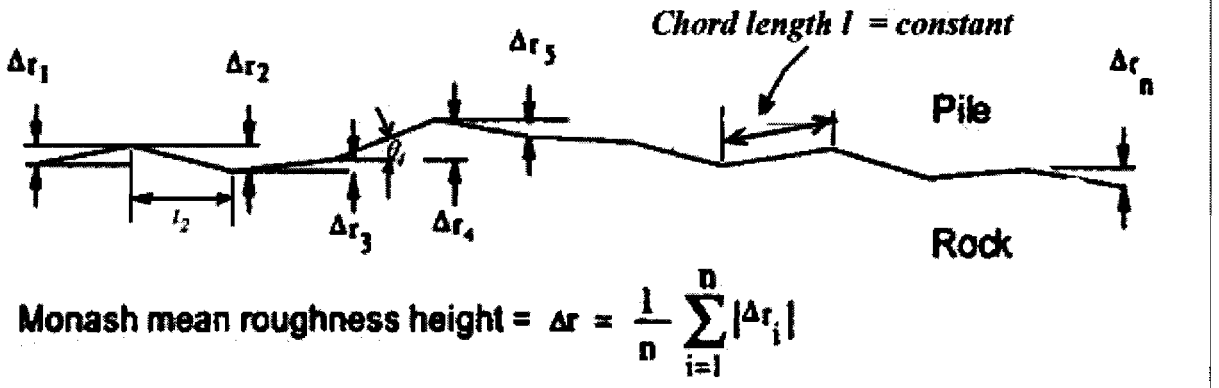

Figure 2.28. Monash Interface Roughness Model (Collingwood, 2000)

The interface is defined by a sequence of connected chords. The maximum chord length l is prescribed corresponding to the primary (longest) wavelength of the general interface roughness pattern. For example, for a very long, undulating interface, l would be in the order of 800 mm according to empirical evidence quoted by Collingwood (2000). Smaller values would be used for shorter primary wave lengths. Seidel and Collingwood (2001) indicate that for most ordinary drilling in Australian mudstone and sandstone this value should be about 50 mm. ROCKET then defines the interface using the prescribed value for l, the longest chord length of the asperity. This is approximately ½ of the wavelength of the longest repetitive pattern along the interface. The mean asperity height Δr corresponding to the value of l that is given is then established by the user and input. This can be done by reference to Fig. 2.28, in which the intersection points between chords of constant length l correspond to points on the actual (measured) or assumed interface roughness profile.

ROCKET then creates a synthetic interface with constant chord lengths l and irregular values of Δr, whose mean value, which has been prescribed, is defined according to Fig. 2.28. This is done by computing the mean value of the offset angle θ from the given values of l and Δr (average). The value of θ is then varied in a semi-random manner from chord to chord assuming a Gaussian distribution of θ around the mean value, producing a surface as indicated schematically in Fig. 2.28.

The concrete domain, which is assumed to deform elastically, is displaced past the rock, which also deforms elastically and later plastically as slip and shear through the various

asperities occur. This process, which is performed in plane strain, produces a tabulation of average shearing resistance (f) at the interface vs. shaft movement (w) and also includes the effect of base loading on the elastic deformations around the sides of the socket and elastic deformations in the asperities themselves. The process may be repeated with additional ROCKET runs using smaller values of *l* (perhaps ½ and ¼ of the maximum value) to create a more representative interface. Each run produces a nonlinear f-w curve. All f-w curves so generated are then enveloped to provide the best-estimate f-w curve (or series of f-w curves for layered rock) for the rock socket, as shown in Fig. 2.29. A socket-head load-settlement curve, incorporating both elastic base load vs. settlement computations and the side shear vs. displacement relation that was generated, is also created and output. The developed f-w curves can then be used in other software to synthesize the load-settlement behavior of longer sockets, or if the assumption can be made that the diameter has only a minor effect on load-settlement behavior, on sockets of different diameter.

A typical ROCKET output, of an analysis performed to simulate the load-settlement behavior of a socket in very soft clay-shale that was tested at the TAMU National Geotechnical Experimentation Site for the FHWA (O'Neill et al., 1996), is shown in Fig. 2.30.

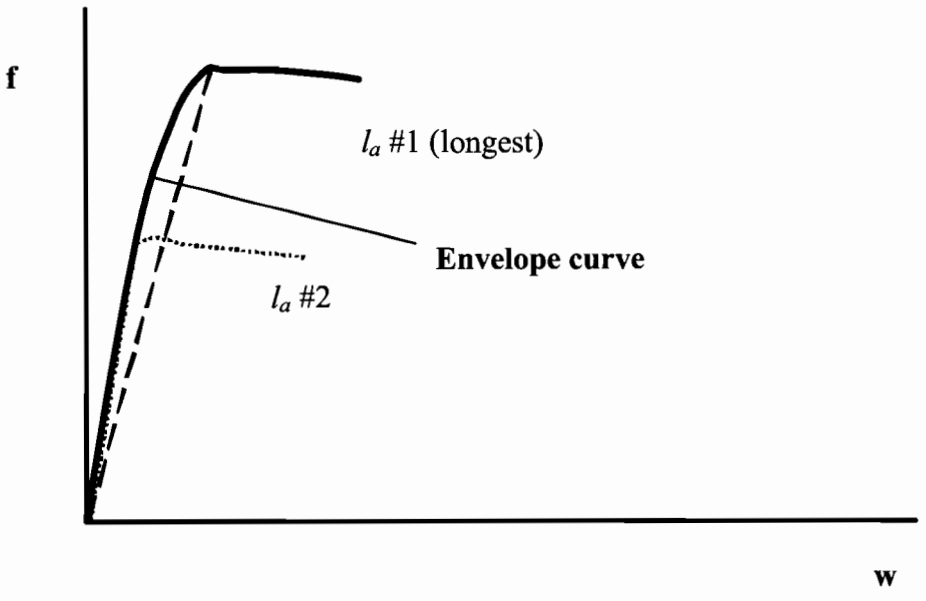

Figure 2.29. Envelope f-w Curve from ROCKET Executed for Different Values of *l*.

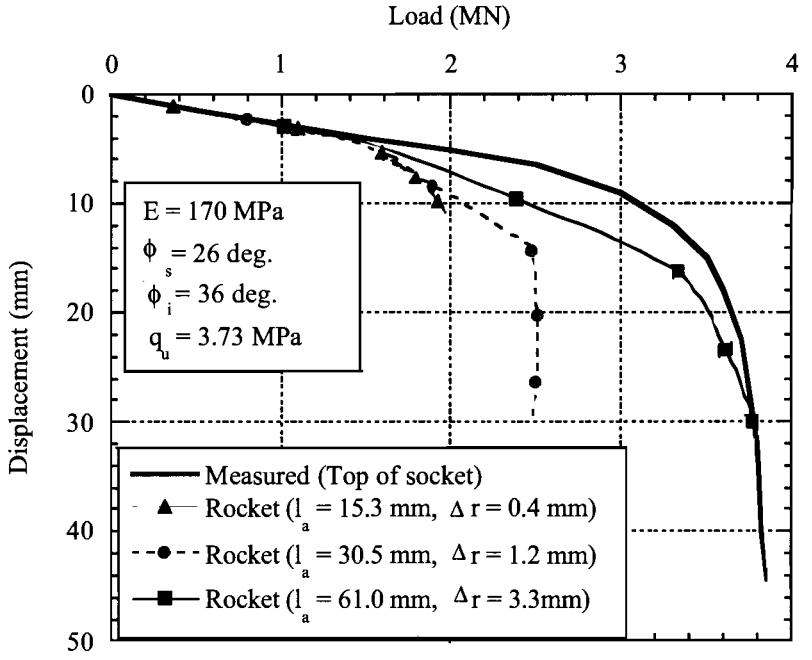

(a) Load-settlement curve

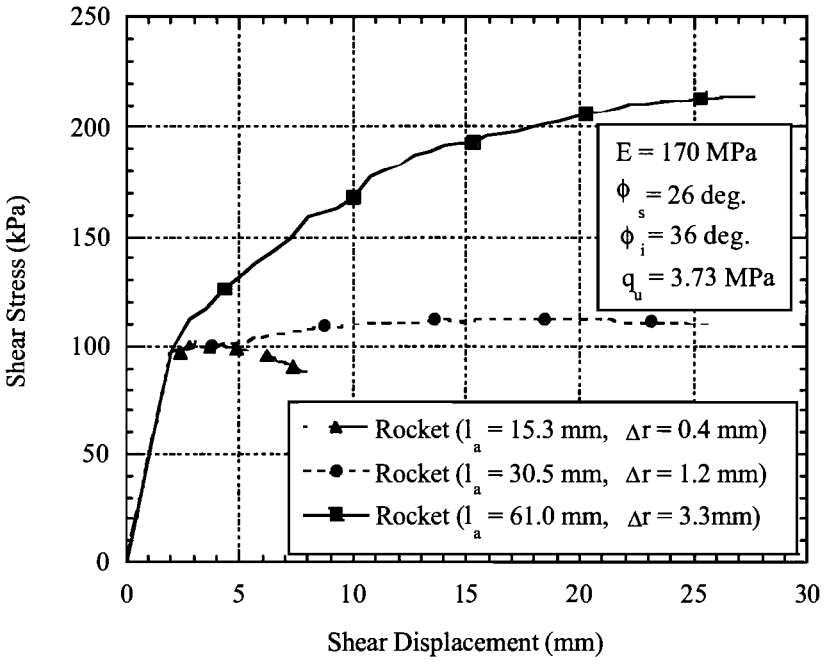

(b) Shear stress-displacement curve

Figure 2.30. Output from Early Version of ROCKET (Test: TAMU NGES, O'Neill et al., 1996).

For small deformations, the shearing resistance (f) is merely an accumulation of sliding frictional resistances on the interface asperities, as described previously, but as the relative shaft-rock deformation increases, the shearing resistance at some (at first) and then all of the asperities is defined by failure through the asperities as indicated in Fig. 2.26. During the process, the concrete and soil are assumed weightless. ROCKET does not consider the effect of interface cohesion (c_s), as it was shown in the CNS laboratory studies that this factor is minor in the rock and simulated rock that was tested at Monash University.

Collingwood (2000) performed a parametric study using ROCKET sufficient to define a method for producing socket side shear – displacement curves by hand to assist designers who wished to compute load-settlement behavior but did not wish to use ROCKET to do so. This method will not be reviewed here because it is assumed that for structures sensitive to settlement load-settlement curves will be generated by TxDOT, or other designers, by executing ROCKET directly. If only total side shear resistance is needed, as is usual TxDOT practice, either ROCKET or the simplified method described in the next section can be utilized.

Simplified Method of Seidel and Collingwood to Compute f_{max}

Seidel (1996), Hassan and O'Neill (1997) and Seidel and Collingwood (2001) recognized that the side shear capacity of a rock socket f_{max} is controlled mainly by the longest wavelength pattern of the interface and the effective height of the rock asperities Δr_e associated with that wavelength. With this postulation, a factor was proposed by Seidel (1996) and subsequently modified by Collingwood (2000) to which f_{max} can be correlated. This factor is defined as the shaft resistance coefficient (*SRC*), which incorporates all the factors influencing shaft resistance (but not settlement). In modified form [Collingwood, 2000)],

$$SRC = \eta_c \frac{n}{(1+\nu)} \frac{\Delta r_e}{D_s} \quad , \tag{2.64}$$

where η_c = construction method reduction factor, equal to 1 for socket with clean unbonded concrete-rock interface but possibly less than 1 for sockets with smear or residual mudcake from mineral drilling muds. (For good drilling mud practice, Collingwood recommends $\eta_c = 0.7 - 0.9$ for bentonite muds and $0.9 - 1.0$ for polymer muds. If

remolded smear is present on the borehole walls, η_c can be as low as 0.3, which is consistent with Kulhawy and Phoon, 1993, and Hassan and O'Neill, 1997.)

n = ratio of rock mass modulus to unconfined compressive strength of the rock (E_m/q_u),

Δr_e = effective asperity roughness height, and

D_s = socket diameter.

Collingwood and Seidel (2001) used ROCKET to perform parametric studies to determine the effect of the SRC with $\eta_c = 1$ on f_{max} by varying the values of the individual parameters that constitute the SRC. This allowed the SRC to be incorporated into a shaft resistance chart to produce theoretical relationships between the adhesion factor, α_q, and the unconfined compressive strength, q_u, for various values of SRC. Figure 2.31 shows the resulting shaft resistance chart. Once q_u is determined, f_{max} is computed from Eq. (2.65).

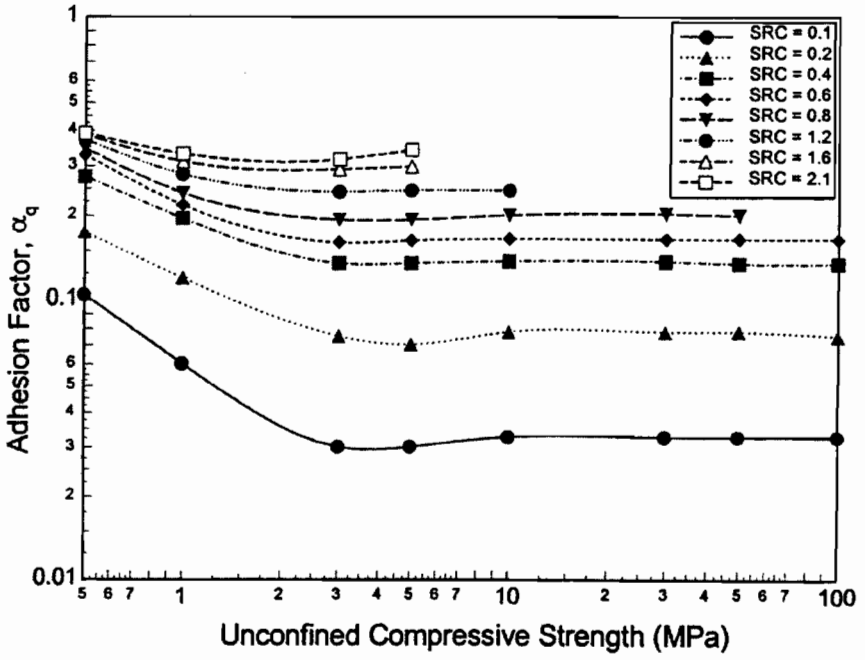

Figure 2.31. Relation between SRC, Unconfined Compression Strength (q_u) and α_q Computed Using ROCKET (Collingwood, 2000)

$$f_{max} = \alpha_q q_u \quad . \tag{2.65}$$

It is the opinion of the UH research team that q_u should be the median, rather than the mean, value along the length of the socket. From a design perspective, if the SRC can be estimated and q_u (median) measured, the peak shaft resistance, f_{max}, for rock sockets in tension or compression over a wide range of rock strengths can be evaluated.

In order to use the SRC method in design, the designer must know Δr_e, E_m, ν, q_u, and D_s. Since pore water pressure behavior in rock is usually drained behavior for normal design loadings (slowly applied loads), ν can usually be assumed to be about 0.3. The diameter of the socket, D_s, would be known by the designer for any trial design. Of the three remaining variables, it would be expected that the designer would extract cores and measure q_u and E_{core} for the rock cores. If the rock contains open seams and joints, or if the RQD is less than 100%, E_{core} will need to be reduced to E_{mass} using, for example, Table 2.6 or some other rational method. However, further reduction in f_{max} will not be needed, as is required by other methods cited in this chapter. (This information is not explicit in Seidel and Collingwood.)

Table 2.6. Ratios of E_{mass}/E_{core} Based on RQD. (from O'Neill et al., 1996; modified after Carter and Kulhawy, 1988)

RQD of rock (%)	E_{mass} / E_{core}	
	Closed joints	Open joints
100	1.00	0.60
70	0.70	0.10
50	0.15	0.10
20	0.05	0.05

Once these measurements have been made, the only remaining unknown is Δr_e. Seidel and Collingwood note that if a load test is performed on a rock socket, f_{max} is measured, and q_u is obtained, it is possible to enter Figure 2.31 with α_q (f_{max}/q_u) and q_u as arguments and infer a value of SRC. This leaves only Δr_e as the only unknown in Eq. (2.64), assuming that the value of η_c is known. For example, η_c is 1 if the sides or the socket are not smeared with soil or

ground-up rock or are coated with residual drilling mud. Δr_e can therefore be computed from the load test using Eq. (2.64), rewritten as Eq. (2.66), even if roughness measurements are not made.

$$\Delta r_e = \frac{D_s(1+\nu)SRC}{\eta_c n} \quad . \tag{2.66}$$

Using a data base of rock-socket load tests at sites at which q_u, E_{mass} and f_{max} had been measured or estimated, Seidel and Collingwood in this way developed relationships between back-calculated values of Δr_e and q_u, shown in Figure 2.32.

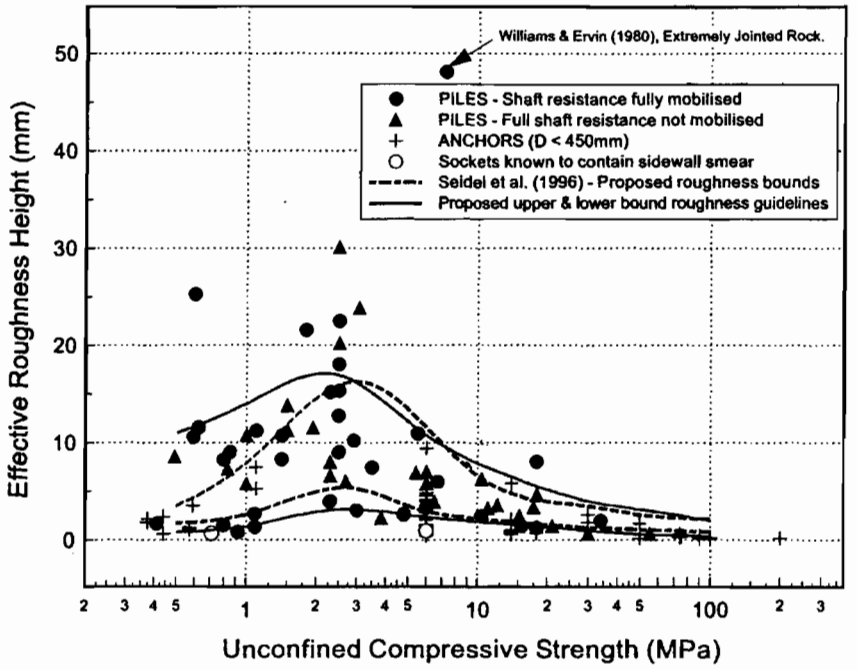

Figure 2.32. Back-calculated Values of Effective Roughness Height (Δr_e) from Load Tests (Seidel and Collingwood, 2001).

The test sites represented by Figure 2.32 contained many types of rock, including shale, mudstone, sandstone, schist, chalk and limestone. Specific results, however, are not identified according to rock type. Drilling tools, and their effect on roughness, likewise are not identified; however, all of the sockets were classified as clear of smear of residual mud, except for the two shown with open circles.

For design purposes, Seidel and Collingwood (2001) examined the data in Fig. 2.32 statistically and used reasonable limits for the modular ratio n to develop the design chart for SRC shown in Figure 2.33.

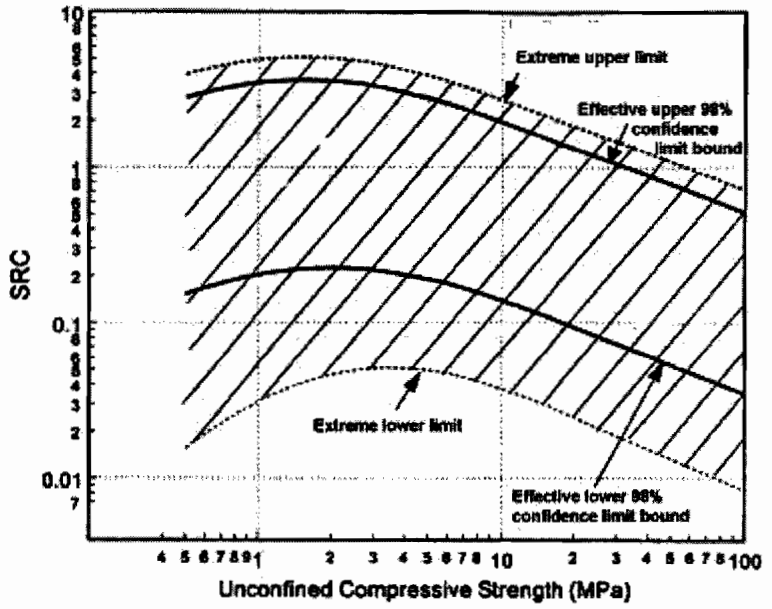

Figure 2.33. Estimated Values of SRC for Various Values of Unconfined Compressive Strength (q_u) (Seidel and Collingwood, 2001).

Seidel and Collingwood verified the accuracy of Figure 2.33 by comparing the results obtained with those in the experimental database of Kulhawy and Phoon (1993).

For design purposes, therefore, with q_u (median value) known, one would presumably, in sequence, use the lower 98% confidence limit line in Figure 2.33 to compute SRC, Figure 2.31 to compute α_q, and Eq. (2.65) to compute f_{max}. Alternatively, Figure 2.32 could be used to estimate Δr_e, from which the computations could proceed in a straightforward way. With either procedure, this general method will be valid only if $f'_c > q_u$.

Design Method of Ng et al.

Ng et al. (2001) reviewed a database of large-scale field load tests on rock-socketed piles with regard to rock-socket side resistance. Sixty-one tests in all were reviewed. Thirty-five tests were in decomposed rock, of which 13 were tests on piles of diameter from 1.0 m to 1.3 m in Hong Kong, and 44 of the tests were in sedimentary rock. The socket tests were studied to

compare with design formulas for side shear proposed in the literature. The investigators analyzed their empirical database by plotting the mean measured value of f_{max} for each test against the mean value of q_u (or f'_c in case f'_c was less than q_u). They concluded that the mean maximum socket side resistance, f_{max}, could be related to q_u, as indicated in Eq. (2.67), below.

$$f_{max}\,(MPa) = 0.19\sqrt{q_u\,(MPa)} \quad . \tag{2.67}$$

Ng et al. stated that Eq. (2.67) is applicable for sockets with length-to-diameter ratios less than 3.5. Figure 2.34 shows α_q versus q_u for various ranges of RQD. Table 2.7 summarizes the test data in their database, from which Fig. 2.32 was developed, and shows the ratio of average unit side resistance f_{max} to compressive strength of the rock, q_u, termed α_q here.

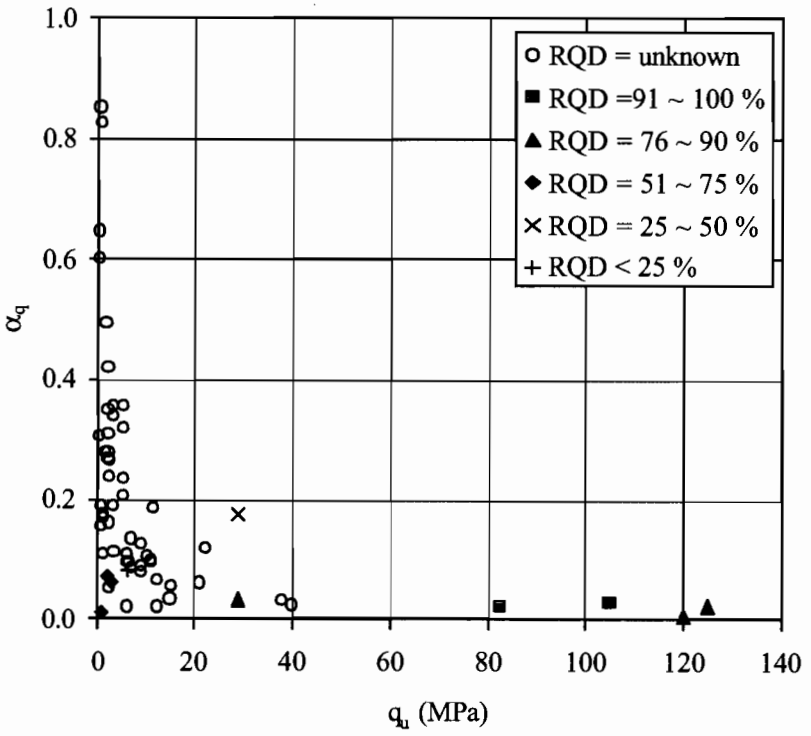

Figure 2.34. α_q versus q_u for Various RQD's from Database of Ng et al., 2001

Table 2.7. Summarized Database of Ng et al., 2001.

Rock type	Compressive Strength (MPa)	Unit Skin Friction (kPa)	α_q	RQD (%)
Fine Ash Tuff	105.00	2900.0	0.03	92
Fine Ash Tuff	156.00	1740.0	0.01	64
Coarse Ash Tuff	40.00	2860.0	0.07	68
Metasandstone	28.80	5100.0	0.18	41
Granodiorite	6.00	480.0	0.08	3
Granite	82.50	1700.0	0.02	100
Granite	10.00	610.0	0.06	69
Granite	125.00	2865.0	0.02	90
Granite	28.80	960.0	0.03	83
Granite	120.00	695.0	0.01	88
Granite	230.00	1000.0	0.00	-
Granite	38.00	1210.0	0.03	-
Granite	12.50	800.0	0.06	-
Siltstone	6.00	560.0	0.09	-
Siltstone	7.00	600.0	0.09	-
Siltstone	9.00	800.0	0.09	-
Siltstone	9.00	700.0	0.08	-
Siltstone	3.50	390.0	0.11	-
Siltstone	6.50	620.0	0.10	-
Marl	0.90	140.0	0.16	-
Diabasic Breccia	15.00	490.0	0.03	-
Gypsum	6.00	120.0	0.02	-
Diabase	40.00	890.0	0.02	-
Limestone	2.50	400.0	0.16	-
Mudstone	3.20	600.0	0.19	-
Siltstone	8.90	1110	0.12	-
Sandstone	11.60	2160	0.19	-
Shale	5.40	1110	0.21	-
Shale	11.10	1110	0.10	-
Shale	5.60	2000	0.36	-
Shale	5.50	1750.0	0.32	-
Shale	10.40	1090.0	0.10	-
Shale	15.20	830.0	0.05	-
Shale	7.00	932.0	0.13	-
Shale	11.10	1040.0	0.09	-
Shale	1.50	417.0	0.28	-
Shale	22.10	2600.0	0.12	-
Mudstone	2.30	800.0	0.35	-
Chalk	1.00	190.0	0.19	-
Marl	1.30	230.0	0.18	-
Diabase	0.40	122.0	0.31	-
Mudstone	2.30	965.0	0.42	-
Mudstone	3.10	1050.0	0.34	-
Mudstone	1.90	940.0	0.49	-
Mudstone	0.80	660.0	0.83	-
Mudstone	0.60	510.0	0.85	-
Mudstone	2.50	600.0	0.24	-
Mudstone	2.30	640	0.28	-
Mudstone	2.30	710.0	0.31	-
Mudstone	2.30	620.0	0.27	-
Mudstone	5.50	1300	0.24	-
Shale	0.48	310.0	0.65	-
Shale	3.10	1100.0	0.35	-
Shale	0.50	300.0	0.60	-
Shale	2.70	720.0	0.27	-
Shale	21.00	1260.0	0.06	-
Sandstone	6.00	650.0	0.11	-
Shale	12.20	242.0	0.02	-
Mudstone	1.10	120.0	0.11	-
Mudstone	1.10	184.0	0.17	-
Chalk	2.40	120.0	0.05	-

As a comment on the method of Ng et al. (2001), f_{max}/q_u trends lower as q_u increases, but there appears to be no clear relation between RQD, q_u and f_{max}. However, this method does not consider either borehole roughness (as does the SRC method), drilling tool or rock type.

Design method of Castelli and Fan

Castelli and Fan (2002) confirmed the design method of McVay, et al. (1992) and Law (1995) that developed correlations between SPT N-values, q_u of limestone and marl and f_{max}. This approach may be useful in the current study in correlating TxDOT PR to f_{max}, since it may be possible to correlate PR to N_{SPT} in Texas limestone. The ultimate f_{max} values used for foundation design by Castelli and Fan are summarized in Table 2.8. The unit skin friction values measured in limestone were generally consistent with design values determined using the method proposed by McVay et al (1992) and Law (1995).

Table 2.8. f_{max} for Limestone Used for Foundation Design (Castelli and Fan, 2002)

Limestone Classification	q_u (MPa)	SPT N-Value	f_{max} (kPa)
Weakly Cemented	< 4.8	25 to 100/300 mm	960
Cemented	4.9 to 12.0	100 to 50/50mm	2870
Well-Cemented	> 12.0	> 50/50mm	8620

Design Method of Kim et al.

Kim et al. (1999) investigated the load transfer behavior of drilled shafts in highly weathered rock by using an analytical study and field load tests. The analytical study was conducted by using a modified load transfer method that considered the continuity of the weathered rock mass by applying Mindlin's solution. Also, they proposed a single-modified hyperbolic model for the shear load transfer function.

The pile toe displacement was expressed as follows:

$$s_2 = \frac{D}{E_s}\sum_{j=1}^{n}\left(I_{bj} f_i\right) \quad , \tag{2.68}$$

where, f_j = unit shear transfer at element j, and

I_{bj} = vertical displacement factor for the base due to shear stress on element j

$$= \pi \int_{(j-1)\Delta L}^{j\Delta L} I_p dc = \frac{(1+\nu)}{8(1-\nu)} \left[\begin{array}{l} \dfrac{z_1}{R_1} - 4(1-\nu)\ln(z_1+R_1) + 8(1-2\nu+\nu^2)\ln(z+R) \\ + \dfrac{2h^2 z/r^2 - 4h - (3-4\nu)z}{R} + \dfrac{2(hr^2 - h^2 z^3/r^2 c)}{R^3} \end{array} \right] \quad (2.69)$$

ΔL = length of elements = L/n

c = embedded depth to element j, and,

I_p = displacement influence factor for vertical point loads, and according to Mindlin's equation

$$= \frac{(1+\nu)}{8\pi(1-\nu)} \left[\frac{z_1^2}{R_1^3} + \frac{(3-4\nu)}{R_1} + \frac{(5-12\nu+8\nu^2)}{R} + \frac{(3-4\nu)z^2 - 2cz + 2c^2}{R^3} + \frac{6cz^2(z-c)}{R^5} \right], \quad (2.70)$$

$z = h + c$

$z_1 = h - c$

$R_2 = z2 + D^2/4$,

$R_1^2 = z_1^2 + D^2/4$,

h =embedded depth, and

r = pile radius.

See Fig. 2.35.

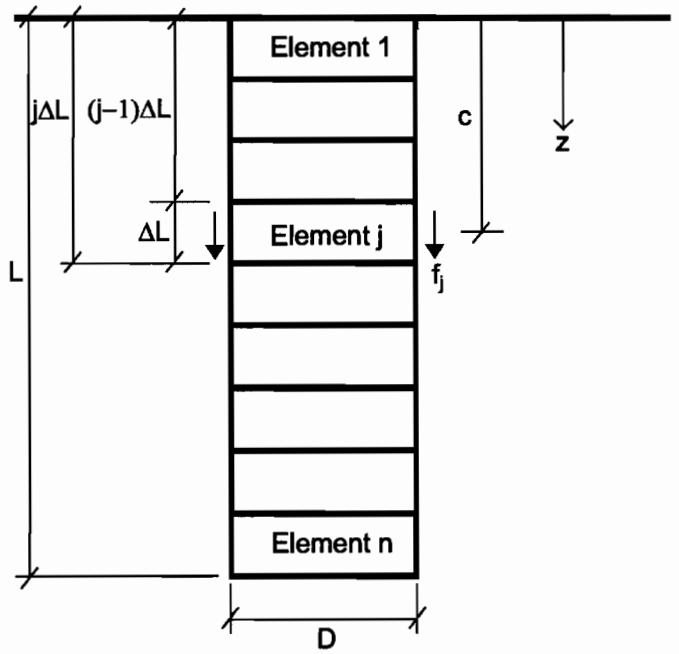

Figure 2. 35. Geometry of pile (After Kim et al., 1999)

The equilibrium of an elastic pile element along the pile axis is as follows:

$$\frac{d^2 w_z}{dz^2} = \frac{f_z C_p}{E_p A_p} \quad , \tag{2.71}$$

where, w_z = vertical displacement of the pile shaft,

E_p = modulus of elasticity of the pile,

C_p = perimeter distance around the pile,

A_p = cross-sectional area of the pile shaft, and

f_z = unit shear transfer resisted by weathered rock at depth z and displacement w_z.

A finite-difference approximation of Eq. (2.71) can be written as follows:

$$\frac{1}{(\Delta L)^2}(w_{i-1} - 2w_i + w_{i+1}) = \frac{C_p}{E_p A_p} f_i \quad . \tag{2.72}$$

The load remaining in the pile at node i is as follows:

$$Q_i = Q_{head} - \sum_{j=1}^{i-1} f_j L_j C_p \tag{2.73}$$

The solution procedure is to formulate a full set of nonlinear equations by applying Eqs. (2.68) - (2.73).

They also proposed single modified hyperbolic f-w function that implicitly considers wall roughness as follows:

$$f = \frac{w}{\frac{1}{S_i} + \frac{w}{\alpha_1 f_{max}}} = \frac{w}{\frac{\sqrt{D}}{C\alpha_1 f_{max}} + \frac{w}{\alpha_1 f_{max}}} \tag{2.74}$$

where, f = mobilized unit skin friction, in kN/m^2,

f_{max} = maximum unit skin friction, in kN/m^2,

w = displacement, in mm,

D = socket diameter, in mm,

S_i = initial tangent of the load transfer function in kN/m^2

$= CE_s / \sqrt{D} = C\alpha_1 f_{max} / \sqrt{D}$, and,

α = curve-fitting constant (≥ 1).

Table 2.9 shows the values for C and α values for highly weathered rocks obtained by linear regression analysis from their study.

Table 2.9. C and α Values for Highly Weathered Rocks (After Kim et al., 1999)

Surface roughness	C	α
Rough	3.86	1.00
Smooth	6.26	1.35

Methods Based on Informal Databases

Osterberg Cell Technique and Database of Osterberg

Figure 2.36 shows the Osterberg load test arrangement, and Fig. 2.37 shows typical Osterberg cell test results. The Osterberg load cell is a flat jack that is placed either on the bottom of the borehole or at an intermediate depth in the shaft. It jacks the socket above the load cell upward while reacting against either the base of the borehole or a reaction socket below the test socket. This testing technique can apply very high loads (thousands of tons) to rock sockets not attainable (or not attainable economically) with standard pile-head loading systems. Several hundred such load tests have been performed worldwide, many in rock sockets, since the test was first performed for a bridge foundation on drilled shafts in Port Orange, Florida, in 1987.

Advantages of the Osterberg load cell testing technique are as follows:

- Any load sequence and test duration can be performed. Sockets can be retested periodically over a period of years. Load applications can be cycled if desired.
- Very high loads can be applied. By using multiple cells and considering the socket and reaction loads separately, loads exceeding 15,000 tons have been applied to drilled shafts.
- Preparation and testing can be accomplished quickly and conveniently. For example, reaction shafts and reaction beams are not required.
- Tests can be performed on crowded sites.
- Tests can be performed over water.
- Tests can be performed where the top of the socket is below the ground surface.
- Tests can be performed on battered shafts with sockets.
- The maximum stresses in the concrete are only about 50% of those in a conventional test.

However, there are also some limitations for drilled shaft testing, as follows:

- The shaft or socket to be tested must be designated before installation.
- The Osterberg cell cannot be retrieved except under special circumstances.
- The stresses in the rock mass are different from those that are developed with top-down loading.

Osterberg (2001) summarized the results of several Osterberg cell load tests in rock sockets. From that data set, the ratio of mean unit side resistance to mean compressive strength of the rock, α_q, was computed by Eq. (2.75), then α_q was plotted versus q_u. The results are shown in Table 2.10 and Fig. 2.38.

$$\alpha_q = \frac{f_{\max}(avg)}{q_u(mean)} \quad . \tag{2.75}$$

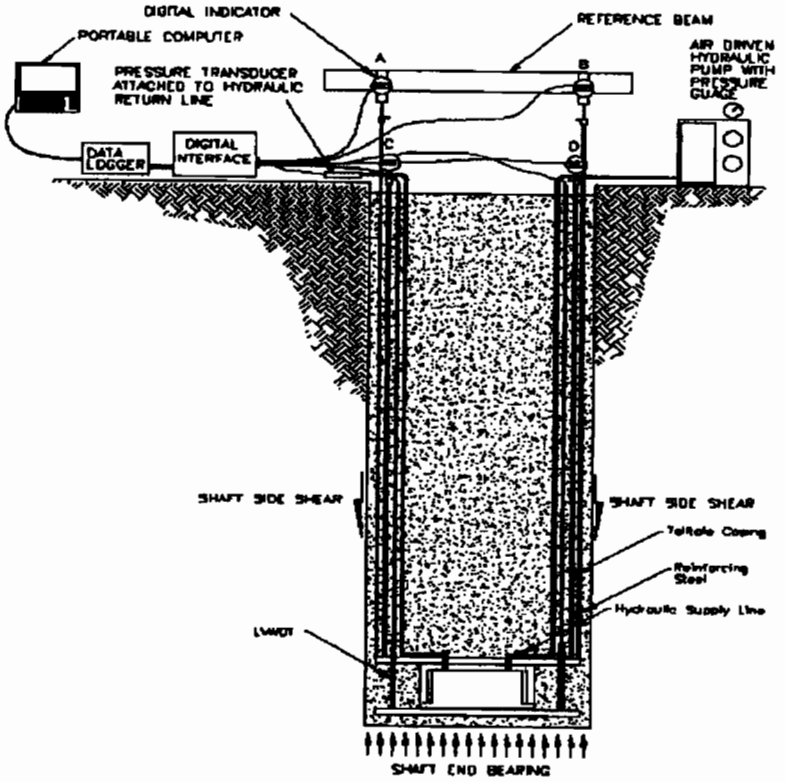

Figure 2.36. Osterberg Load Test Arrangement

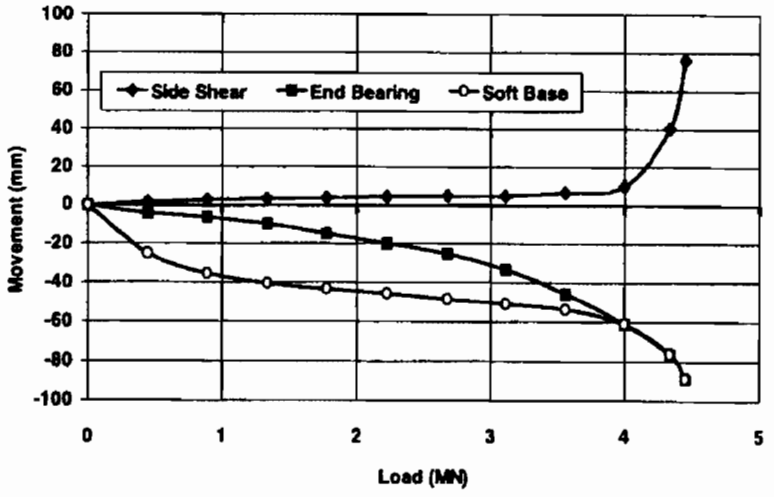

Figure 2.37. Typical Osterberg Cell Test Results

Table 2.10. Ratio of f_{max} to q_u, α_q (after Osterberg, 2001)

Rock type	Compressive Strength, q_u (MPa)	Unit Skin Friction, f_{max} (kPa)	α_q	RQD (%)
Hard Limestone	120.66	1819.44	0.02	
Medium Hard Limestone	127.56	1915.20	0.02	
Shale with Coal Seams	2.93	890.57	0.30	
Argilite Shale	22.06	1436.40	0.07	17
Hard Limestone	84.12	1915.20	0.02	50
Moderated Wethered Gypsum with Clay Shale	37.92	1627.92	0.04	
Gray-Black Shale with thin Limestone & Coal Seams	0.84	768.95	0.92	
Gray-Black Shale with Thin Limestone & Coal Seams	2.32	847.48	0.37	

As with other databases, there is a clear relationship between α_q and q_u, with α_q decreasing as q_u increases. For the two tests for which RQD was known, the rock with the lower RQD had the higher value of α_q, although it exhibited the lower actual value of f_{max}.

Field Load Tests by The University of Texas in the Late 1960's and Early 1970's

The University of Texas at Austin conducted a series of drilled shaft load tests in intermediate geomaterials for TxDOT in the late 1960's and early 1970's. Reese and Hudson (1968) report the load testing of a 24-in.- (0.61-m-) diameter shaft 12 ft (3.7 m) deep in hard clay with calcareous matter (which can be described as extremely soft rock, or "intermediate geomaterial"). The average value of f_{max} along the shaft was 1.40 tsf (133 kN/m^2), and the average developed point resistance was 14.3 tsf (1370 kN/m^2), although the point did not experience complete failure. The mean unconfined compression strength (q_u) of this geomaterial was about 5.0 tsf (480 kN/m^2). Aurora and Reese (1976) reported TxDOT cone PR values at this site ("Montopolis"—located near the present Austin-Bergstrom Airport) to be about 1 m (40 in.)

per 100 blows. Using Fig. 1.4 and extrapolating to such a large value of PR, the ultimate unit point bearing would be about 10.0 tsf (960 kN/m^2), and the ultimate unit skin friction would be about 2.1 tsf (200 kN/m^2). For the test of Reese and Hudson, the TxDOT PR method slightly overpredicts side resistance and underpredicts point resistance.

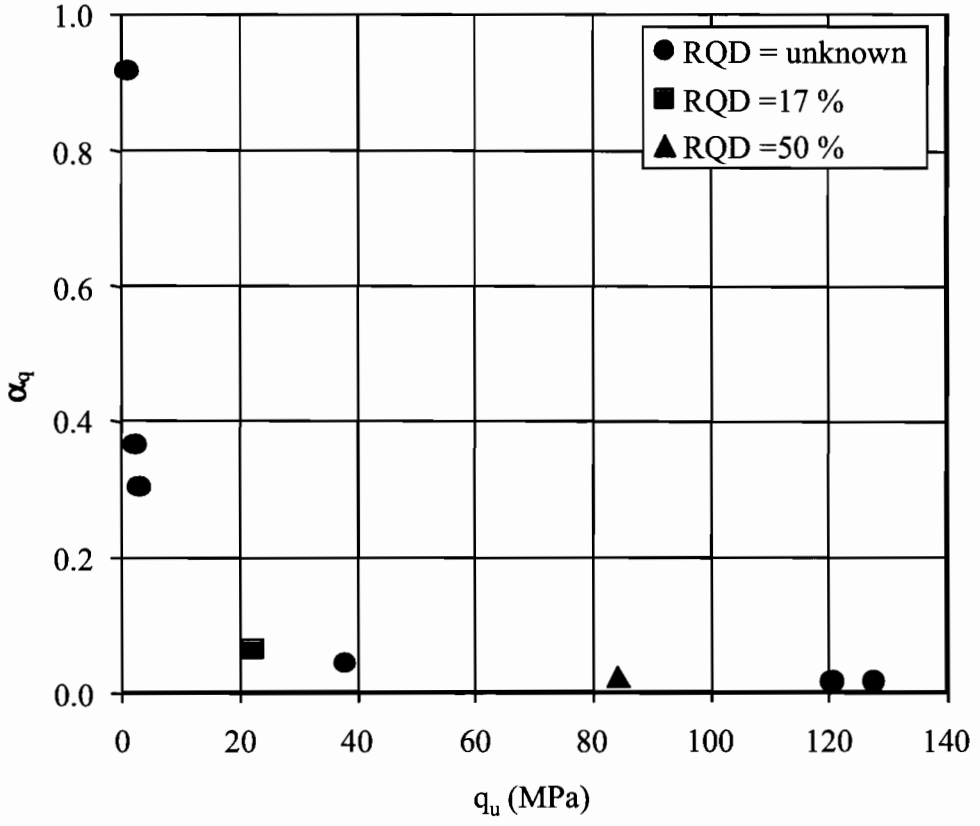

Figure 2.38. α_q versus q_u from Database of Osterberg, 2001

Vijayvergiya, Hudson and Reese (1969) reported the results of a compressive load test on a 30-in.- (0.76-m-) diameter drilled shaft that penetrated to a depth of about 27 ft (8.2 m) in the highly weathered Upper Midway clay-shale formation near Lackland Air Force Base in San Antonio. The average TxDOT cone PR was about 7 in. (175 mm) per 100 blows in the less weathered material below a depth of 18 ft. (5.5 m), and the unconfined compression strength of that geomaterial was about 4.5 tsf (430 kN/m^2). The ultimate skin friction in this lower zone was measured to be about 9.0 tsf (860 kN/m^2), and the average ultimate unit point bearing in the test sequence was 32.7 tsf (3130 kN/m^2). These values compare with values of 2.9 tsf (280 kN/m^2)

and 18.8 tsf (1800 kN/m^2) from Fig. 1.4 using a cone PR of 7 in. (175 mm) / 100 blows. In this case, the current TxDOT design method was conservative for both skin friction and end bearing.

Aurora and Reese (1976) also reported the results of other load tests at the Montopolis site on shafts that were deeper than the shaft described by Hudson and Reese (1968). These deeper shafts extended into a true clay-shale formation beneath the intermediate geomaterial of the earlier test Dry, casing and slurry methods were used for construction. The TxDOT cone PR was about 3 in. (75 mm) per 100 blows in the clay-shale, and the unconfined compression strength of this geomaterial was about 14.8 tsf (1420 kN/m^2). Load transfer data are given in the clay-shale unit for the shaft that was constructed in the dry and which penetrated the clay-shale to a depth of about six ft (2 m). The average measured unit skin friction in the clay-shale was 7.2 tsf (670 kN/m^2), which compares with 6.6 tsf (630 kN/m^2) from Fig. 1.4. The average measured unit point bearing was 66.1 tsf (6330 kN/m^2), which compares with 42.8 tsf (4100 kN/m^2) from Fig. 1.4. For this test the current TxDOT design chart is slightly conservative for both skin friction and point bearing.

Aurora and Reese (1976) also reported an additional drilled shaft load test in the Dallas District, at I-35 E near Spur 354. This test was conducted on a shaft that was very similar to the shaft described above at Montopolis, except that it was constructed using casing to stabilize the borehole. The average TxDOT cone PR was about 5 in. (125 mm) per 100 blows in the clay-shale, and the unconfined compression strength of this geomaterial was about 6.4 tsf (610 kN/m^2). The measured unit skin friction was 3.0 tsf (288 kN/m^2), compared with 3.9 tsf (375 kN/m^2) from Fig. 1.4. Because of some instrument problems, point bearing resistance could not be measured, but the ultimate value from Fig. 1.4 is 25.6 tsf (2450 kN/m^2).

Engeling and Reese (1974) reported a drilled shaft load test in " hard clay" in the Bryan District. This geomaterial was similar to the geomaterial above the clay-shale at Montopolis - not truly a clay-shale but a material that exhibited low cone PR. Between depths of about 32 ft (9.8 m) and 42 ft (12.8 m) (top of hard clay to bottom of shaft), the cone PR averaged about 8 in. (200 mm) per 100 blows, and at the base of the shaft, the PR was about 7in. (175 mm) per 100 blows. The unconfined compression strength of this geomaterial was about 2.0 tsf (190 kN/m^2). The measured skin friction in this material was 1.1 tsf (102 kN/m^2), while the measured point bearing was about 39 tsf (3750 kN/m^2). These values compare with 2.5 tsf (240 kN/m^2) and 16.2 tsf (1550 kN/m^2) from Fig. 1.4. As with the Montopolis test of Reese and Hudson (1968), the skin

friction was overpredicted and the point bearing underpredicted by the current TxDOT method that uses the PR of the TxDOT cone.

Based on The University of Texas (UT) reports, Table 2.11 and Figure 2.39 were developed to show the relationship between α_q and q_u that were obtained in the clays-shales and hard clays of central Texas. Figure 2.40 shows the relation of PR values to f_{max} from the UT test sites compared with the predictions from the TxDOT design method (2000). Figure 2.41 shows the relationship between PR and q_{max} based on these reports. These data are sparse and need to be improved upon in order to use ROCKET or similar models for developing new design charts.

The values of α_q in Fig. 2.39 are about twice as high as the values determined by O'Neill and Hassan (1993) for load tests in Eagle Ford shale in the Dallas area. This difference may have been due to the relative quality of the soft rock samples that were available for testing in both data sets, or they may be due to possible differences in borehole roughness that was developed by the drilling process at the UT sites as opposed to the sites investigated by O'Neill and Hassan (Fig. 2.7). The extremely high value of α_q (2.0) for the Lackland site is most likely the result of poor sample quality due to innate fracturing in the formation and consequent underestimation of compressive strength.

Table 2.11. Summary of Load Tests Performed by UT for TxDOT in Hard Clays/Soft Clay-Shales.

	Measured Values				α_q	Ultimate Values from Fig 1.4 (TxDOT, 2000)	
Site	Compressive Strength (MPa)	Unit Skin Friction (kPa)	Unit Point Bearing (kPa)	PR (mm / 100 blows)		Unit Skin Friction (kPa)	Unit Point Bearing (kPa)
Montopolis / Shallow	0.48	133	1370	1000	0.28	200	960
Lackland	0.43	860	3130	175	2.00	280	1800
Montopolis / Deep	1.42	670	6330	75	0.47	630	4100
Dallas	0.61	288	-	125	0.47	375	2450
Bryan	0.19	102	3750	200	0.53	240	1550

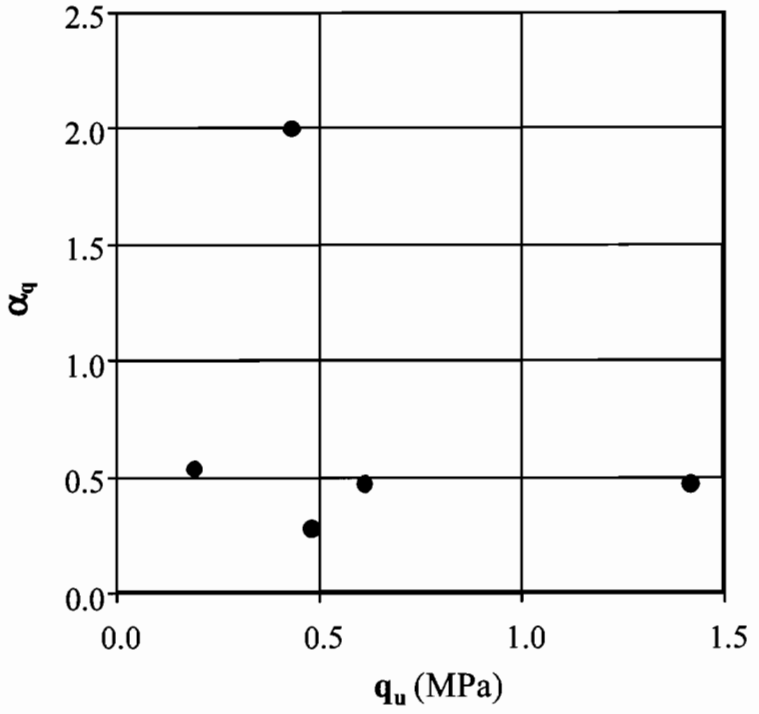

Figure 2.39. Relation between α_q (from Measurements) and q_u for UT Test Sites

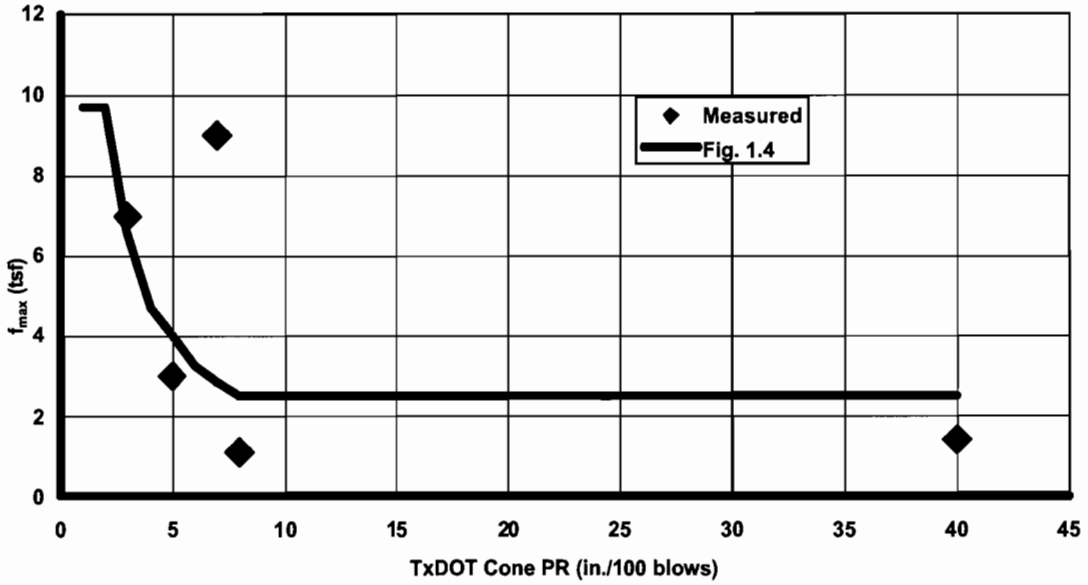

Figure 2.40. Comparison of Measured PR vs. f_{max} from UT Reports and PR vs. f_{max} Predicted by Current TxDOT Design Method (2000)

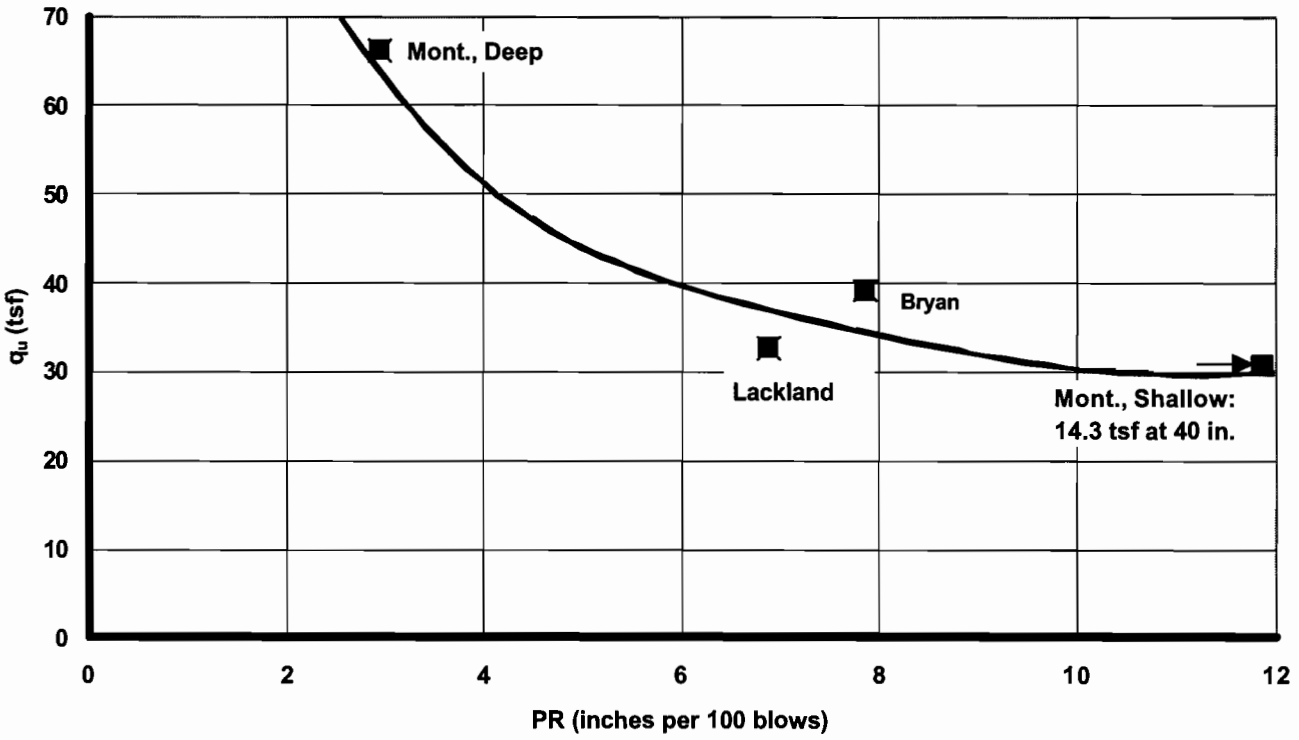

Figure 2.41. q_u vs. PR from UT Test Reports

Summary and Commentary

The following comments can be made concerning the studies that have been reported in the literature and summarized in this chapter.

1. The most important parameters that affect the capacity of a drilled shaft socket in soft rock are the compression strength of the rock, the Young's modulus of the rock, the pattern of roughness that develops on the interface due to construction (possibly a function of drilling tool and rock formation), the diameter of the socket, the presence or absence of smear on the socket walls, and the size, orientation and infill characteristics of the rock joints.
2. The most important characteristics that influence the side resistance (skin friction) appear to be strength of the rock mass and the roughness of the sides of the borehole.
3. Several models, including those of Seidel and Collingwood, Kulhawy and Phoon, Hassan and O'Neill, Williams, and Rowe and Armitage appear appropriate for developing

relations between q_u and f_{max} in soft rocks of the types found in central Texas, with varying degrees of socket interface roughness. These models, in various forms, also allow for the computation of f-w and/or load-settlement relations. (Computation of load-settlement behavior will not be a primary focus of this research.)

4. The models of Zhang and Einstein and the Canadian Foundation Manual appear to provide a sound basis for developing relations between q_u and q_{max} in soft rock profiles with closed and open joints, respectively.
5. Both the ROCKET model and the simplified method of Seidel and Collingwood appear to be especially promising for the development of improved design charts (i. e., Figs. 1.3 and 1.4) for TxDOT. One way to apply the simplified method to TxDOT's design process would be to acquire data on Δr_e, q_u, E_{core} and RQD for each design zone (grouping of borings) at each bridge site. From these data, SRC can be computed using Eq. (2.64). [E_{core} is corrected according to Table 2.4 if necessary.] The SRC can then be used to obtain α_q from Fig. 2.31, and f_{max} can be computed from Eq. (2.65). However, it is not TxDOT's current practice to recover cores and measure borehole roughness (Δr_e), q_u, E_{core} and RQD. In TxDOT practice, the rock is characterized using the TxDOT cone penetration test. The penetration resistance (PR) is the number of inches that the cone advances per 100 blows of the hammer. The highly fractured and laminated nature of much of the soft rock in central Texas has dictated this method of characterization, as contrasted to the standard method of recovering and testing cores, because cores often cannot be recovered intact for proper laboratory testing. In order to transform the simplified method of Seidel and Collingwood into a usable method for TxDOT practice, correlations will first need to be made between PR, q_u and E_{mass} at sites representative of common rock formations in Texas so that the parameter n in Eq. (2.64) can be replaced by a function of PR. Figure 2.41 provides a basis for making this correlation, but that figure is at present inadequate because of an insufficient number of data points and inconsistency in some of the relations. More measurements will need to be made at other sites. Correspondingly, measurements will need to be made of borehole roughness (specifically to obtain Δr_e) produced in such rock formations with common types of drilling tools (augers, core barrels) before proceeding to develop design charts relating PR to f_{max} (and possibly also to rock type, such as shale or limestone). Finally, the values

of f_{max} developed from this computational method will need to be verified both with socket load tests and complete simulations using ROCKET or other procedures. This approach is preferable to the approach outlined below because it will allow the final design charts to be tailored to Texas rock formations, drilling techniques and drilling tools.

6. Should this approach not prove successful, a simple correlation between PR and q_u can be developed, building upon the preliminary data in Fig. 2.41, which will allow for the use of Fig. 2.33 to obtain SRC, Fig. 2.31 to obtain α_q and Eq. (2.65) to compute f_{max}, from which a relationship between PR and f_{max} can be plotted for use by TxDOT designers after verification with socket load tests and more detailed simulations, such as the ROCKET model or a finite element model such as described by Hassan and O'Neill (1997).
7. Two factors should be considered when using the methods based on the research of Seidel and Collingwood. (1) Concerning the characterization of tightly laminated clay shales of the type found in central Texas formations, such as the Eagle Ford clay-shale, for any design method, RQD may not be a good indicator of modulus reduction as suggested in Table 2.6. The joints in those formations are closed *in situ.* RQD should perhaps be estimated based on the spacing between seams of soft soil (such as bentonite seams, which occur occasionally in clay-shales in Texas), rather than the actual RQD of the rock itself, which easily breaks apart along horizontal seams once extracted. (2) Concerning the disregard of interface cohesion, direct interface shear tests conducted on samples of Eagle Ford shale by Hassan (1994) indicated that there appears to be essentially zero cohesion for smooth interfaces. See Fig. 2.42. This is consistent with the ROCKET model. Whether this is also true for limestones common to the I-35 corridor or whether a cohesive interface model such as that of McVay et al. (1992) in limestone formations of central Texas will need to be considered.
8. Little information was found on the addition of side resistance in overburden soil to that in rock sockets. Shear deformation to failure is about 5 to 10 mm in most soils. It remains to determine corresponding values for rock sockets. This can be accomplished through load tests and simulations. Should similar values be found for rock sockets, then it should be safe to add side resistance in the overburden soil to that in the rock socket.

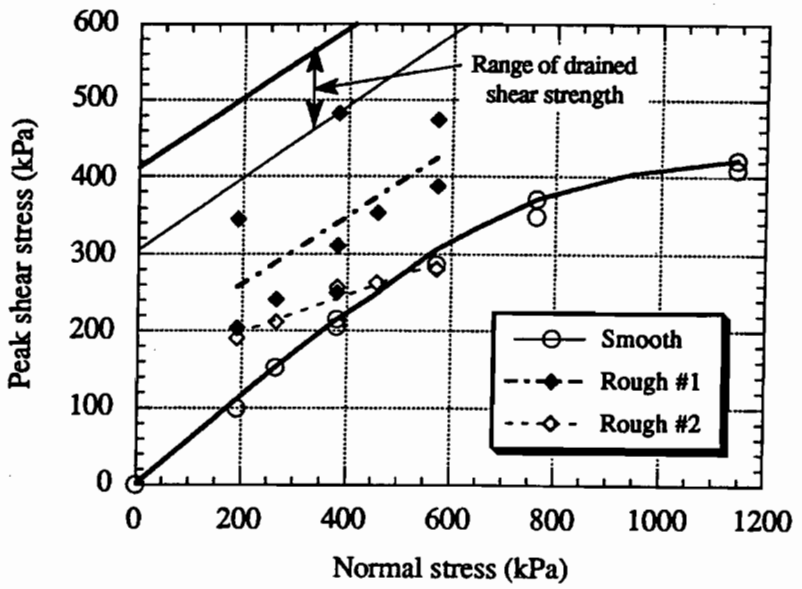

Figure 2.42. Mohr-Coulomb Envelopes for Interface Shear (Constant Normal Stress) on Samples of Soft Eagle Ford Clay Shale / Shear Perpendicular to the Planes of Lamination (Hassan, 1994)

References

AASHTO (1996). *"Standard Specifications for Highway Bridges,"* Sixteenth Edition, American Association of State Highway and Transportation Officials, Washington, D. C.

Aurora, R. P., and Reese, L. C. (1976). "Behavior of Axially Loaded Drilled Shafts in Clay-Shales," *Research Report 176-4*, Center for Highway Research, The University of Texas at Austin, March.

Baycan, S. (1996). "Field Performance of Expansive Anchors and Piles in Rock," *Ph. D. Thesis*, Department of Civil Engineering, Monash University, Clayton, Vic., Australia, October.

Canadian Geotechnical Society (1985). *Canadian Foundation Engineering Manual,* Second Edition, BiTech Publishers, Vancouver, BC.

Carter, J. R., and Kulhawy, F. H. (1988). "Analysis and Design of Drilled Shaft Foundations Socketed Into Rock," *Report No. EPRI EL-5918,* Geotechnical Engineering Group, Cornell University, August.

Castelli, R. J., and Fan, K. (2002). "O-Cell Test Results for Drilled Shafts in Marl and Limestone," *Geotechnical Special Publication No. 116, Deep Foundations Congress,* Vol. 1, Edited by O'Neill, M. W., and Townsend F., ASCE, February, pp. 807 – 823.

Collingwood, B. (2000). "The Effects of Construction Practices on the Performance of Rock Socketed Bored Piles," *Ph. D. Thesis*, Department of Civil Engineering, Monash University, Clayton, Vic., Australia, November.

Deere, D. U., and Miller, R. P. (1968). "Engineering Classification and Index Properties for Intact Rock," *Technical Report No. AWWL-TR-116*, Air Force Weapons Laboratory, Kirtland Air Force Base, New Mexico.

Engeling, D. E., and Reese, L. C. (1974). "Behavior of Three Instrumented Drilled Shafts Under Short Term Axial Loading," *Research Report 176-3*, Center for Highway Research, The University of Texas at Austin, May.

Hassan, K. M. (1994). "Analysis and Design of Drilled Shafts Socketed into Soft Rock," *Ph. D. Thesis*, Department of Civil & Environmental Engineering, University of Houston, Houston, Texas.

Hassan, K. M., and O'Neill, M. W. (1997). "Side Load-Transfer Mechanisms in Drilled Shafts in Soft Argillaceous Rock," *Journal of Geotechnical and Geoenvironmental Engineering*, Vol. 123, No. 2, ASCE, pp.145 – 152.

Hoek, E., and Brown, E. T. (1980). "Empirical Strength Criterion for Rock Masses," *Journal of the Geotechnical Engineering Division*, Vol. 106, ASCE, pp. 1013 - 1035.

Hoek, E. (1983). 'Strength of Jointed Rock Masses," *Geotechnique*, Vol. 33, No. 3, September, pp. 187 – 223.

Horvath, R. G., and Chae, K-J. (1989). "Long-Term Settlement of Rock-Socketed Piers," *Canadian Geotechnical Journal*, Vol. 26 No. 3, August, pp. 348 – 358.

Horvath, R. G., Kenney, T. C., and Kozicki, P. (1983). "Methods of Improving the Performance of Drilled Piers in Weak Rock," *Canadian Geotechnical Journal*, Vol. 20, pp. 758 - 772.

Jumikis, A. R. (1983). *Rock Mechanics*, Second Edition, Trans Tech Publications.

Kalinski, M. E., Ata, A., Stokoe, II, K. H., and O'Neill, M. W. (2001). "Use of SASW Measurements to Evaluate the Effect of Lime Slurry Conditioning of Drilled Shafts," *Journal of Environmental and Engineering Geophysics*, Dec., pp. 147 – 156.

Kim, S., Jeong, S., Cho, S., and Park, I. (1999). "Shear Load Transfer Characteristics of Drilled Shafts in Weathered Rocks, *Journal of Geotechnical and Geoenvironmental Engineering*, Vol. 125, No. 11, ASCE, pp. 999~1010.

Kulhawy, F. H., and Phoon, K-K (1993). "Drilled Shaft Side Resistance in Clay Soil to Rock," *Design and Performance of Deep Foundations, GSP No. 38,* Ed. by P. P. Nelson, T. D. Smith and E. C. Clukey, ASCE, October, pp. 172 - 183.

Law Engineering and Environmental Services, Inc. (1995). "Revised Report No. 2 of Geotechnical Exploration, Fuller Warren Bridge Replacement," *Law Project No. 442-06326-02.*

McVay, M. C., Townsend, F. C., and Williams, R. C. (1992). "Design of Socketed Drilled Shaft in Limestone," *Journal of Geotechnical Engineering*, Vol. 118, No. 10, ASCE, pp.1626 – 1637.

Ng, C. W. W., Yau, T. L. Y., Li, J. H. M., and Tang, W. H. (2001). "Side Resistance of Large Diameter Bored Piles Socketed into Decomposed Rocks," *Journal of Geotechnical and Geoenvironmental Engineering*, Vol. 127, No. 8, ASCE, pp.642 – 657.

O'Neill, M. W., and Hassan, K. M. (1993). "Perimeter Load Transfer in Drilled Shafts in the Eagle Ford Formation," *Design and Performance of Deep Foundations, GSP No. 38,* Ed. by P. P. Nelson, T. D. Smith and E. C. Clukey, ASCE, October, pp. 229 -244.

O'Neill, M. W., and Reese, L. C. (1999). "Drilled Shafts: Construction Procedures and Design Methods," *FHWA Publication No. FHWA-IF-99-025.* Department of Transportation, Federal Highway Administration, Office of Implementation, McLean, VA, August.

O'Neill, M. W., Townsend, F. C., Hassan, K. M., Buller, A., and Chan, P. S. (1996). "Load Transfer for Drilled Shafts in Intermediate Geomaterials," *FHWA Publication No. FHWA-RD-95-172,* Department of Transportation, Federal Highway Administration, Research and Development, McLean, VA, November.

Osterberg, J. (2001). "Load Testing High Capacity Piles: What Have We Learned?" *Proceedings of the 5th International Conference on Deep Foundation Practice,* Singapore, April 2001.

Osterberg, J.(2001). "Side Shear and End Bearing in Drilled Shafts," *Proceedings*, 18th Annual Geotechnical Seminar, Geo-Omaha 2001, ASCE, February, pp. 1-8.

Pells, P. J. N., Rowe, R. K., and Turner, R. M. (1980). "An Experimental Investigation into Side Shear for Socketed Piles in Sandstone." *Proceedings of the International Conference on Structural Foundation on Rock*, Sydney, Vol. 1., Balkema, pp. 291 – 302.

Randolph, M. F., and Wroth, C. P. (1978). "Analysis of Deformation of Vertically Loaded Piles," *Journal of the Geotechnical Engineering Division*, Vol. 104, No. GT12, ASCE, pp. 1465 – 1488.

Reese, L. C., and Hudson, W. R. (1968). "Field Testing of Drilled Shafts to Develop Design Methods," *Research Report 89-1*, Center for Highway Research, The University of Texas at Austin, April.

Rowe, P. K., and Armitage, H. H (1987a). "Theoretical Solutions for Axial Deformation of Drilled Shafts in Rock," *Canadian Geotechnical Journal,* Vol. 24, pp. 114 – 125.

Rowe, P. K., and Armitage, H. H. (1987b). "A Design Method for Drilled Piers in Weak Rock," *Canadian Geotechnical Journal,* Vol. 24, pp. 126 – 142.

Sellards, E. H., Adkins, W. S., and Plummer, F. B. (1932). "The Geology of Texas – Volume I, Stratigraphy," *The University of Texas Bulletin No. 3232*, Bureau of Economic Geology, August.

Seidel, J. P., Gu, X. F., and Haberfield, C. M. (1996). "A New Design Factor for Improved Prediction of the Resistance of Pile Shafts in Rock," in *Geomechanics in a Changing World, Proceedings of the 7th ANZ Conference on Geomechanics*, Adelaide, July, Institute of Engineers, Australia, pp. 693 – 697.

Seidel, J. P. (2000). *ROCKET Executable File*, Department of Civil Engineering, Monash University, Melbourne, Victoria, Australia.

Seidel, J. P., and Collingwood B. (2001). "A New Socket Roughness Factor for Prediction of Rock Socket Shaft Resistance," *Canadian Geotechnical Journal,* Vol. 38, February.

TxDOT (2000). *"Geotechnical Manual* (On-Line Version)," Texas Department of Transportation, Bridge Division, Austin, Texas.

Vijayvergiya, V. N., Hudson, W. R., and Reese, L. C. (1969). "Load Distribution for a Drilled Shaft in Clay Shale," *Research Report 89-5*, Center for Highway Research, The University of Texas at Austin, May.

Williams, A. F., and Johnston, I. W., and Donald, I. B. (1980). 'The Design of Socketed Piles in Weak Rock," *Proceedings of the International Conference on Structural Foundations on Rock*, Balkema, Sydney, pp.327-347, 1980.

Williams, A. F. (1980). "The Design and Performance of Piles Socketed Into Weak Rock," *Ph. D. Thesis,* Department of Civil Engineering, Monash University, Clayton, Vic., Australia, March.

Zhang, L., and Einstein, H. H. (1998). "End Bearing Capacity of Drilled Shafts in Rock," *Journal of Geotechnical and Geoenvironmental Engineering*, ASCE, Vol. 124, No. 7, July, pp. 574 – 584.

Chapter 3: Selection of Sites for Field Tests

Candidate Field Test Sites

Five candidate field test sites in the Dallas-Fort Worth area have been identified with the assistance of personnel in the Dallas District of the Texas Department of Transportation and the South Central Chapter of ADSC: The International Association of Foundation Drilling. One additional site, in Lone Star Office Park in Dallas, in which a drilled shaft load test was conducted approximately 10 years ago by Hassan et al. (1997), has also been identified to assist in the development of the final design curves. With the exception of the single site proposed by ADSC, these sites were all explored during May and June of 2002 by HBC, Inc., of Dallas, under the direction of the University of Houston. Figure 3.1 shows the general locations for each site. These test sites are identified as follows:

- ***Belt Line Road Site*** (immediately west of Belt Line Road, 0.3 miles north of I-30). This site consists of about 18 feet of mixed soil overburden overlying soft clay shale. The site is in the flood plain of the south fork of the Trinity River and was inaccessible for drilling and sampling during several attempts to sample there. However, in late June, 2002, TxDOT cone tests were performed and samples of the shale and overburden were recovered for laboratory testing. The average TxDOT cone penetration resistance in the depth range of 20 to 30 feet, the likely depth range for a test socket at this site, is 2.7 inches per 100 blows. Penetration resistances were relatively constant with depth; however, thin layers of bentonite were noted by the logger. Laboratory UU triaxial compression testing indicated that for the likely depth range for a test socket at this site, the average compressive strength in the depth range of 20 to 28 feet was about 380 psi, with a range from 614 to 285 psi, and the average compressive strength in the depth range of 28 to 30 feet was 250 psi, with a range from 282 to 246 psi. For the likely depth range for a reaction socket at this site, the average compressive strength in the depth range of 30 to 35 feet was 180 psi, with a range from 399 to 140 psi, and the average compressive strength in the depth range of 35 to 40 feet was 150 psi, with a range from 173 to 102 psi. As mentioned before, the site is in the flood plain of the south fork of the Trinity River and may be inaccessible for drilled shaft construction equipment for long periods of time. Because of this feature of the site, the unfavorable pattern of the rock

strength (decreasing with depth) and the availability of another site (Denton Tap) with nearly the same geologic setting and mean value of compressive strength, the Belt Line Road site will not be the location of a field load test. However, the laboratory strength and field penetration resistance data from this site will be used to develop correlations that will be used in the development of the final design charts.

- ***Hampton Road Site*** (approximately 50 feet east of the south abutment of the existing Hampton Road Viaduct over the Trinity River). The site consists of about 20 feet of mixed overburden overlying a deposit of clay shale having an average penetration resistance of about 9.6 inches per 100 blows in the proposed socket test zone (depth of approximately 25 to 35 feet). Penetration resistances generally decreased with increasing depth, below 35 feet, making this a suitable site for Osterberg Cell load testing. Laboratory UU triaxial compression tests on the samples from this site, recovered in May, 2002, indicate an average compressive strength in the depth range of 25 to 35 feet of 170.8 psi, with a range from 95 to 412 psi. The average compressive strength of the clay shale from 35 to 45 feet, which would be the potential location of a reaction socket for an Osterberg Cell, is approximately the same (191.3 psi); however, the compressive strength variation is from about 93 psi at 35 feet to about 200 psi at 45 feet, requiring a fairly long reaction socket. The site is dry and flat and easily accessible for drilled shaft construction equipment and is selected as a test site representing soft clay-shale rock.

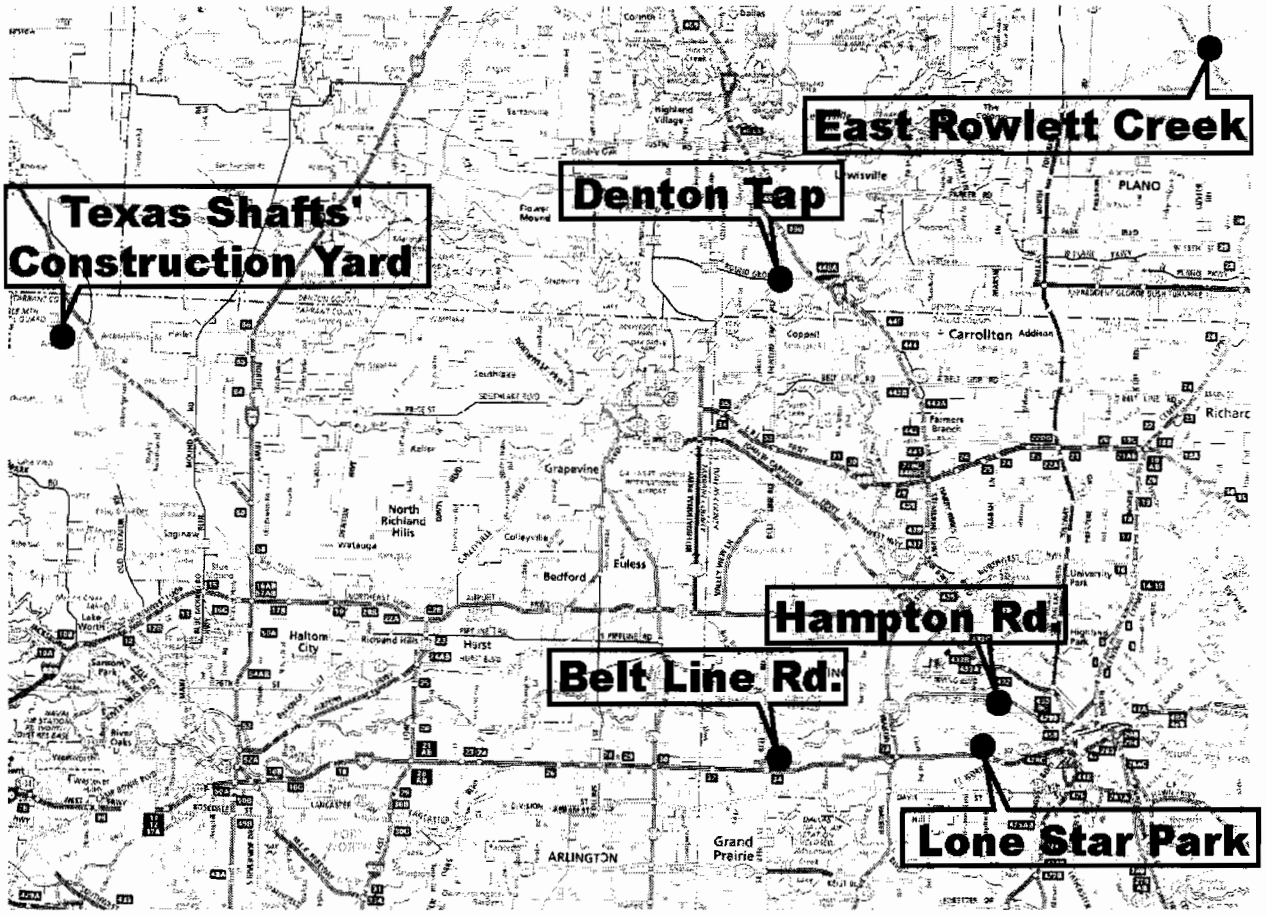

Figure 3.1 Map of the Locations for Candidate Field Test Sites

- ***Denton Tap Site*** (near the centerline of SH 121, 55 feet east of the eastern turnaround for Denton Tap Road). The site consists of about 19 feet of mixed overburden overlying a deposit of clay shale that is approximately 21 feet thick and which becomes sandy near the base of the unit. The clay shale has an average penetration resistance of about 6 inches per 100 blows in the proposed socket test zone (depth of approximately 20 to 27 feet). Penetration resistances generally decreased with depth.

  Below a depth of 40 feet was found a deposit of friable sandstone, extending to a depth of about 85 feet. Penetration resistances in the sandstone unit varied from about 4 inches to 8 inches per 100 blows. The sandstone is waterbearing. A socket test could conceivably be performed in the friable sandstone at a depth of about 45 to 55 feet; however, underwater construction is likely to be required, and this is a variable that the authors

would prefer not to introduce into the study. The underwater socket would also not be accessible to the laser caliper described later, resulting in unknown variations in diameter and surface roughness of the completed shaft. Therefore, the test socket at this site will be placed in the clay shale in the upper depth range. UU triaxial testing on core samples has revealed an average compression strength of 384.4 psi in the clay shale in the 20 to 27 foot depth range (depth range for the test socket). In the depth range of 28 to 36 feet, which would provide the reaction for an Osterberg load test, the average compression strength is only 210 psi, which will necessitate a relatively long reaction socket. The site is dry and flat and easily accessible for drilled shaft construction equipment. This site will represent a hard clay-shale rock.

- ***East Rowlett Creek Site*** (south side of SH 121 on the east side of East Rowlett Creek). The site consists of about 6 feet of clay overburden overlying relatively hard limestone (Austin formation). The average penetration resistance was about 1.8 inches per 100 blows in the proposed socket test zone (depth of approximately 10 to 17.5 feet), and it was about 1.2 inches per 100 blows in the proposed reaction socket zone (depth of approximately 19 to 24 feet). Laboratory unconfined compression testing has not been completed on the samples from this site, recovered in May, 2002. However, the average compressive strength from the tests performed so far in the depth range of 10 to 17.5 feet was 1360 psi, with a range from 1221 to 1574 psi. The average compressive strength of the limestone at about 19 to 24 feet was 1412 psi, with a range from 1144 to 1567 psi. Because this is a site at the high-end of rock strength among the sites investigated, it was chosen for testing. This site is representative of medium-strength limestone rock.

- ***Lone Star Office Park Site*** (2275 Lone Star Drive, Dallas, Texas). A drilled shaft load test was conducted at this location approximately 10 years ago by Hassan et al. (1997). A crude shaft roughness profile was measured on the extracted shaft, and the skin friction capacity of the shaft was also measured during a load test to failure. While further load testing at this site is not proposed, TxDOT cone penetration test results were obtained on June 3, 2002, in order to assist in the development the deliverable design chart, which will relate penetration resistance to unit skin friction. At this site, the penetration

resistance was about 11 inches per 100 blows, and the average undrained compression strength of this clay shale was only about 55 psi, which places the site at the lowest end of soft clay shale sites.

Analysis of the older test data from this site and new data from the East Rowlett Creek site should help "anchor" the ends of the design curves that will be developed as part of this project.

- ***Texas Shafts' Construction Yard Site*** (private contractor's yard near Blue Mound, Tarrant County, Texas, proposed by ADSC). No subsurface exploration has taken place at this site; however, the site is known to be underlain by limestone. This site will not be used for a load test, but it is proposed to drill full-sized boreholes there in order to make measurements of borehole roughness in the limestone. These data will supplement those that we plan to make in the limestone at the East Rowlett Creek site and will therefore increase the level of confidence in the developed correlations between drilling tool, rock formation and hole roughness parameter, which will be used in the process of developing the final design curves.

Figure 3.2 shows photos of rock compressive strength testing with clay shale (Belt Line site) and limestone (East Rowlett Creek site). The clay shale was tested in UU triaxial compression using the Trautwein triaxial test system in the University of Houston geotechnical laboratory, and the limestone was tested in unconfined compression test using a Tinus Olsen universal testing machine in the University of Houston materials laboratory because of its high strength. With both testing systems, complete axial stress-strain curves were obtained for later use in modeling socket behavior and developing the design curves.

The Hampton Road, Denton Tap and East Rowlett Creek sites were selected for Osterberg cell testing. These sites represent soft clay shale, hard clay shale and medium limestone rock, respectively. Correlations between TxDOT cone penetration resistance, splitting tension and point load index values, compression strength and rock sample modulus will be developed for each of these three sites plus the Belt Line Road site and the Lone Star Park site. This information will be of use in developing design charts.

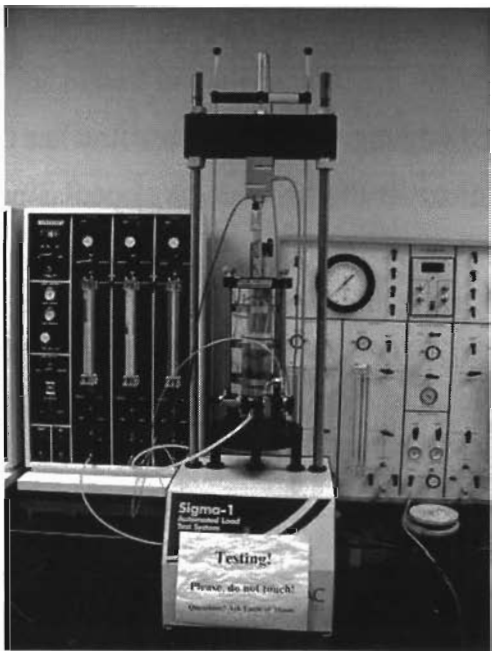

(a) Testing clay shale

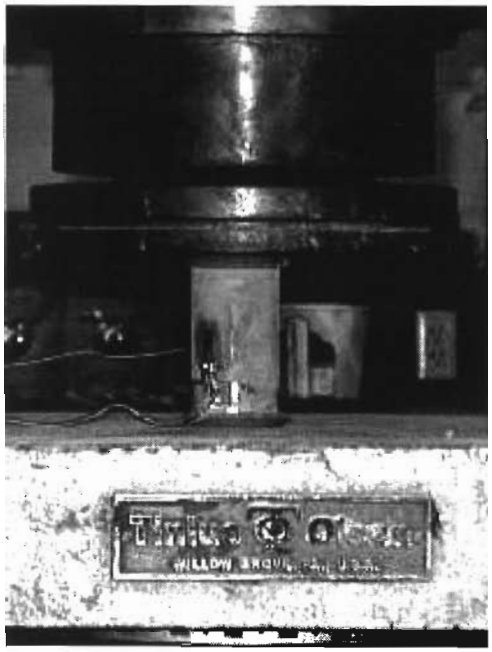

(b) Testing limestone

Figure 3.2 Photos of Rock Compressive Strength Testing

Criteria for Selection of Load Test Sites

Site accessibility, lithology, compressive strength, and average TxDOT cone penetration resistance were the main criteria for site selection. Test sites should be easily accessible to drilled shaft construction equipment, and the rock characteristics should be distinctly different at each site and yet representative of the soft rock conditions in the Dallas-Fort Worth area. Using these criteria, the Hampton Road, Denton Tap, and East Rowlett Creek sites were chosen for Osterberg Cell testing.

Load testing of a rock socket together with overlying soil will be carried out at the Denton Tap site in order to assess whether side resistance in the socket can be added to skin friction in the overburden soil. The Denton Tap site was chosen for this test because the compressive strength and modulus of the clay shale layer is relatively high, while the indicated strength of the overburden soil is relatively low, making this site (among the three clay shale sites) the most likely to experience socket failure and overburden failure at different values of

movement. Rock-socket-only load tests will be performed at the Hampton Road and East Rowlett Creek sites. Loading will be carried out using Osterberg Cells. In order to assure failure, 1000-ton Osterberg Cells will be installed at the Hampton Road and Denton Tap sites, and an 1800-ton Osterberg Cell will be installed at East Rowlett Creek site.

The Osterberg Cells will be placed beneath test sockets in selected depth ranges where there is the greatest probability that skin friction failure will occur in the socket above the cell. Reaction sockets are needed below the cell for all test sites to facilitate failure of the test sockets in side shear.

Activities for Field Tests

The literature survey indicated that borehole roughness is a very important factor in determining skin friction capacity of sockets in soft rock. The borehole roughness is influenced by the type of rock encountered, the flaws in the rock (joints, seams, vugs, etc.) and the type of drilling tool used to excavate the rock. Two common types of rock drilling tools will be used at the field test sites: (1) the rock auger and (2) the core barrel. The roughness of the interface between the concrete in a rock socket and the surrounding will likely vary with the drilling tool, so two boreholes will be drilled in close proximity at each of the three test sites plus the Texas Shafts' site. One hole will be drilled with a rock auger, and one will be drilled with a single-walled core barrel.

In order to quantify the roughness of each borehole a laser profiler that has been developed by the Department of Electrical and Computer Engineering at the University of Houston will be lowered down the completed borehole to obtain the roughness profile. This laser profiler is described briefly in the appendix to this report.

Following profiling, a simple mechanical tool will be affixed to the Kelly bar of the drill rig and pushed (under the weight of the Kelly bar) into the bottom of the borehole. This device, developed in the Department of Civil and Environmental Engineering at the University of Houston, also described briefly in the appendix, is a crude index tool to assess whether the geomaterial at the bottom of the borehole is rock or soil. It is intended that this tool, if successful, be used in the future by TxDOT personnel to verify the location of rock in boreholes that will be drilled into clay shales under slurry. In such situations clay shales are ground into fine

geomaterials that are mixed with slurry before they are removed, making it impossible for inspectors to distinguish the parent material by examining the cuttings.

Next, concrete with reduced coarse aggregate size will be placed by directed free fall into the reaction sockets.

Reinforcing cages with Osterberg Cells and instruments attached (assembled prior to construction of the test sockets) will then be placed into the borehole.

Finally, concrete will be placed in the test socket (and overburden at Denton Tap), and concrete cylinders will be taken for measuring the compressive strength and elastic modulus of the concrete.

Surface and/or perched water was observed at each test site above the elevation of the top of the test socket. In order for the borehole to be accessible to the laser caliper and the rock index test device it is necessary for the test socket to remain dry. It is therefore likely that a length of surface casing will need to be placed through the overburden above the test socket as soon as the overburden is excavated, sealed at the top of the test socket and left in place until after the load test is completed.

About one month later, load tests (TxDOT quick load tests) will be performed. The details of activities for load tests at each site are summarized in Table 3.1.

A test socket will not be constructed at the Texas Shafts' site because of funding limitations. However, two boreholes will be drilled there to a depth of about 10 feet with a rock auger and a core barrel, respectively, and the boreholes will be profiled with the laser profiler.

Table 3.1 List of Activities at Three Test Sites

Activities	Remarks
Drill two boreholes	Core barrel Rock auger
Make Laser profiles	Core barrel hole Rock auger hole
Read Bottom hole penetrometer	Core barrel hole (two depths) Rock auger hole (in the rock)
Place concrete in reaction socket (TxDOT Class C with Grade 5 coarse aggregate)	
Place cage with Osterberg cell & instruments	
Place concrete in test socket (TxDOT Class C with Grade 5 coarse aggregate)	Recover samples
Perform Load tests	TxDOT quick tests

Design of Test Shafts

Several design models, including those of TxDOT, O'Neill and Hassan [only applied for clay shale ($q_u \leq 5.0$ MPa)], O'Neill et al., FHWA, Seidel and Collingwood, Kulhawy and Phoon, Williams, and Rowe and Armitage (Chapter 2), were used for the design of the test rock sockets and reaction sockets because they appear appropriate for developing relations between q_u and f_{max} in soft rocks of the types found in North Texas.

The design concept is as follows:

- The test and reaction sockets will all be 30 inches (0.76 m) in diameter.
- Osterberg Cells were available with capacities of 1000 tons and 1800 tons.
- The reaction sockets will have factors of safety of at least 1.5 with respect to the test socket capacities.
- Likewise, the Osterberg Cells will have factors of safety of at least 2.0 with respect to the computed test socket capacities.

Therefore, the relationship of Osterberg Cell and the skin friction of rock socket / overburden soil (test shaft) is,

$$Q_o \geq 2.0\, R_S \quad , \tag{3.1}$$

where, Q_o= the capacity of Osterberg Cell, and

R_S = the skin friction of the test shaft.

The relationship of the skin friction and end bearing in the rock socket and reaction socket is

$$Q_R = Q_{SR} + Q_B \geq 1.5\, R_S \tag{3.2}$$

where, Q_R = the capacity of the reaction socket below the Osterberg Cell,

Q_{SR} = the skin friction of the reaction socket and,

Q_B = the end bearing capacity of the reaction socket

The design of both the reaction and test sockets should be sufficient to satisfy both Eqs. (3.1) and (3.2). Figure 3.3 shows a schematic of the rock and reaction socket, and the designs for each site are summarized as follows.

Hampton Road Site. The test socket was placed in the depth range of 25 to 35 feet with a diameter of 30 in., and the reaction socket was placed in the depth range of 36.5 to 46.5 feet, also with a diameter of 30 in. The depth range 35 to 36.5 feet is the height of the Osterberg Cell. The clay shale in the test socket zone has an average compressive strength of 170.8 psi, RQD of 94.2 %, and an average penetration resistance of about 9.6 inches per 100 blows. Similarly, the reaction zone has an average compressive strength of 191.3 psi, RQD of 100 %, and an average penetration resistance of about 5 inches per 100 blows, which indicate that the reaction socket zone consists of slightly better quality rock than the test socket zone.

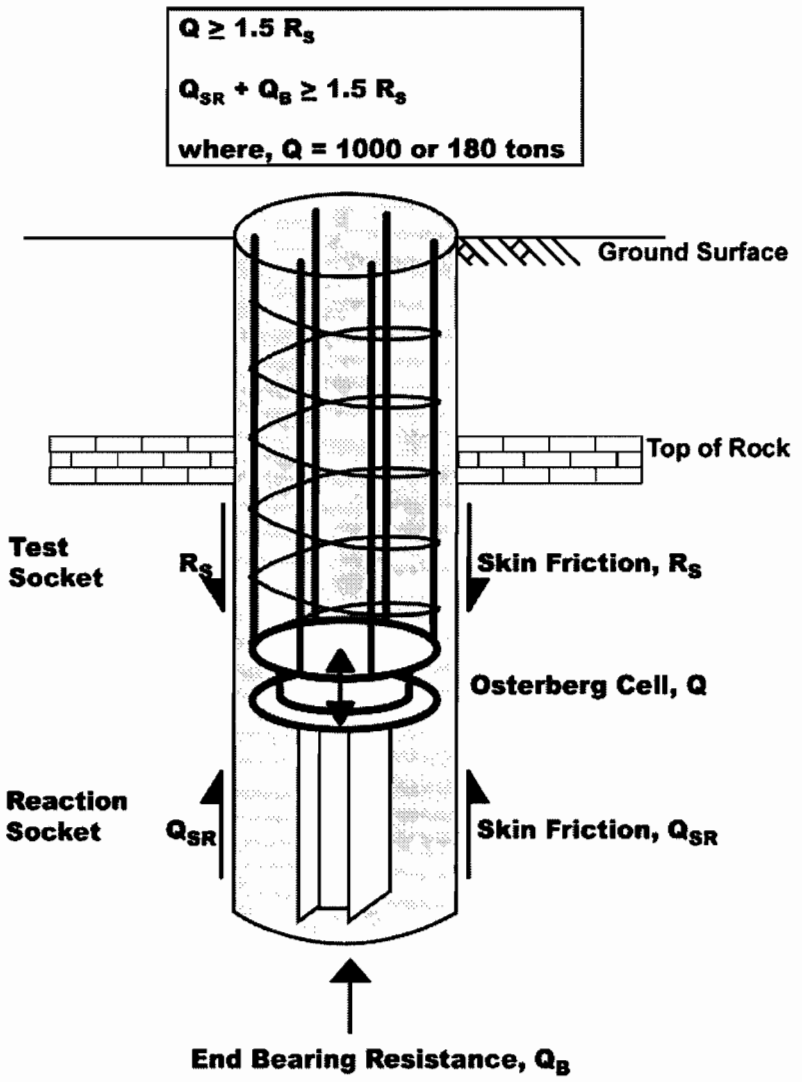

Figure 3.3 Schematic of Rock and Reaction Socket

Several design methods were used for designing the rock and reaction sockets, as mentioned before. The average skin friction resistance for the test socket was 241.0 tons, and the average capacity of the reaction socket was 453.9 tons; these values were sufficient to satisfy Eqs. (3.1) and (3.2). Therefore, the Hampton Road Site test arrangement was acceptable with a test rock socket length of 10 feet and a reaction socket length of 10 feet. Table 3.2 describes the design values obtained by the design methods employed, and Figure 3.4 shows the geomaterial and test shaft profiles for the Hampton Road Site. From a practical perspective it is likely that the cased portion of the borehole will need to be 36 in. in diameter to facilitate construction of a 30-in.-diameter test socket.

Table 3.2. Summary of Design Values for Hampton Road Site By Several Design Methods

Design Methods	Skin Friction of Test Socket, R_S (Tons)	Capacity of Reaction Socket, Q_R (Tons)	Remarks
TxDOT (2000)	212.1	436.9	- Using Figure 1.4.
O'Neill and Hassan (1993)	122.3	313.3	- Using Eq. (2.4), (2.5), (2.6) for skin friction. - Using Eq. (2.13) for end bearing.
O'Neill et al. (1996)	144.7	347.5	- Using Figure 2.8 for skin friction. - Using Eq. (2.13) for end bearing. - Assuming non-bond and smooth interface, $\sigma_n/\sigma_p = 1.25$, and $\phi = 30°$.
FHWA (1999)	183.7	379.8	- Using Eq. (2.58) for skin friction. - Using Eq. (2.55) for end bearing. - Assuming smooth socket.
Collingwood and Seidel (2001)	193.0	401.5	- Using Figure 2.31 and 2.33 for skin friction. - Using Eq. (2.13) for end bearing. - Assuming SRC = 0.6.
Kulhawy and Phoon (1993)	399.8	608.5	- Using Eq. (2.29) for skin friction. - Using Eq. (2.13) for end bearing. - Assuming $\psi = 2$ / normal drilling conditions.
Williams (1980)	386.0	617.7	- Using Figure 2.19 for skin friction. - Using Eq. (2.13) for end bearing.
Rowe and Armitage (1987b)	286.3	525.8	- Using Eq. (2.19) for skin friction. - Using Eq. (2.13) for end bearing. - Assuming clean socket with roughness R1, R2 or R3.
Average	***241.0***	***453.9***	$1.5 \times 241.0 = 361.5 \leq 453.9$ and $361.5 \leq 1000$ $\Rightarrow$ ***O. K!***

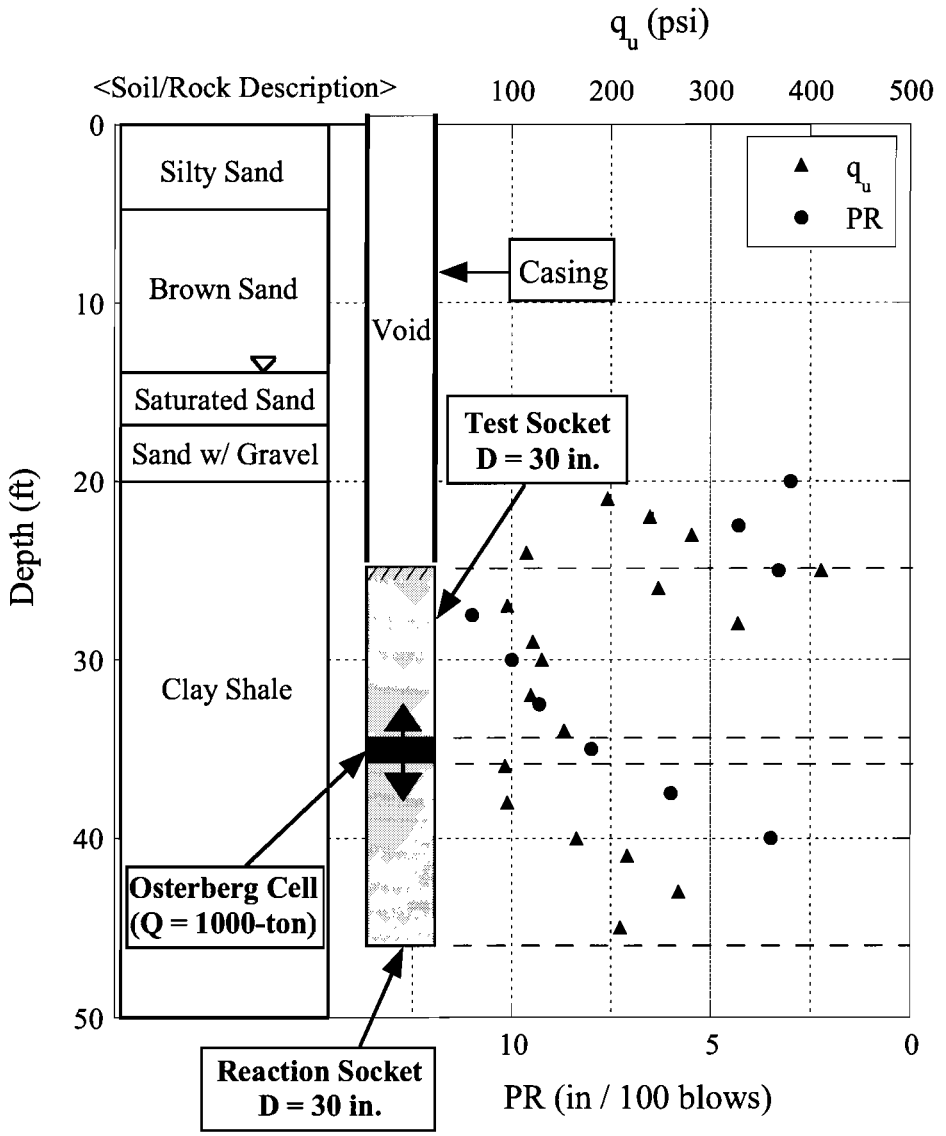

Figure 3.4. Geomaterial and Test Shaft Profile for Hampton Road Site

Denton Tap Site. There are low RQD values (about 20%), and a high degree of fracturing in the friable sandstone layers in the zone at depths of around 40 to 45 feet, so it was decided to keep the reaction socket out of his zone because of the uncertainty in capacity evaluation. That is, the reaction socket should extend no deeper than about 37 feet, leaving a depth of shale equal to one shaft diameter beneath the reaction shaft base. By considering this limitation the test shaft depth range was set at depths of 7.0 to 25.5 feet. From depths of 7.0 to 19.0 feet the shaft will be cast against overburden soil. Below 19.0 feet the shaft will socket into the rock. The diameter of the shaft and socket

will be 30 in. The Osterberg Cell will be placed in the depth range of 25.5 to 27.0 feet. The reaction socket will be placed in the depth range of 27.0 to 36.0 feet and will also have a diameter of 30 in. The laboratory test for overburden soils have not been completed, so the skin friction in the overburden soil was assumed to 0.6 tsf. The socket zone (20 ~ 27.5 ft) has the average compressive strength of 384.4 psi, an RQD of 72.2 %, and an average penetration resistance of about 6 inches per 100 blows. On the other hand, the reaction zone has the average compressive strength of 210.0 psi, RQD of 84.2 %, and an average penetration resistance of about 7 inches per 100 blows, which indicate that the quality of the rock in that zone is somewhat worse than in the test socket zone.

As before, several design methods were used to size the test shaft and reaction socket. The TxDOT method did not satisfy Eq. (3.2), but the other methods all satisfied Eqs. (3.1) and (3.2). The value of the base capacity for the reaction socket by the TxDOT method was lower than the values from other methods. The computed skin friction in the overburden was 56.5 tons, the average computed skin friction of the rock socket was 220.9 tons, yielding a combined capacity of 277.4 tons if both capacities can be added (on objective of the test). The average capacity of the reaction socket was 512.4 tons. The skin friction for the full shaft and the average capacity of the reaction socket were sufficient to satisfy Eqs. (3.1) and (3.2). Therefore, the Denton Tap site test shaft was judged acceptable with an overburden length of 12.0 feet, a test rock socket length of 6.5 feet, and a reaction socket length of 9.0 ft. Table 3.3 summarizes the design value computations by several design methods, and Figure 3.5 shows the geomaterial and test shaft profile for the Denton Tap site.

Table 3.3. Summary of Design Values for Denton Tap Site by Several Design Methods.

Design Methods	Skin Friction of Test Socket, R_S (Tons)	Skin Friction of Test Shaft, R_T (Tons)	Capacity of Reaction Socket, Q_R (Tons)	Remarks
TxDOT (2000)	153.2	209.7	286.3	- Using Figure 1.4. - Does not satisfy Eq. (3.2).
O'Neill and Hassan (1993)	102.6	159.1	417.9	- Using Eq. (2.4), (2.5), (2.6) for skin friction. - Using Eq. (2.56) for end bearing.
O'Neill et al. (1996)	141.2	197.7	448.3	- Using Figure 2.8 for skin friction. - Using Eq. (2.56) for end bearing. - Assuming non-bond and smooth interface, $\sigma_n/\sigma_p = 1.25$, and $\phi = 30°$.
FHWA (1999)	179.2	235.7	482.2	- Using Eq. (2.58) for skin friction. - Using Eq. (2.56) for end bearing. - Assuming smooth socket.
Collingwood and Seidel (2001)	197.6	254.2	501.7	- Using Figure 2.31 and 2.33 for skin friction. - Using Eq. (2.56) for end bearing. - Assuming SRC = 0.6.
Kulhawy and Phoon (1993)	389.8	446.4	697.8	- Using Eq. (2.29) for skin friction. - Using Eq. (2.56) for end bearing. - Assuming $\psi = 2$ / normal drilling conditions.
Williams (1980)	282.3	338.9	683.2	- Using Figure 2.19 for skin friction. - Using Eq. (2.56) for end bearing.
Rowe and Armitage (1987b)	321.0	377.6	582.0	- Using Eq. (2.19) for skin friction. - Using Eq. (2.56) for end bearing. - Assuming clean socket with roughness R1, R2 or R3.
Average	***220.9***	***277.4***	***512.4***	$1.5 \times 277.4 = 416.1 \leq 512.4$ and $416.1 \leq 1000 \Rightarrow$ ***O. K!***

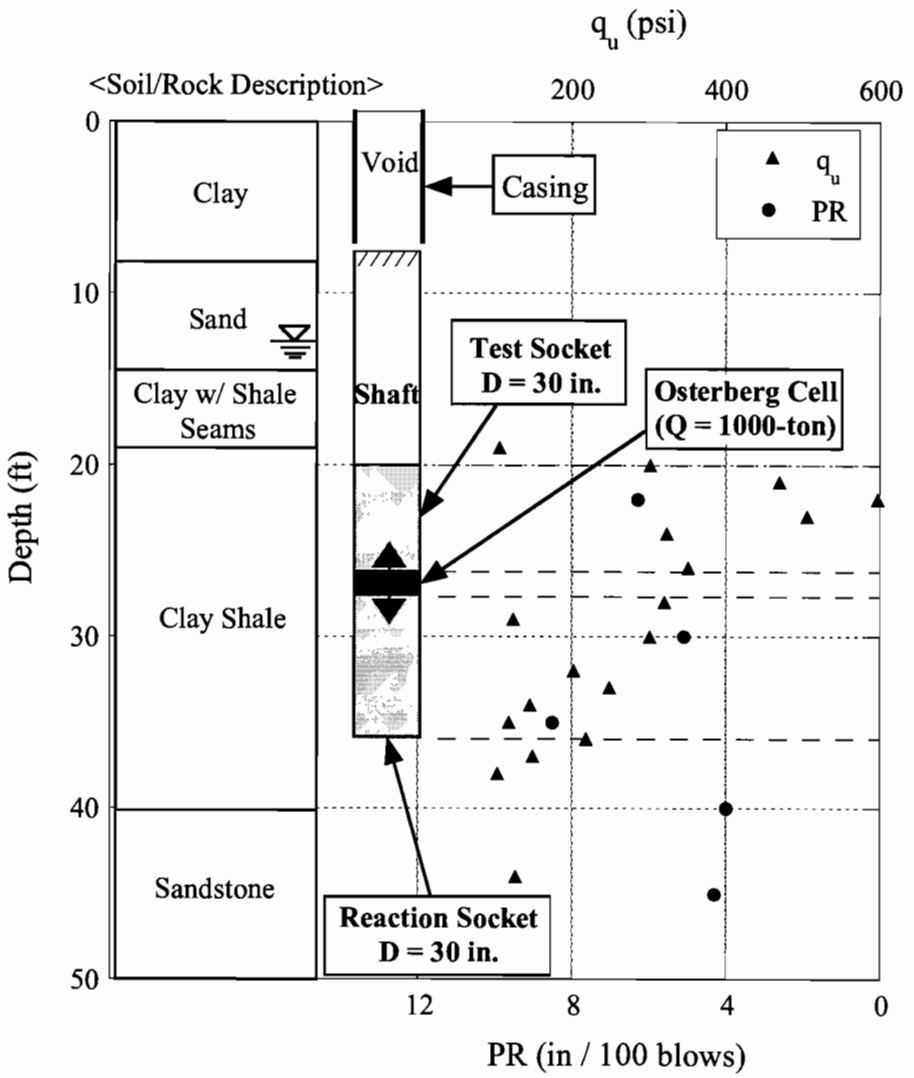

Figure 3.5. Geomaterial and Test Shaft Profile for Denton Tap Site.

East Rowlett Creek Site. The rock socket will be placed in the depth range of 10.0 feet to 17.5 feet, with a diameter of 30 in. The reaction socket will be placed in the depth range of 19.0 feet to 24.0 feet, also with a diameter of 30 in. The depth range 17.5 feet to 19.0 feet is for the placement of the Osterberg Cell. The limestone in the test socket zone has an average compressive strength of 1360.3 psi, RQD of 85.4 %, and an average

penetration resistance of about 1.8 inches per 100 blows. Similarly, the reaction zone has an average compressive strength of 1412.2 psi, RQD of 96.5 %, and an average penetration resistance of about 1 inch per 100 blows, which represent a slightly higher quality rock than that in the test socket zone.

As before, several design methods were used to size the rock and reaction sockets. The average skin friction of test socket from those methods was 720.7 tons, and the average capacity of reaction socket was 1275.1 tons. The Rowe and Armitage design method produced higher skin friction in the test socket than the others, but the reaction capacity was also accordingly higher. The values from the Rowe and Armitage method did not satisfy Eq. (3.2). However, the reaction capacity had a safety factor of about 1.3 against skin friction in the test socket. The others design methods all satisfied Eqs. (3.1) and (3.2). Therefore, the design of the test arrangement for the East Rowlett Creek site was considered acceptable with a test socket length of 7.5 feet and a reaction socket length of 5.0 feet. Table 3.4 summarizes the design values obtained by several design methods discussed in Chapter 2, and Figure 3.6 shows the geomaterial and test shaft profile for East Rowlett Creek site.

The results for all sites are summarized in Table 3.5. In addition, for the Lone Star Office Park site is profiled in Figure 3.7, and the Belt Line Road site is profiled in Figure 3.8.

Rebar cages are needed to provide support for Osterberg Cell hoses, telltales and leads for instrumentation along the shafts, in addition to assuring that failure will not be by exceeding the structural capacity of the shaft. The rebar cages were designed with a 24-inch OD, with 1 % longitudinal rebar (8 No. 8 bars equally spaced) and No. 3 smooth bar used as spiral steel with a 6-inch pitch. The concrete mix for the test and reaction sockets shall be TxDOT Item 421 (1993) Type C concrete with a No. 5 coarse aggregate gradation (3/4 inch maximum aggregate size). However, the desired slump range is modified to 7 inch (minimum) to 8 inch (maximum). This may require the cement factor to be increased beyond that specified by TxDOT. The reasons for the concrete specifications are primarily related to the fact that the steel in the reaction sockets (twin channels to support the weight of the steel in the test socket and the Osterberg Cell) must be pushed through the standing concrete, which should offer minimal resistance to placement.

Table 3.4. Summary of Design Values for East Rowlett Creek Site by Several Design Methods

Design Methods	Skin Friction of Socket, R_S (Ton)	Capacity of Reaction, Q_R (Ton)	Remarks
TxDOT (2000)	500.7	785.4	- Using Figure 1.4.
O'Neill et al. (1996)	317.0	1005.3	- Using Figure 2.8 for skin friction. - Using Eq. (2.56) for end bearing. - Assuming non-bond and smooth interface, $\sigma_n/\sigma_p = 1.25$, and $\phi = 30°$.
FHWA (1999)	388.9	1054.0	- Using Eq. (2.58) for skin friction. - Using Eq. (2.56) for end bearing. - Assuming smooth socket.
Collingwood and Seidel (2001)	864.6	1388.2	- Using Figure 2.31 and 2.33 for skin friction. - Using Eq. (2.56) for end bearing. - Assuming SRC = 0.4.
Kulhawy and Phoon (1993)	846.2	1364.6	- Using Eq. (2.29) for skin friction. - Using Eq. (2.56) for end bearing. - $\psi = 2$ normal drilling conditions.
Williams (1980)	576.4	1148.9	- Using Figure 2.19 for skin friction. - Using Eq. (2.56) for end bearing.
Rowe and Armitage (1987b)	1551.1	2002.5	- Using Eq. (2.19) for skin friction. - Using Eq. (2.56) for end bearing. - Assuming clean socket with roughness R1, R2 or R3. - Does not satisfy Eq. (3.2).
Average	***720.7***	***1275.1***	$1.5 \times 720.7 = 1081 \leq 1275.1$ and $1081 \leq 1800 \Rightarrow$ ***O. K!***

Table 3.5. Average Capacity Results for Each Test Site.

Sites		Hampton Road	Denton Tap	East Rowlett Creek
Overburden	Depth (ft)	-	7.0~ 19.0	-
	Skin Friction (tons)	-	56.5	-
Test Socket	Depth (ft)	25.0 ~ 35.0	19 ~ 25.5	10 ~ 17.5
	Skin Friction (tons)	241.0	220.9	720.7
Reaction Socket	Depth (ft)	36.5 ~ 46.5	27.0 ~ 36.0	19.0 ~ 24.0
	Total Available Reaction (tons)	453.9	512.4	1275.1

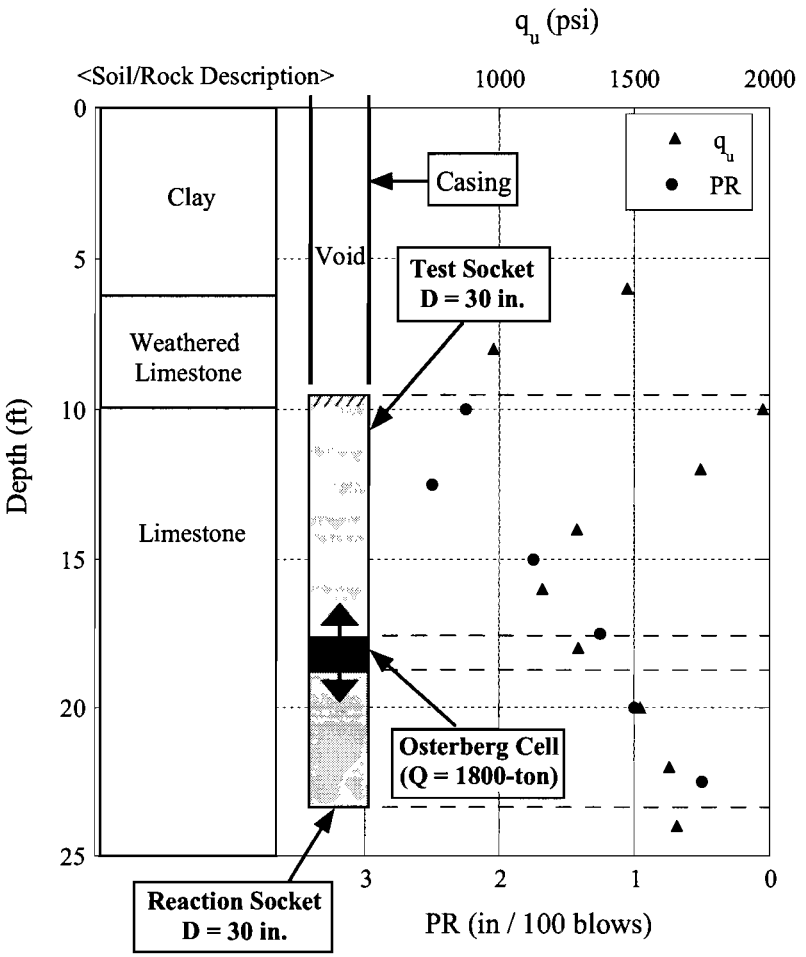

Figure 3.6. Geomaterial and Test Shaft Profile for East Rowlett Creek Site.

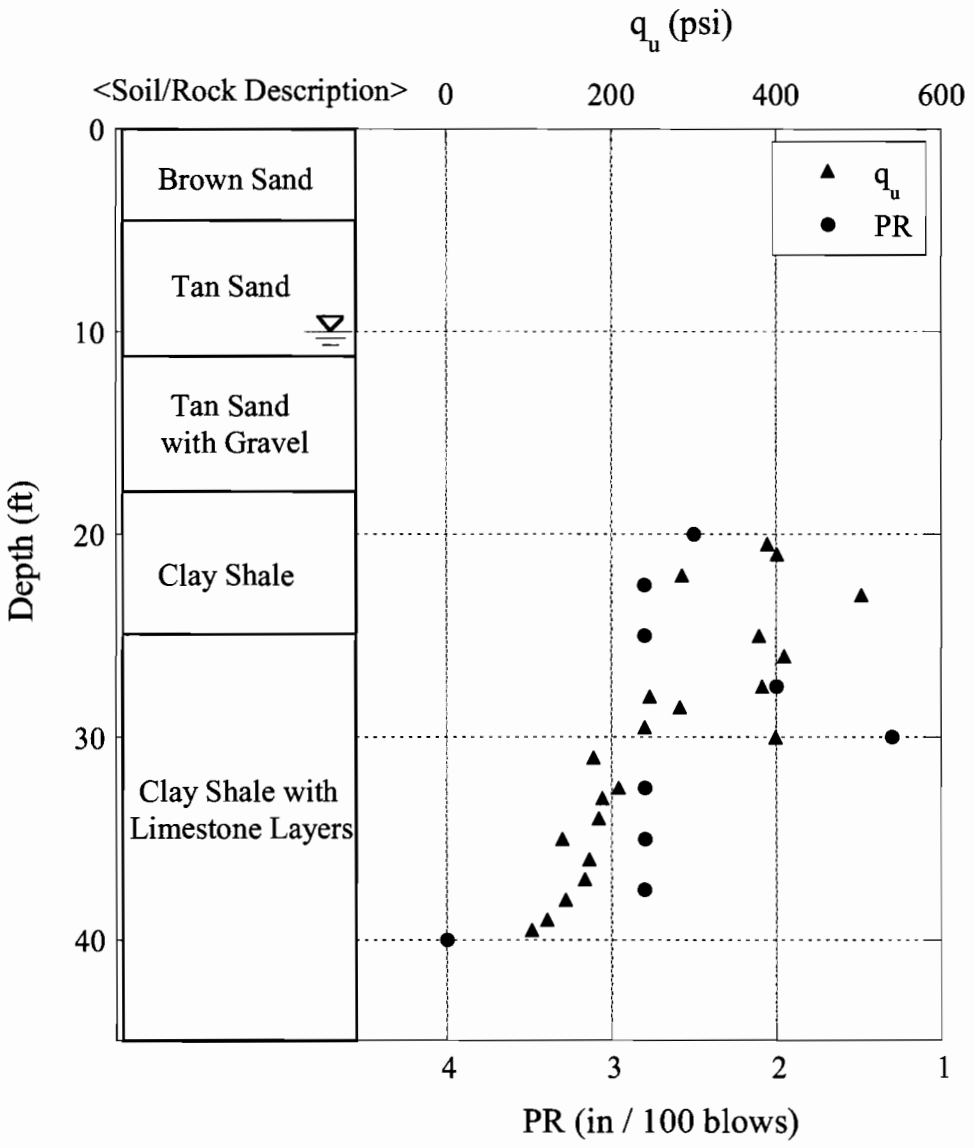

Figure 3.7. Geomaterial Profile for Belt Line Road Site.

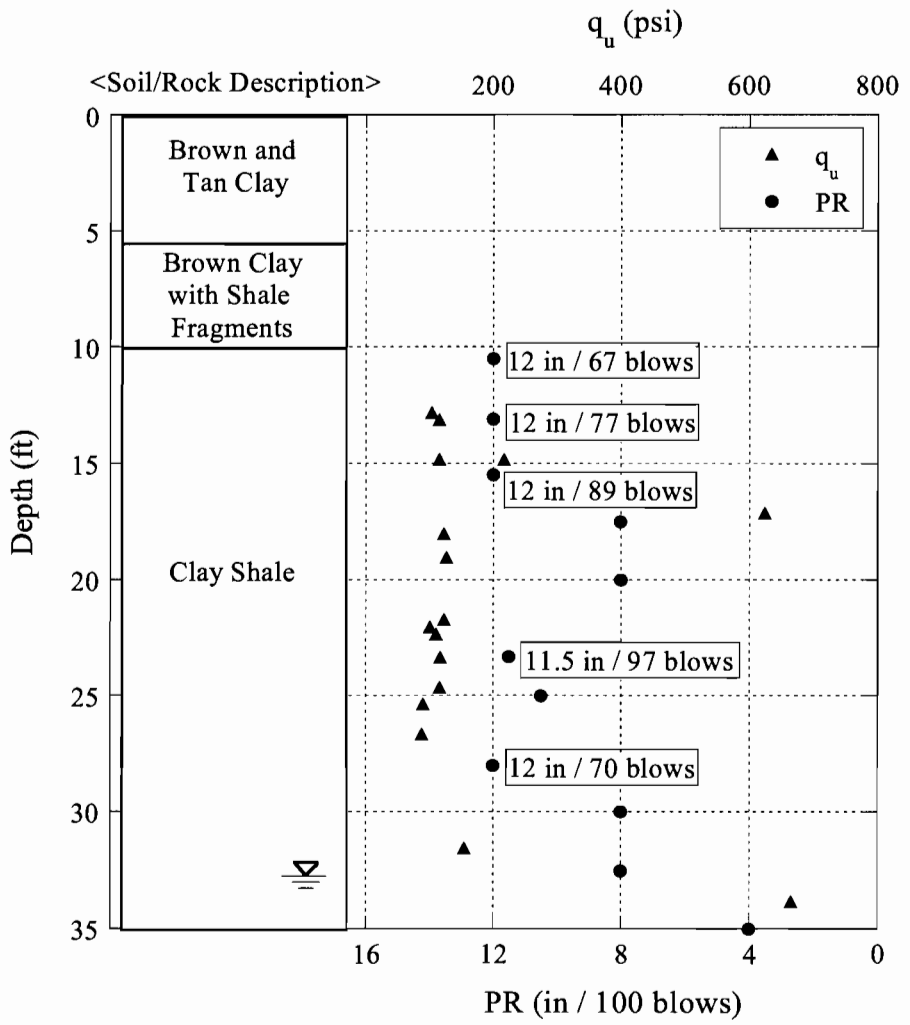

Figure 3.8. Geomaterial Profile for Lone Star Office Park Site.

Drawings of Cages, Instruments and Osterberg Cell for Each Test Shaft

Drawings of cages, instruments and Osterberg Cells for each test shaft will be provided to the South Central Chapter of ADSC, which has volunteered to construct the test sockets. The drawings include the cages, Osterberg cells, and connections between the cells and the cages (including telltales and instruments). The Osterberg Cells will be purchased from Loadtest, Inc., of Gainesville, Florida, which is providing the cells and technical assistance to this project at cost. Mr. Robert Simpson of Loadtest has provided input into the design of the plates and connections

between the Osterberg Cells and longitudinal steel. The instruments will consist of vibrating wire sister bars attached to the reinforcing cages, which will be purchased from GeoKon, Inc., of Lebanon, New Hampshire. Figure 3.9 locates the borings and test shafts. Figures 3.10 to 3.12 are drawings of cages, instruments and Osterberg Cell for the test shafts.

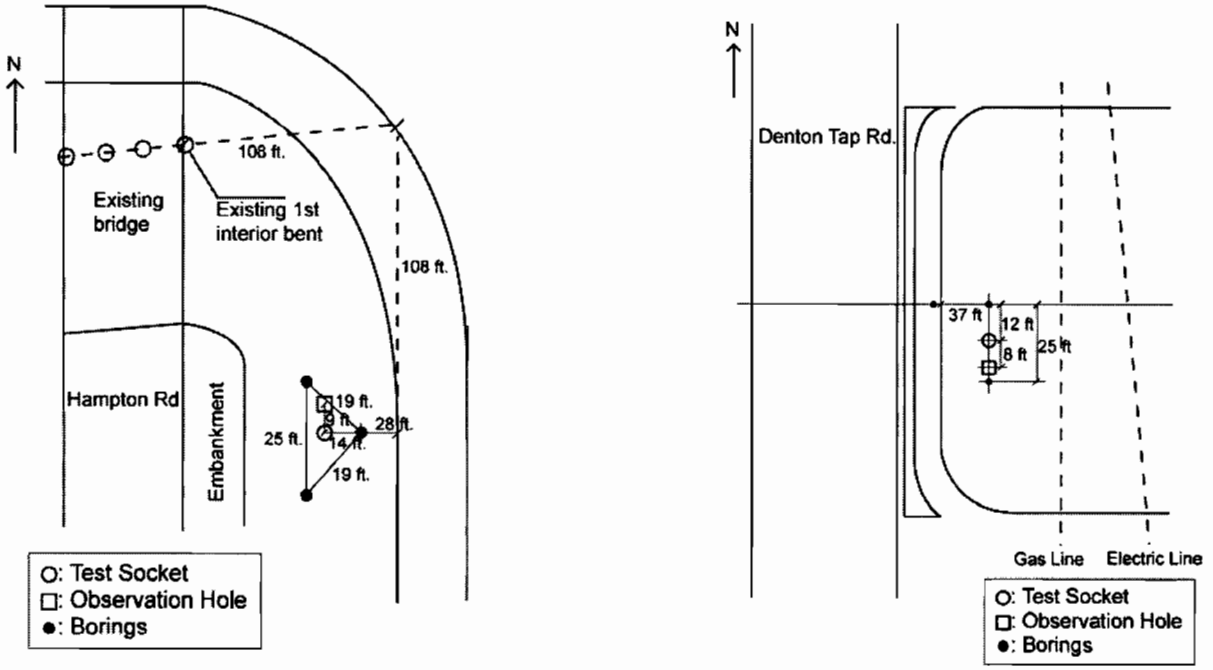

a. Hampton Road Site

b. Denton Tap Road Site

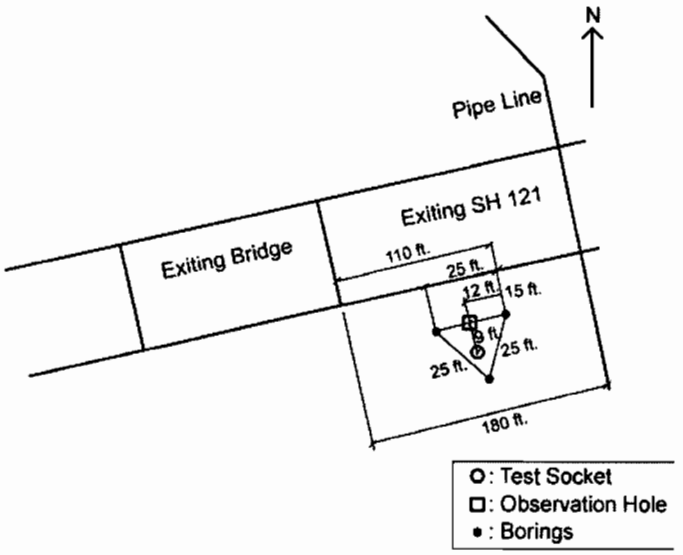

c. East Rowlett Creek Site

Figure 3.9. Location Drawings for Borings and Test Shafts.

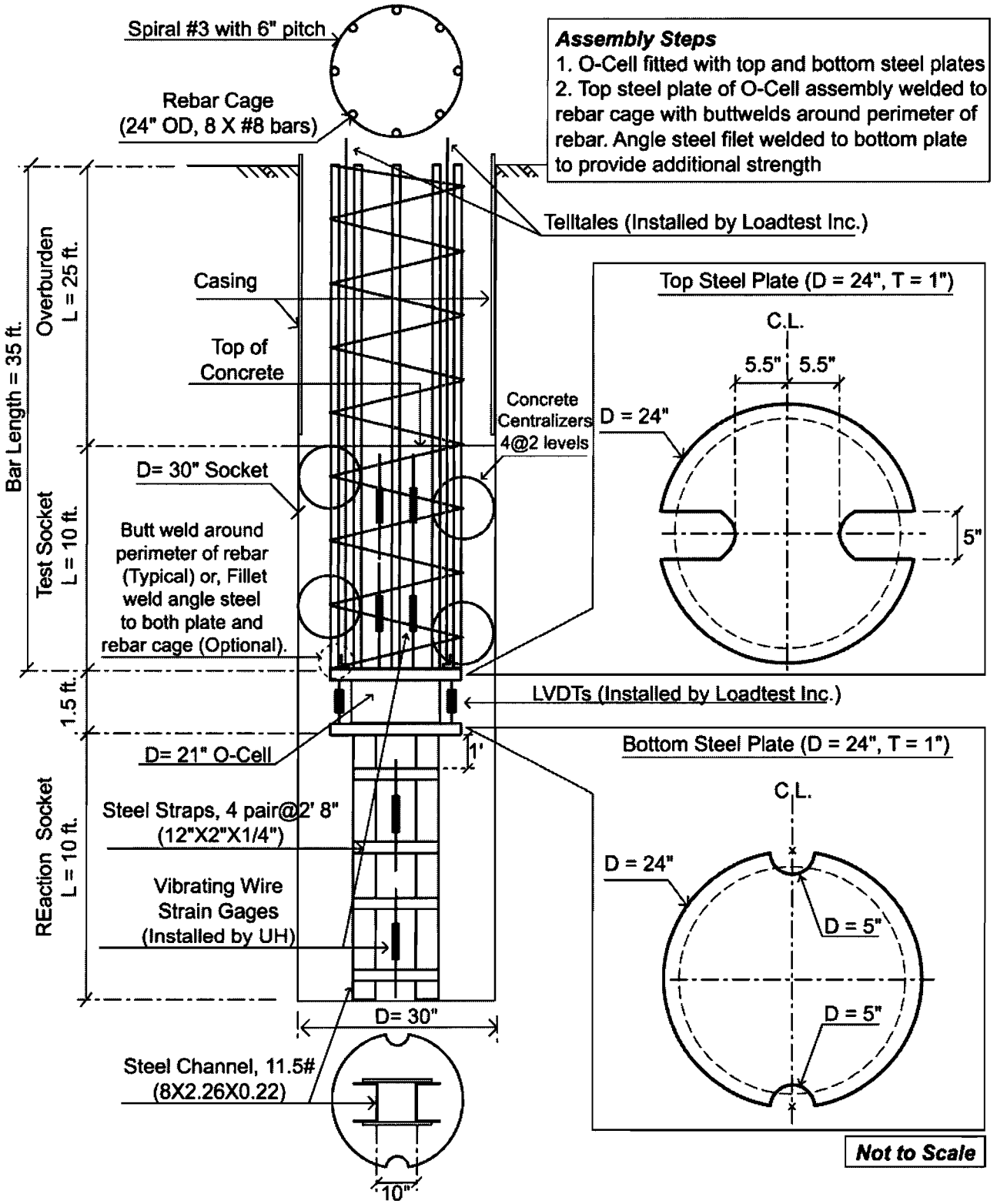

Figure 3.10. Drawing of Cage, Instruments and Osterberg Cell for Hampton Road Site.

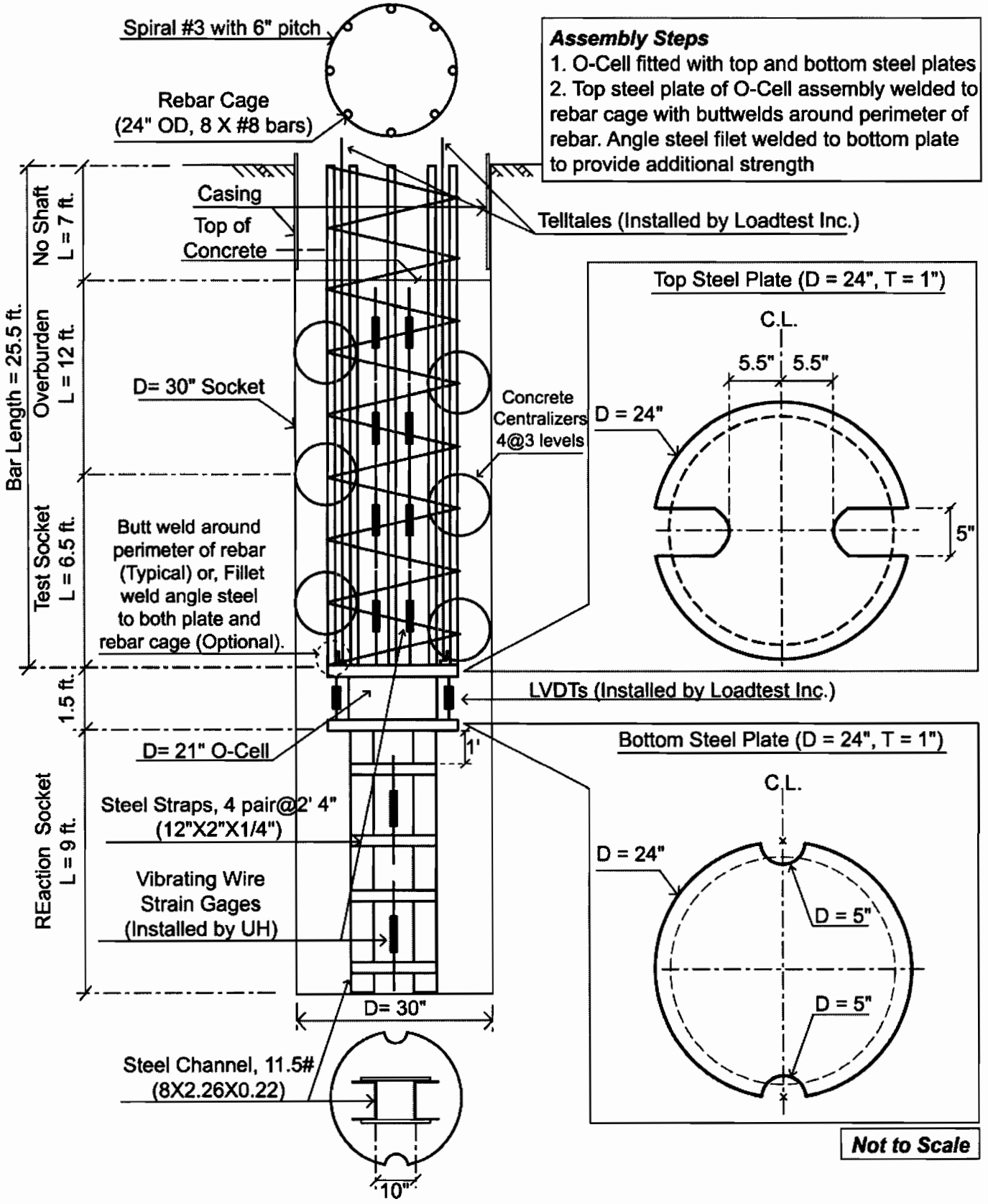

Figure 3.11. Drawing of Cage, Instruments and Osterberg Cell for Denton Tap Site.

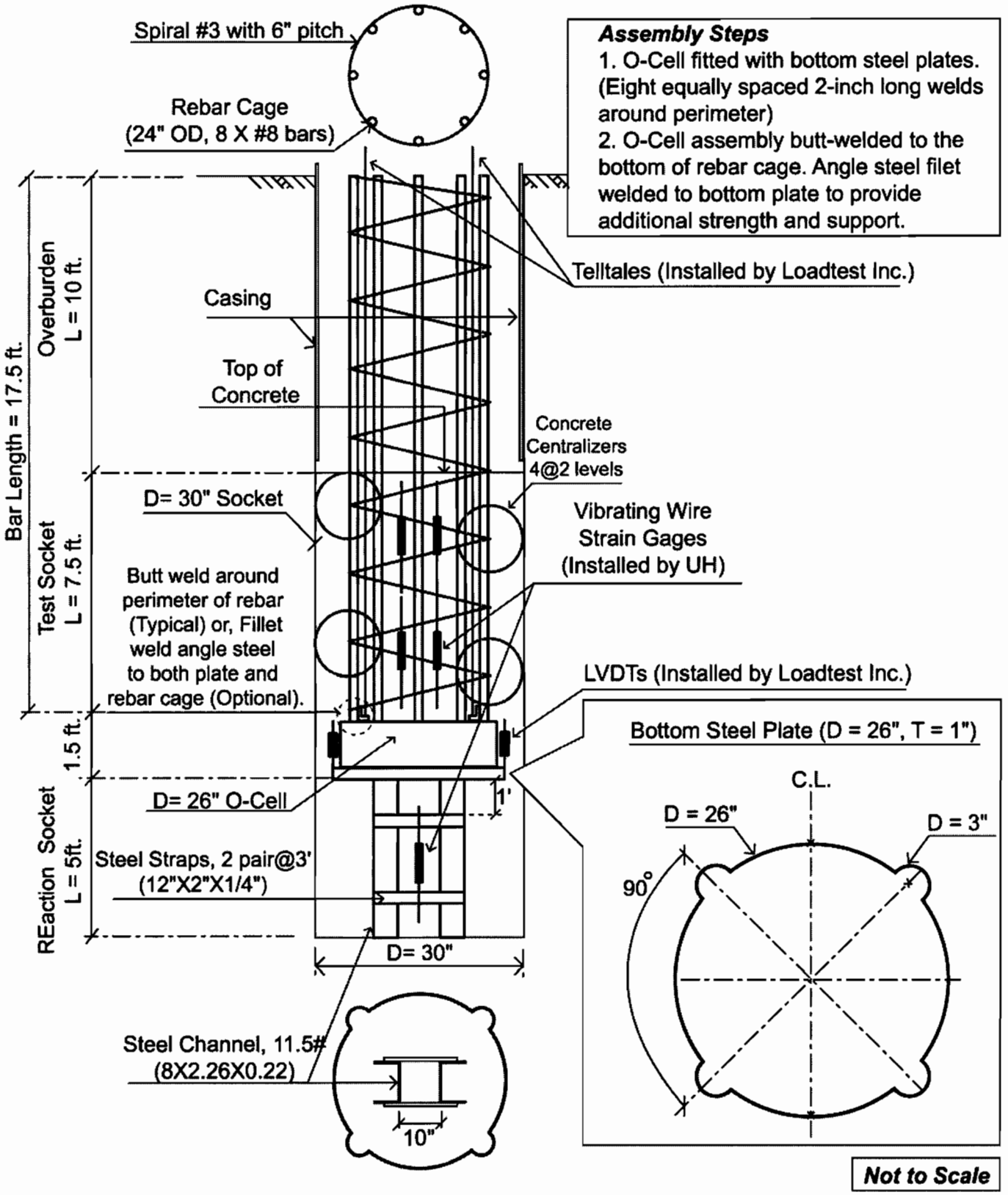

Figure 3.12. Drawing of Cage, Instruments and Osterberg Cell for East Rowlett Creek Site.

Static Penetrometer

The static penetrometer documented briefly here is intended to be used as a tool for verification that a rock stratum has been reached, especially when drilling under a drilling slurry, in which the bottom of the borehole cannot be observed and the cuttings may be so disturbed that overburden (soil) cuttings cannot be easily distinguished from cuttings in soft rock. The static penetrometer is a simple mechanical device that is attached to the bottom of the Kelly bar on the drilling contractor's drill rig using the same pin (Kelly pin or tool pin) that is used to attach drilling tools (augers, core barrels, etc.). It is based on the concept of the "pocket penetrometer," which has been used by field geotechnical boring loggers in soil for many years.

Sketches showing the design of the static penetrometer are given in the Sheets and Materials list that follow this text. At present, most parts need to be made and the device assembled in a machine shop. A key part is the spring (Item 3 on Sheet 1), which must have a spring constant equal to or very close to that shown in the materials list. The height of the reading ring and the location of the score marks are also critical items.

Calibration

The assembled penetrometer was calibrated in a load frame using an electronic load cell. Three score, or calibration, marks were placed on the body of the penetrometer based on this calibration. These marks are intended to represent soils or rocks with unconfined compression strengths (q_u) of 100 psi (Mark A), 200 psi (Mark B), and 300 psi (Mark C), representing hard soil (A), very soft or weathered clay shale (B), and sound clay-shale to soft limestone (C). It was assumed that the bearing failure induced by the piston of the penetrometer is undrained, since penetration takes only a few seconds. It was also assumed that the bearing capacity factor for the toe of the piston would be 4 with respect to q_u. Using the known area of the toe of the piston and values of ultimate bearing capacity of 400 psi (A), 800 psi (B) and 1200 psi (C), spring forces

corresponding to the three marks were computed and the score marks were placed as shown in Table X.X.

Table X.X. Spring Forces Corresponding to Score Marks on Static Penetrometer: Spring Constant = 1728 pounds/inch.

Score Mark	Geomaterial Represented	q_u (psi)	Bearing Capacity (psi)	Toe area (in^2)	Spring Force (pounds)	Location of Score Mark (in. aboveTop of Protector Plate)
A	Hard soil (overburden)	100	400	1.720	688.1	1.50
B	Soft or highly weathered clay-shale	200	800	1.720	1376.3	1.90
C	Sound clay-shale or soft limestone	300	1200	1.720	2064.4	2.30

The static penetrometer was then calibrated in the field in boreholes that were drilled at the test sites (Rowlett Creek, Denton Tap, Hampton Road). The readings at these sites, together with the values of q_u measured in cores taken from the same elevation as the penetrometer test and TxDOT penetration resistance values at the same elevation in nearby boreholes, are given in Table X.X. The readings were all made in open boreholes, not under slurry.

Based on this research, a static penetrometer reading between score marks B and C ("B-C") is indicative of soft, sound clay shale, and a reading of C or higher is indicative of sound limestone or sound, hard clay shale. Readings of B, A-B and A are indicative of overburden materials.

Table X.X. Static Penetrometer Readings at Test Sites (October 21 – 26, 2002)

Site	Depth (ft)	Geomaterial	Reading	q_u (psi)	Penetration Resistance (TxDOT) - in. per 100 Blows
Rowlett Creek	0.5	Medium stiff wet clay	Less than A (min.)	-	-
	3	Stiff, gravelly clay	B-C	-	-
	3.5	**Soft, blocky, highly weathered rock**	**A-B (failures along blocks)**	**-**	**-**
	6	***Sound gray limestone***	***Higher than C (max)***	***950***	***2.2***
Hampton Road	0.5	Soft, moist clay	Less than A (min)	-	-
	2.5	Tan, moist sand	Less than A (min)	-	-
	21	**Gray, soft, slightly blocky clay-shale**	**B-C**	**197**	**3.0**
	22	**Gray, soft, slightly blocky clay-shale**	**B-C**	**197**	**3.0**
	40	**Gray, stiff laminated clay-shale**	**B-C w/o crowding Kelly C w/ crowd**	**170**	**3.5**
Denton Tap	16	Stiff clay / clay-shale mixture	A-B	-	-
	20	Soft, slightly blocky clay shale	B	302	6.5
	36.5	**Dark gray clay shale, slightly sandy**	**B-C**	**212**	**8.5**

Entries in **boldface** indicate sound soft rock with q_u generally above 200 psi. The entry in ***italicized boldface*** indicates sound, relatively hard rock with q_u of about 1000 psi.

Operation

The details of operation of the static penetrometer are important. These details are reviewed in the following. Figures X.X – X.X are photos of the penetrometer that show most of the elements referred to below.

1. Note the weight of the Kelly bar. Hollow Kelly bars may weigh 2000 to 2500 pounds for an "LDH" or similar drilling rig. This weight may not be sufficient to push the penetrometer toe at least 2 inches into sound geomaterial at the bottom of the borehole, which is necessary in order to obtain the correct reading. Solid Kelly bars for LDH or similar rigs generally weigh 4000 to 4500 pounds, which should be sufficient to affect a 2-inch penetration, or at least a C reading. If the weight is in the lower range, tell the rig operator to be prepared to "crowd" the penetrometer very slightly when its toe is resting on the bottom of the borehole.

2. Slide the reading ring / sliding ring assembly until it is resting firmly against the reading ring pins (Item 7 on Sheet 2).

3. Slip the Kelly adaptor (Item 1, Sheet 3) over the bottom tip of the Kelly bar and secure the penetrometer to the Kelly bar with a standard tool pin. Note that the adaptor is designed for use with a square Kelly bar with a side dimension of 4.25 inches.

4. Lower the Kelly bar with the penetrometer until the penetrometer toe rests on the bottom of the borehole. Avoid the middle of the hole, where a "stinger hole" may be present (Fig. X.X). After a brief (2 – 3 second) pause, let the weight of the Kelly rest on the penetrometer. This will force the piston into the geomaterial until the geomaterial fails and at the same time push the reading ring into a position on the outside of the penetrometer body that reflects the force required to cause geomaterial failure (through the relation between spring movement and force). The reading ring will stop moving even though the penetrometer is pushed farther into the geomaterial than is necessary to

produce failure. [The protector plate (Item 10, Sheet 2) is included to limit the drag on the reading ring if the piston is over-pushed.] If the Kelly is hollow (light, especially when buoyed in slurry), place a small crowd on the Kelly to make sure that the toe penetrates at least two inches.

5. Extract with Kelly with the penetrometer. The reading ring will stay in place during this operation.

6. Wipe off the penetrometer around the reading ring and score marks, being careful not to move the reading ring, and read the penetrometer value (less than A, A, A-B, B, B-C, C, greater than C).

7. Decide whether the reading is satisfactory, and inform the contractor what base elevation will be acceptable. For example, if the penetrometer test is performed to identify top of rock, the acceptable base elevation will be the current elevation minus the design length of the socket in the soft rock, if the penetrometer test is successful. If the penetrometer test is performed to identify the bearing surface, inform the contractor whether or not the geomaterial at the current elevation will suffice as the bearing material. Note that this penetrometer test is not sensitive enough to identify loose cuttings at the bottom of the borehole. Even though the parent geomaterial is acceptable, careful cleanout procedures should always be followed.

8. Remove the penetrometer by first removing the tool pin. It may be necessary to drive the pin out with a sledge hammer. The penetrometer is quite robust and should not be damaged by such action.

9. Once the penetrometer is removed from the Kelly, wipe and wash all of the slurry, soil and rock off its surfaces. At the end of the day, apply a little light oil lubricant

to the space between the piston and the bushing shown in Sheet 1. The penetrometer should then be ready for further use.

The penetrometer was designed to be handled by one person. However, it is a heavy object. The user should therefore decide whether he or she can maneuver the penetrometer safely. If it cannot be maneuvered safely a second person should be called upon to help.

References

Hassan, K. M., O'Neill, M. W., Sheikh, S. A., and Ealy, C. D. (1997). "Design Method for Drilled Shafts in Soft Argillaceous Rock," *Journal of Geotechnical and Geoenvironmental Engineering*, Vol. 123, No. 3, ASCE, pp.272 – 280.

TxDOT (1993). *"Standard Specifications for Construction of Highways, Streets and Bridges,"* Texas Department of Transportation, Austin, Texas.

Appendix

Appendix A.1. Laser Borehole Roughness Profiling System Summary

Figures A.1.1 through A.1.8 summarize the laser borehole roughness profiling system. The system was calibrated in the laboratory and found to have an accuracy of approximately 0.2 mm on both vertical distance and interface roughness (radial distance). It was then tested under field conditions and found to provide reasonable roughness profiles of a borehole drilled in stiff clay soils in Houston. Occasional spurious signals were output during field testing, which were likely caused by very small clods of soil that stuck to the sides of the borehole and produced reflected laser ray angles that are outside the limits of the system. These spurious signals appear as very sharp spikes of very short wave length (e. g., $\leq$ 0.1 in.), which can easily be filtered out of the data set if desired. It is noted that the profiles shown in Figure A.1.8 are roughness profiles referred to an arbitrary zero radius. That is, these profiles are not an indication of true borehole radius or diameter.

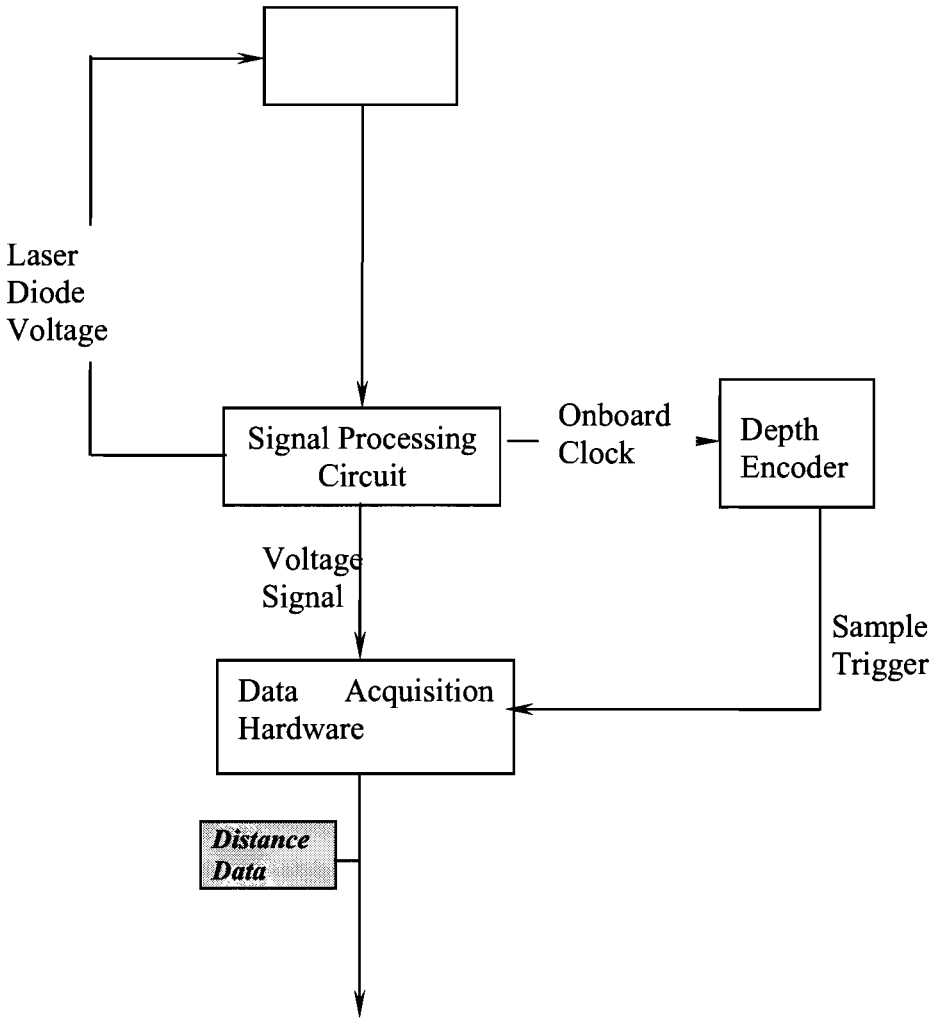

Figure A.1.1. Overall Schematic of Laser Borehole Roughness Profiling System

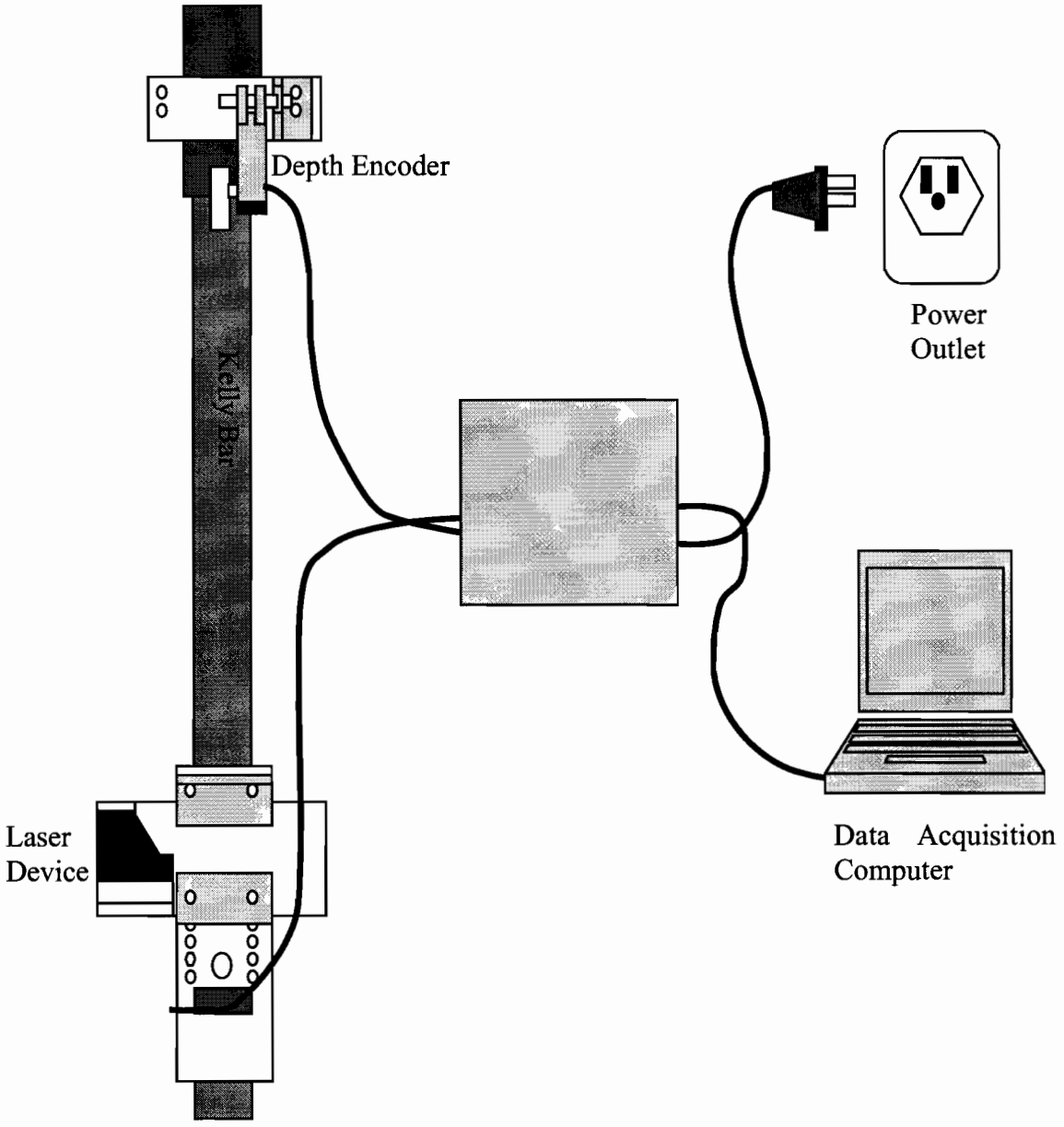

Figure A.1.2. Physical Arrangement of Laser Borehole Profiling System Hardware

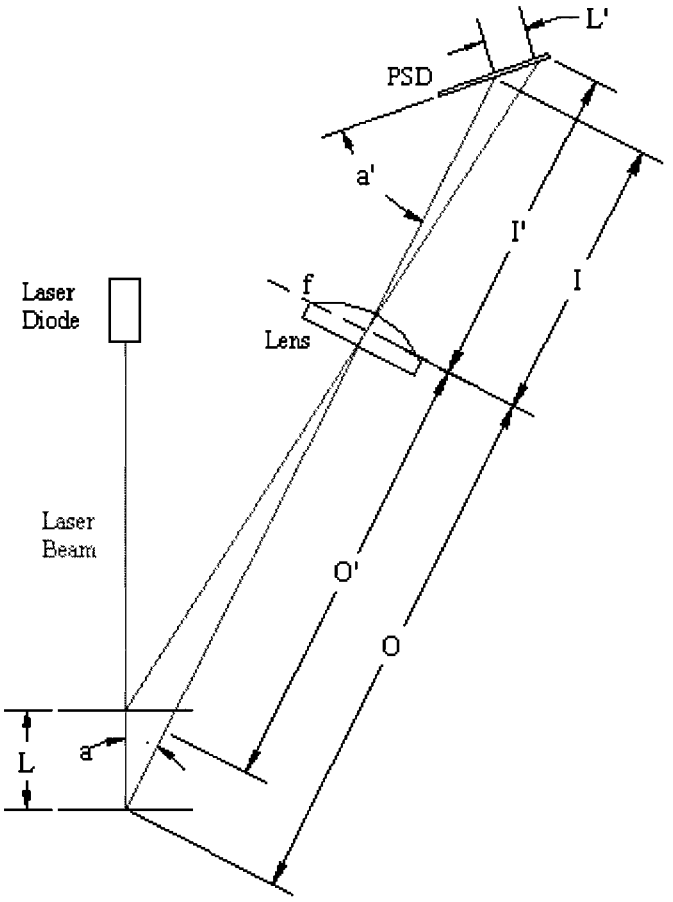

Basic Optics:

$$L = \frac{(O-f)L' \sin a'}{L' \cos a \sin a' + f \sin a}$$

$$\tan a' = \frac{L' \sin a'}{I - I'} = \frac{fL \sin a}{O - L\cos a - f} \times \frac{(O-f)(O - L\cos a - f)}{f^2 L \cos a'}$$

$$I = \frac{Of}{O-f}$$

L' is sensed on the position sensitive detector (PSD); f is the known focal length of the lens, a (angle) is a designed property of the profiler (constant); the above three equations are solved simultaneously using software in the data acquisition system to obtain L.

Figure A.1.3. Principle of Operation of Laser Borehole Roughness Profiler

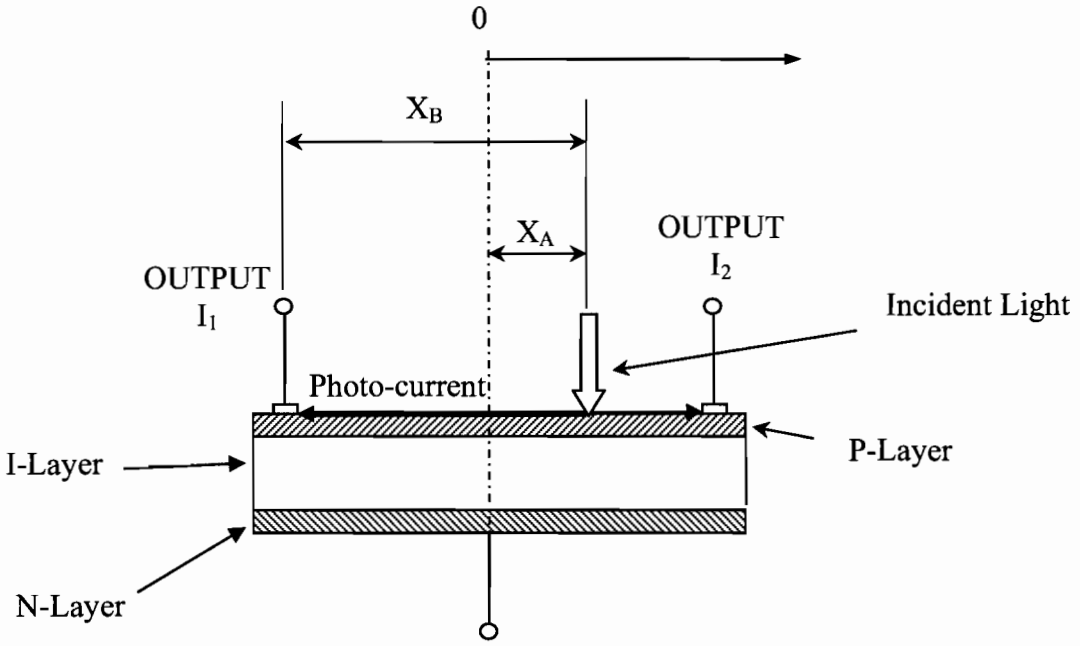

Figure A.1.4. Schematic of Position-Sensitive Detector

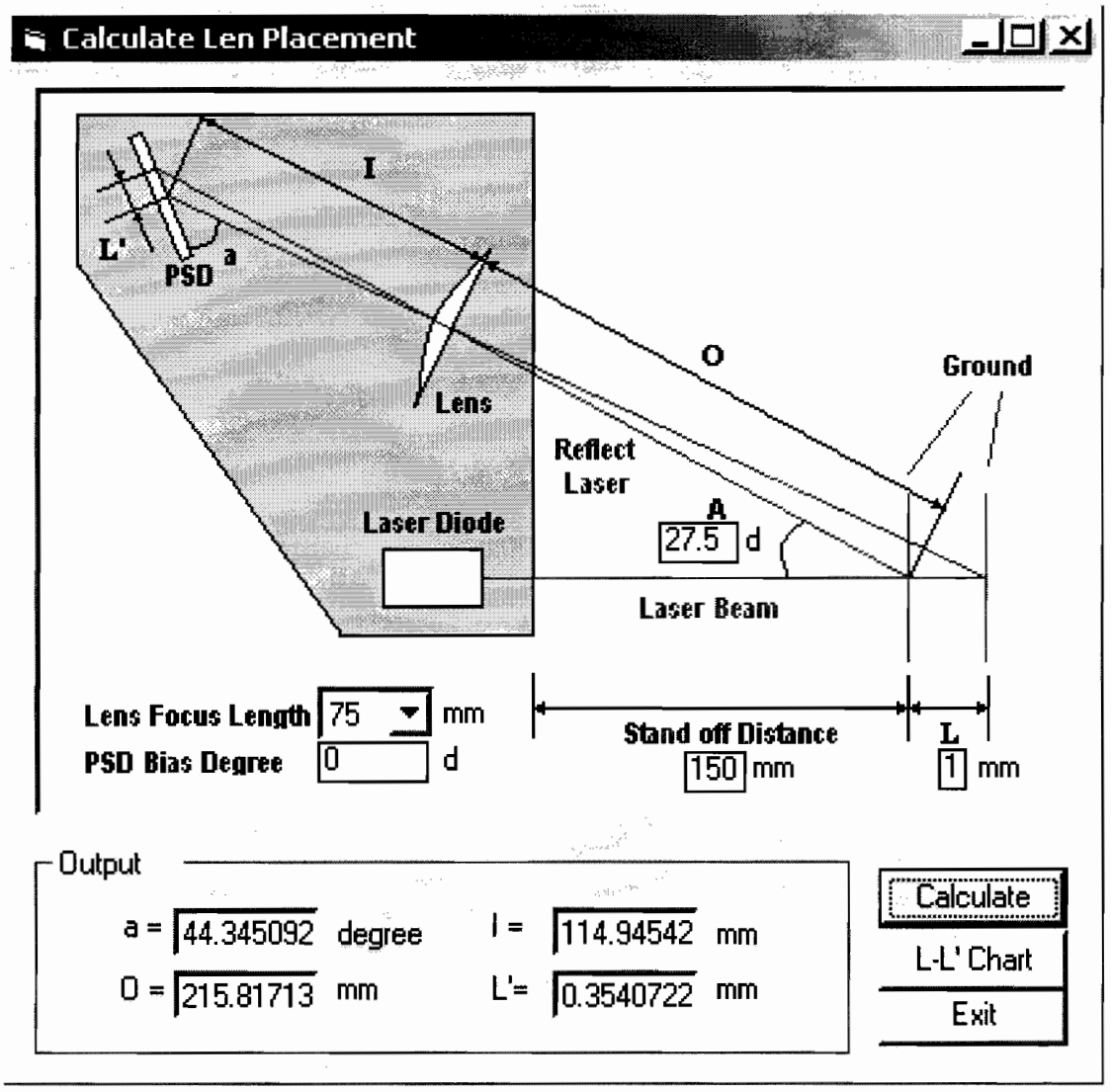

Figure A.1.5. Initial Set-up Screen (Visual Basic) for Data Acquisition Program (Field Readout Device)

Figure A.1.6. Photo of Placement of Depth (Distance) Encoder on Kelly Bar and Kelly Bar Drive Shaft

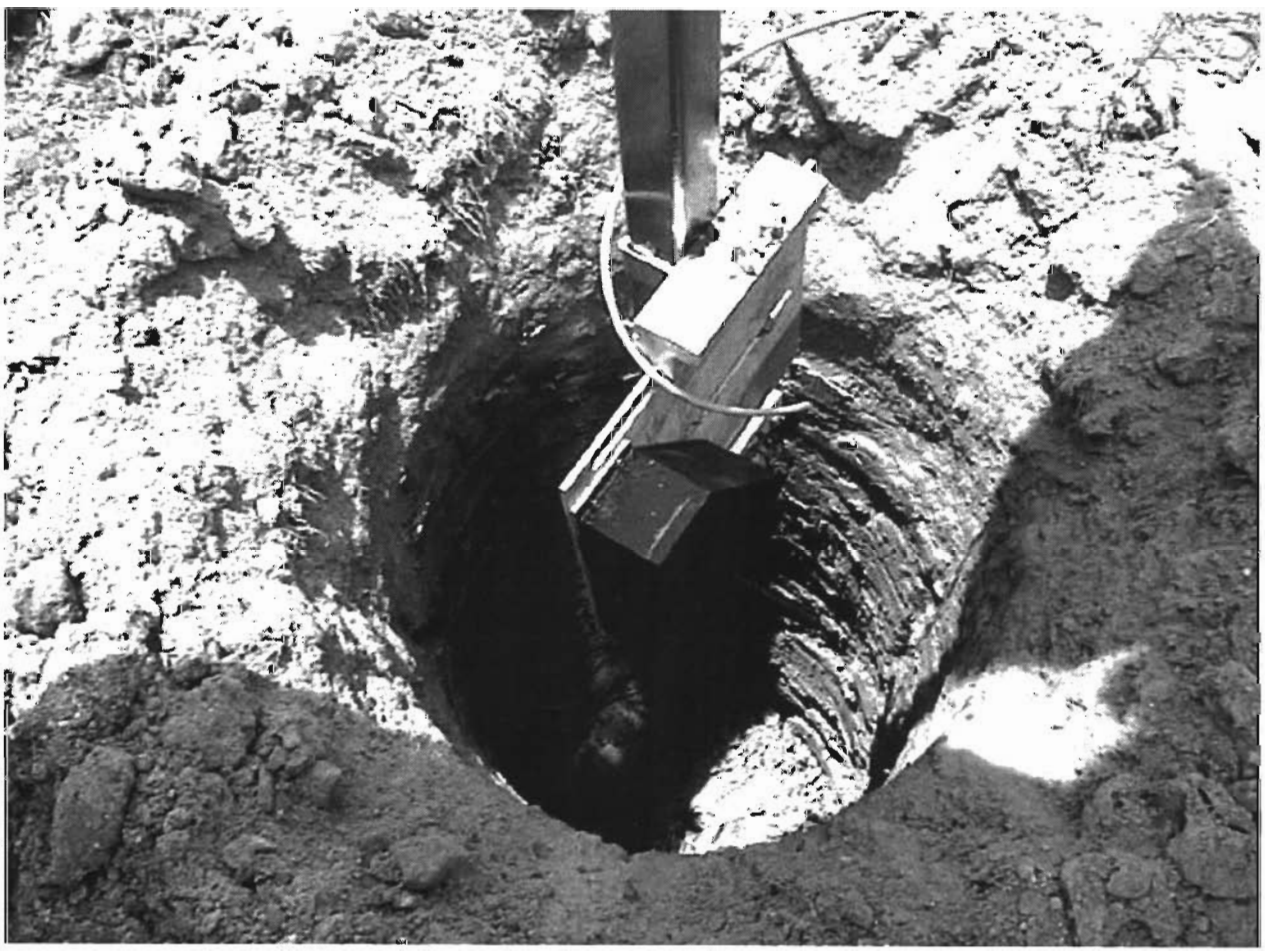

Figure A.1.7. Photo of Laser Borehole Roughness Profiler Affixed to Kelly Bar under Test in Stiff Clay at University of Houston Site.

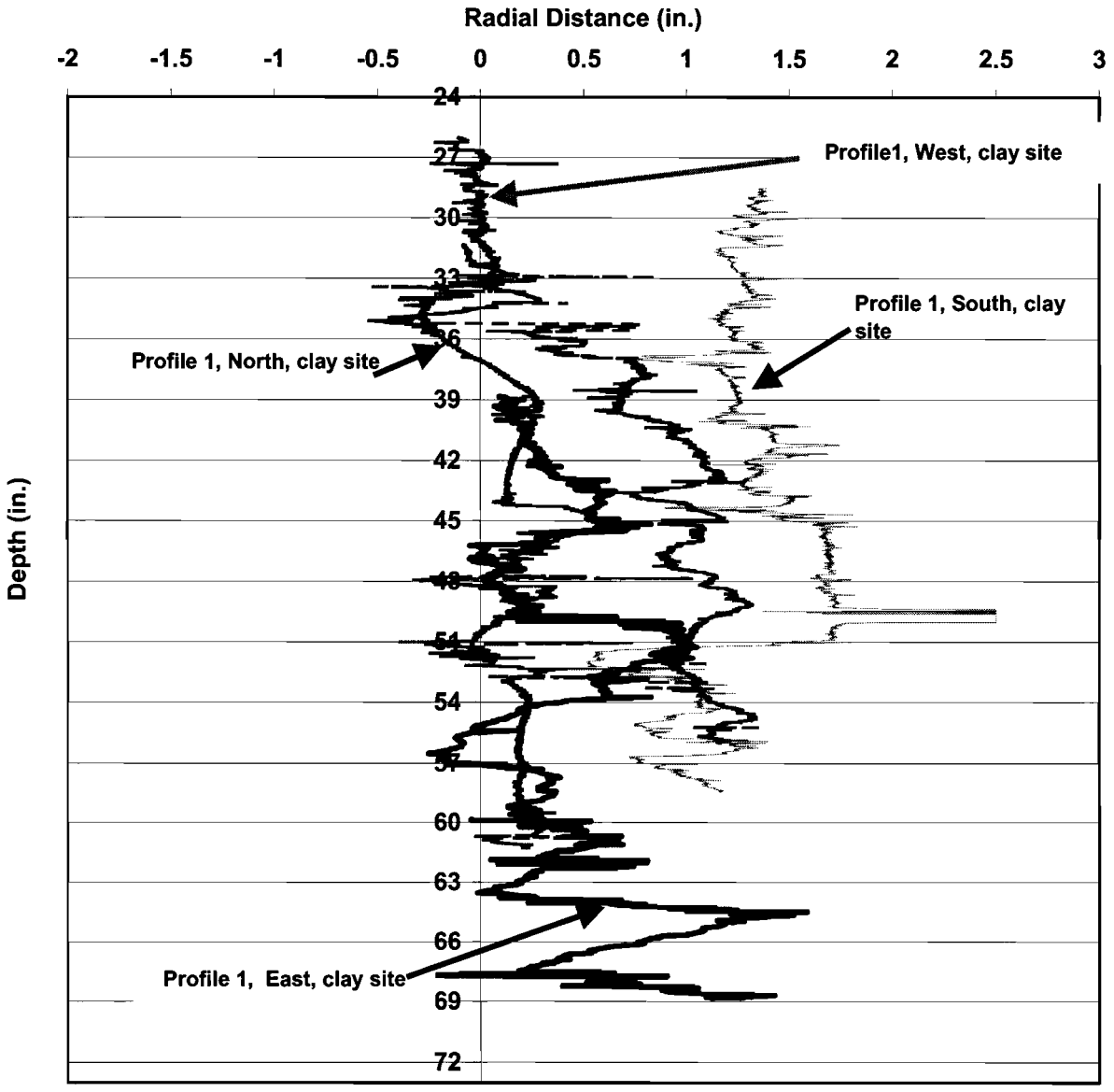

Figure A.1.8. Example of Roughness Profiles Measured with Laser Borehole Roughness Profiler at UH Stiff Clay Site.

Appendix A.2. Static Penetrometer Design Sketches (including minor modifications made following field tests in October, 2002)

All dimensions are shown in inches

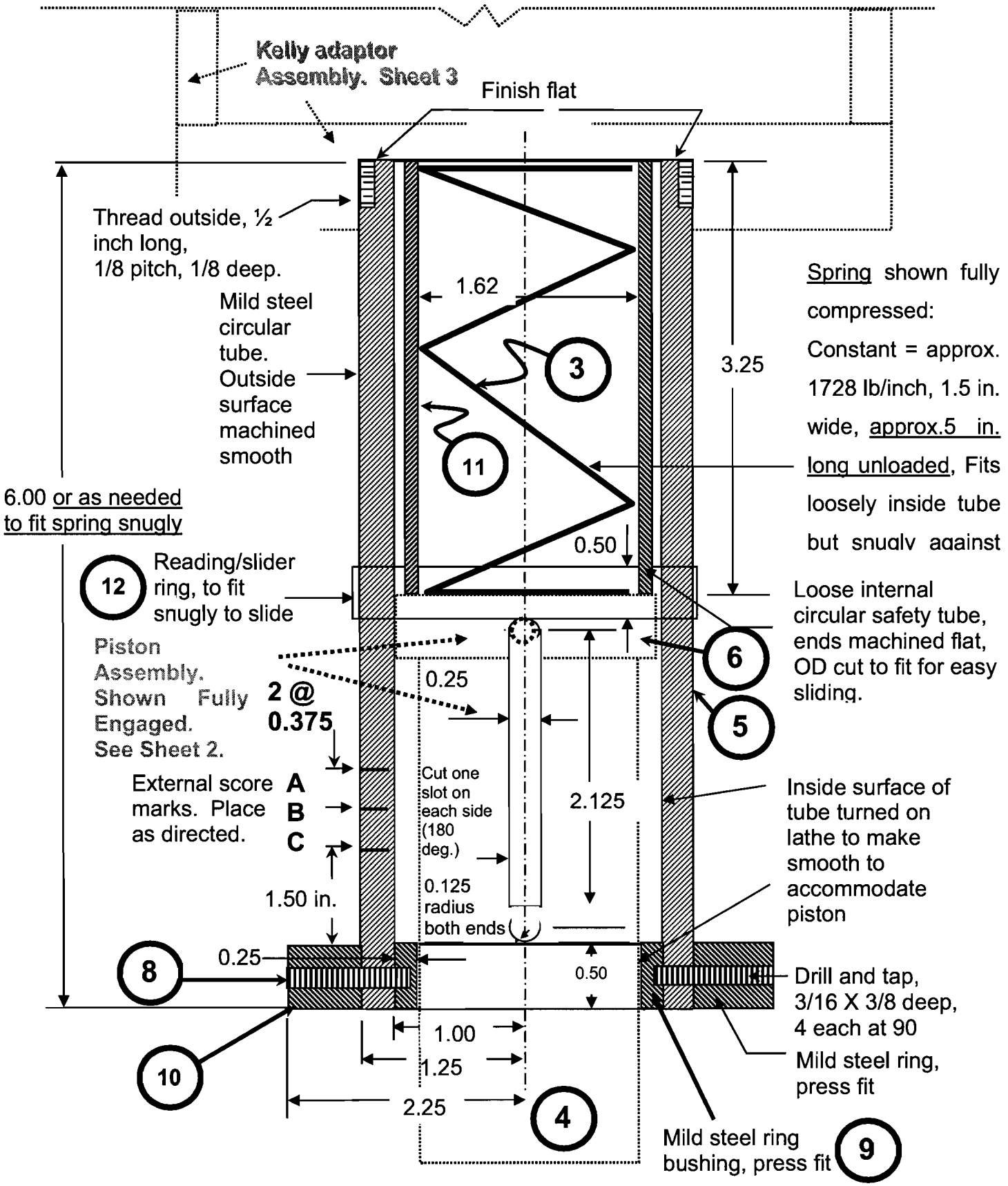

Sheet 1. Body of Penetrometer

Not to scale

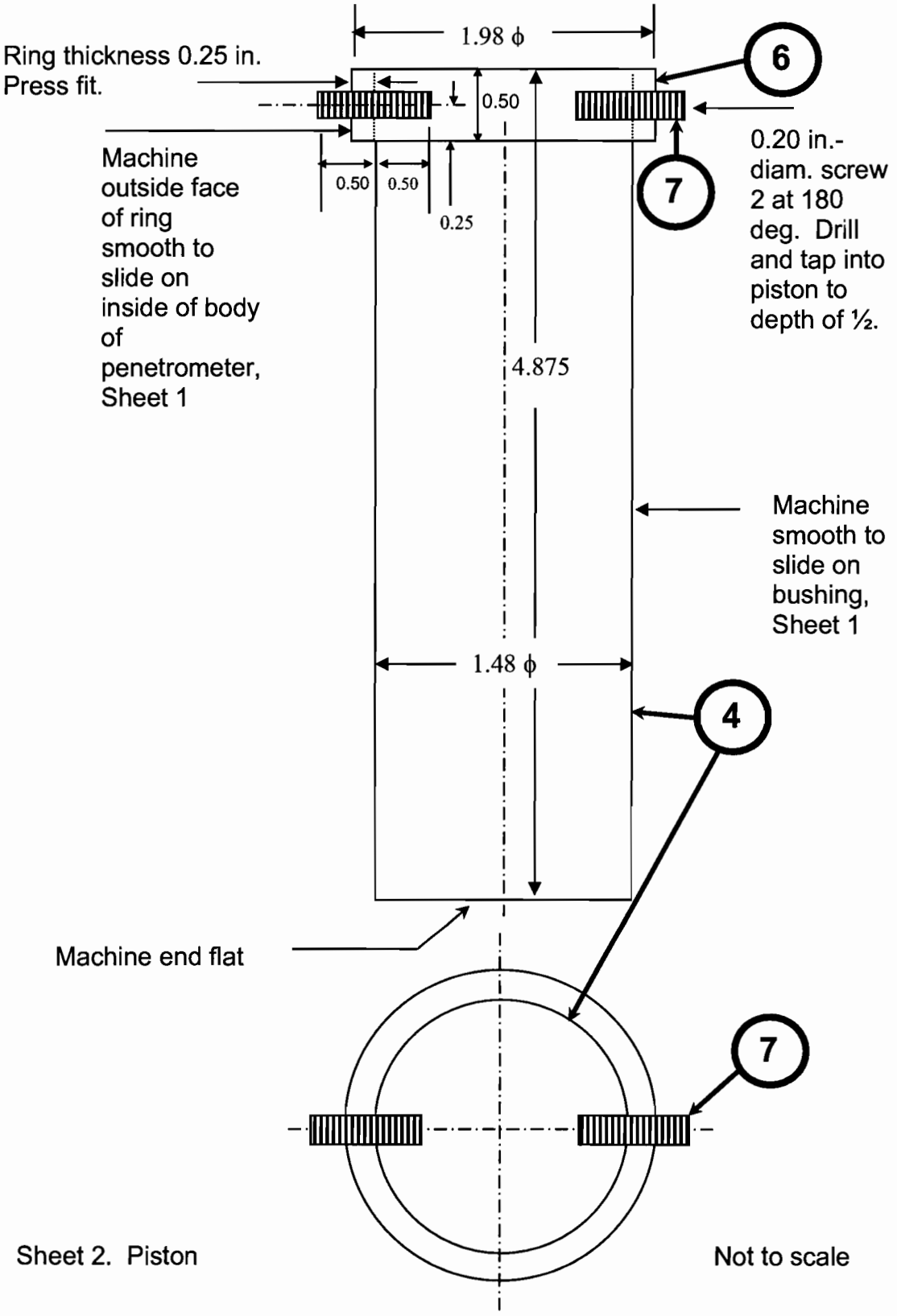

Sheet 2. Piston

Not to scale

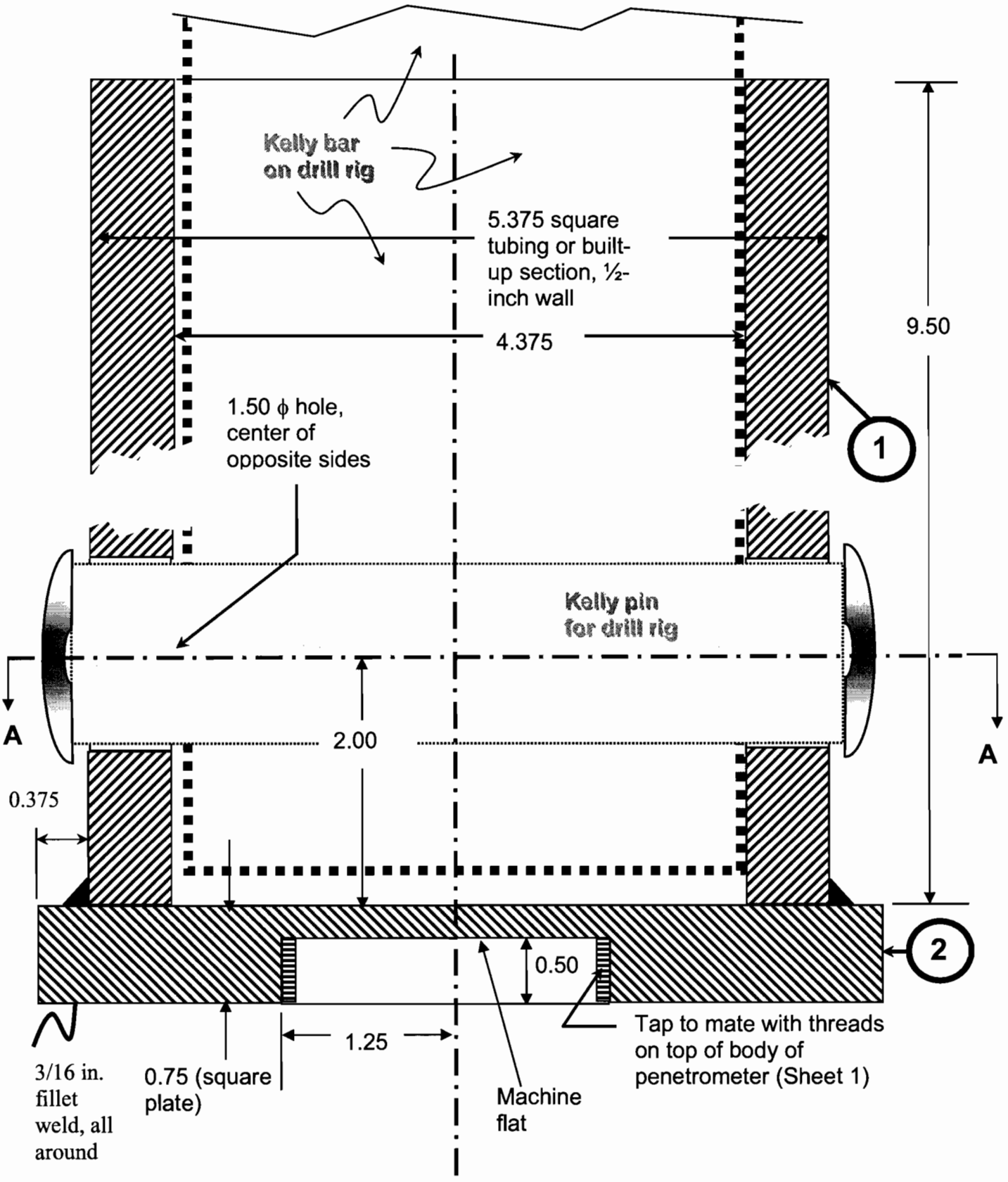

Sheet 3. Kelly Attachment (Elevation) Not to scale

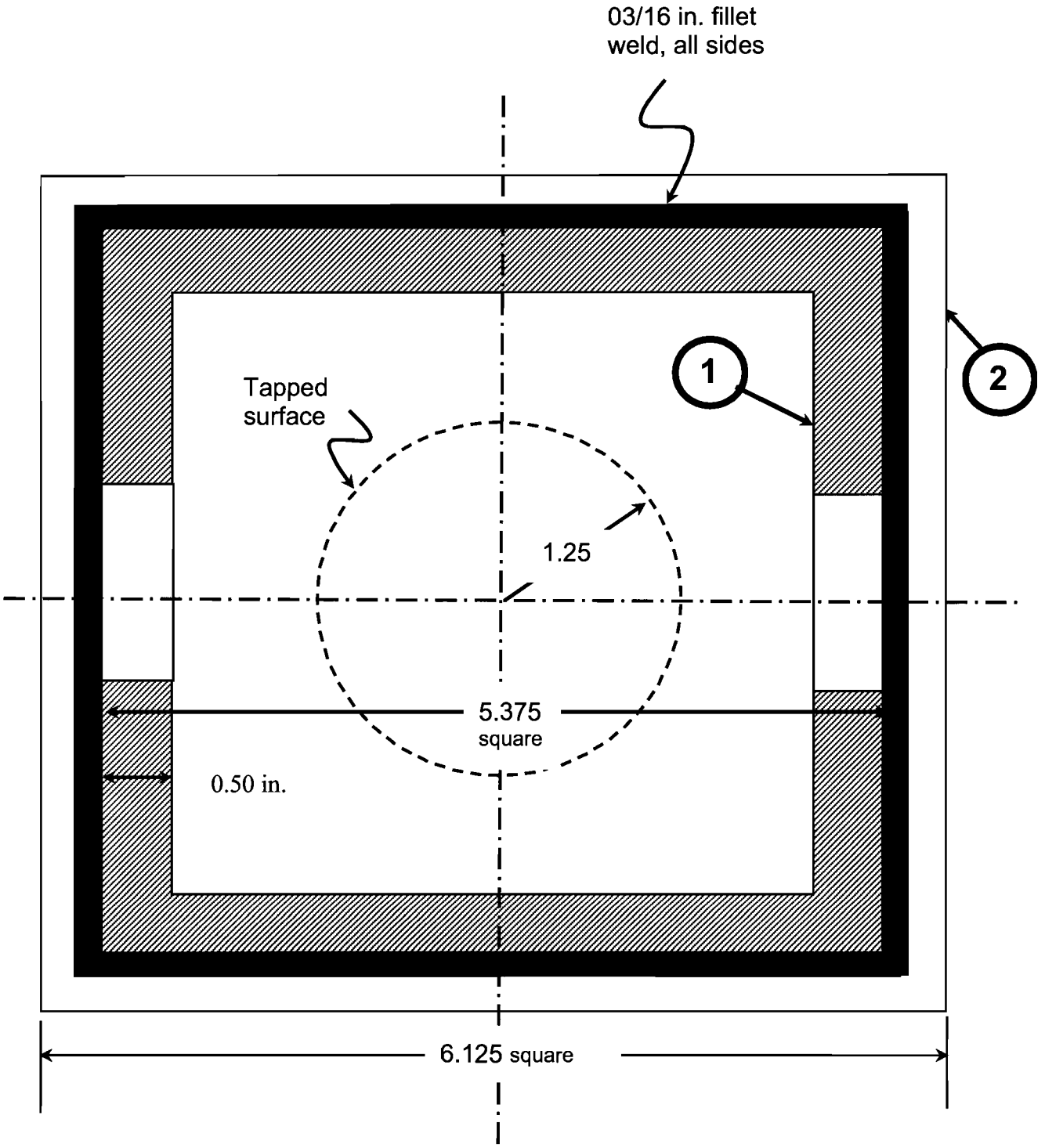

Sheet 4. Kelly Attachment (Plan) Not to scale

Static Penetrometer Materials List *(Dimensions in inches)*

Part* No.	Description	Material	Qty
1	Square tube, 5.375 OD X 0.50 wall X 9.5 in. length (may be made by welding 0.50-inch plate in square tube configuration)	Mild steel	1
2	Square plate, 6.125 X 6.125 X 0.75 (drilled and tapped per Sheet 3)	Mild steel	1
3	Spring, linear, 1728 pounds /inch. For example, Marathon Sales, Inc., Part No. 16820, Length = 5 inches, diameter = 1.5 inches	Treated Steel	1
4	Circular bar piston, 1.48 OD, 4.875 long	Mild Steel	1
5	Circular tube, 6.00 long, 0.25 wall	Mild Steel	1
6	Flat ring, 0.50 in. high, 1.98 OD, 0.25 wall	Mild Steel	1
7	Flathead screws w/ Allen-head-wrench slot, 0.20 diameter X 1.0 long (Reading ring pins)	Mild Steel	2
8	Screws, 0.1875 diameter X 1.375 long	Mild Steel	4
9	Flat ring bushing, 0.50 high, 2.00 OD, 0.25 wall	Mild Steel	1
10	Flat ring protector plate, 0.50 high X 2.50 ID X 1.00 X 1.00 wall (machine from flat plate stock)	Mild Steel	1
11	Stop device (may be loose fitting steel cylinder or 0.5 diameter rod screwed or welded to top of Part 4), 3.25 long	Mild Steel	1
12	Reading ring / slider ring. Slider ring made of Teflon® tubing, 2.50 in diameter, 0.50 in height with 0.125 wall thickness. Reading ring (fits over slider ring) made of slotted mild steel tubing, 0.50 in height with 0.0625 wall thickness (to hold slide ring snugly in place but free to slide).	Mild Steel Teflon®	1

*See Sheets 1 - 4

Fig. A.1.1 Penetrometer, Inverted, Prior to Mounting on Kelly

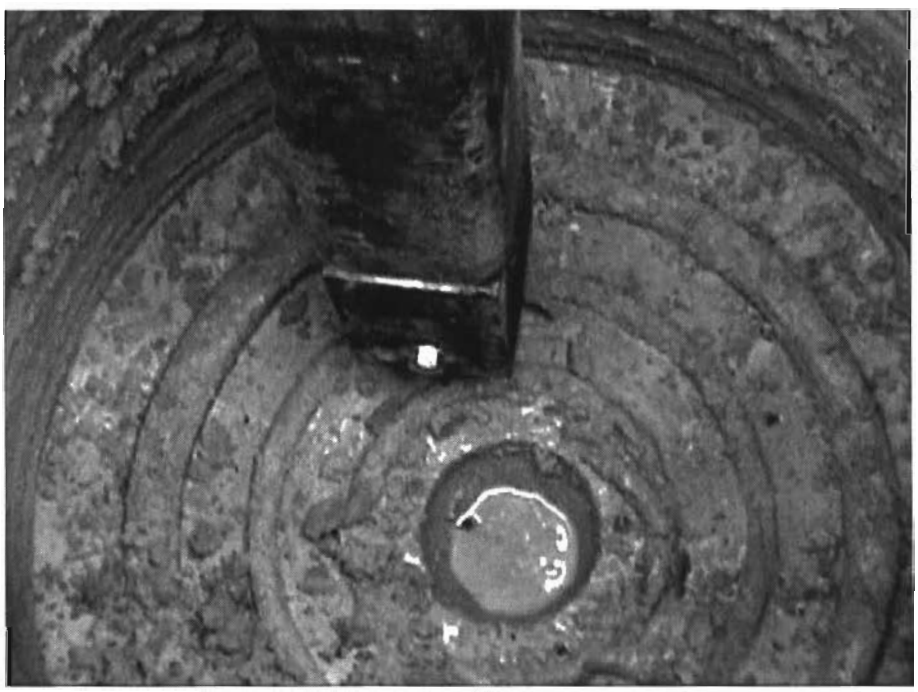

Fig. A.1.2 Static Penetrometer Mounted on Kelly Being Pushed by Weight of Kelly at the Bottom of a Drilled Shaft Borehole

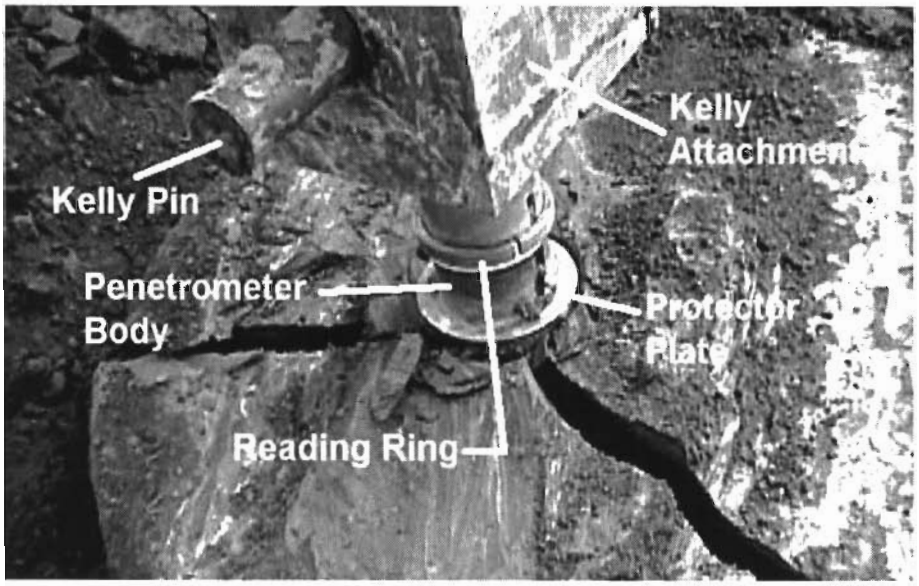

Fig. A.1.3 Close-Up of Penetrometer in Section of Clay-Shale Core

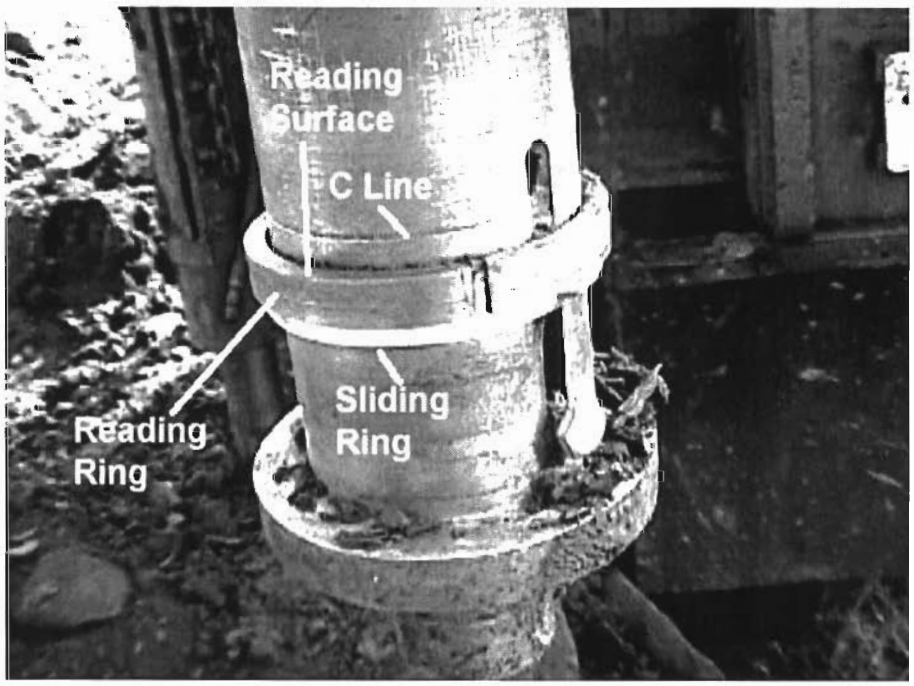

Fig. A.1.4 Photo of Penetrometer after Extraction – Score Marks (A, B, C) and Reading Ring (B-C Reading is Shown)